2007-01-29

Banda Forearc Metamorphic Rocks Accreted to the Australian Continental Margin: Detailed Analysis of the Lolotoi Complex of East Timor

Carl Eldon Standley
Brigham Young University - Provo

BANDA FOREARC METAMORPHIC ROCKS ACCRETED TO THE AUSTRALIAN CONTINENTAL MARGIN: DETAILED ANALYSIS OF THE LOLOTOI COMPLEX OF EAST TIMOR

by

Carl E. Standley

A thesis submitted to the faculty of

Brigham Young University

in partial fulfillment of the requirement for the degree of

Master of Science

Department of Geological Sciences

Brigham Young University

April 2007

BRIGHAM YOUNG UNIVERSITY

GRADUATE COMMITTEE APPROVAL

of a thesis submitted by

Carl E. Standley

This thesis has been read by each member of the following graduate committee and by majority vote has been found to be satisfactory.

Date	Ronald A. Harris, Chair
Date	Bart J. Kowallis
Date	Michael J. Dorais

BRIGHAM YOUNG UNIVERSITY

As chair of the candidate's graduate committee, I have read the thesis of Carl E. Standley in its final form and have found that (1) its format, citations, and bibliographical style are consistent and acceptable and fulfill university and department style requirements; (2) its illustrative materials including figures, tables, and charts are in place; and (3) the final manuscript is satisfactory to the graduate committee and is ready for submission to the university library.

_____ _____

Date

Ronald A. Harris
Chair, Graduate Committee

Accepted for the Department

_____

Jeffery D. Keith
Department Chair

Accepted for the College

_____

Thomas W. Sederberg
Associate Dean, College of Physical and Mathmatical Sciences

ABSTRACT

BANDA FOREARC METAMORPHIC ROCKS ACCRETED TO THE AUSTRALIAN CONTINENTAL MARGIN: DETAILED ANALYSIS OF THE LOLOTOI COMPLEX OF EAST TIMOR

Carl Standley

Department of Geological Sciences

Master of Science

Petrologic, structural and age investigations of the Lolotoi Complex of East Timor indicate that it is part of a group of thin metamorphic klippen found throughout the region that were detached from the Banda forearc and accreted to the NW Australian continental margin during Late Miocene to Present arc-continent collision. Metamorphic rock types are dominated by (in order of greatest to least abundance), greenschist, graphitic phyllite, quartz-mica schist, amphibolite and pelitic schist. Mineral, whole rock, and trace element geochemical analyses of metabasites indicate that protolith compositions are consistent with tholeiitic basalt and basaltic andesite with mixed MORB and oceanic arc affinities. Metapelitic schist compositions are consistent with mafic to intermediate oceanic to continental arc provenance. Geothermobarometric calculations show peak metamorphic

temperatures in pelitic rocks range from 530°C to 610° C for garnet-biotite pairs and peak pressures of 5 to 8 kbar for garnet-aluminosilicate-quartz-plagioclase assemblages. Analyses of amphibole in amphibolites yield temperatures of 550°C to 650°C and pressures of 6 to 7 kbar. Lu-Hf analyses performed on garnet samples from two massifs in East Timor yielded four ages with a mean of 45.36 ± 0.63 Ma, which is interpreted to represent the approximate age of peak metamorphism. Detrital zircons from one amphibolite sample in East Timor yields a bimodal U-Pb age distribution of 560 Ma and 80 Ma, indicating deposition occurred after the 80 Ma closure of the zircon grains. The sequence of deformation as indicated by field measurements is similar to that reported from other klippen throughout the Timor region. Contact relationships with adjacent units indicate that the metamorphic terrane is in thrust contact with underlying Gondwana Sequence rocks. Overlying the metamorphic rocks are Asian affinity volcanic and sedimentary cover units found mostly in normal fault contact on the edges of Lolotoi Complex klippen. Geochemical, age, petrological and structural data imply the Lolotoi Complex formed part of the eastern Great Indonesian arc, which began to collapse in the Eocene, was incorporated into the Banda arc in the Miocene, and accreted to the Austrailian continental margin from Pliocene to Present.

ACKNOWLEDGEMENTS

I would like to thank to all of the individuals who assisted me in the completion of this thesis project. I would like to especially thank Dr. Ron Harris for his help with all aspects of the project from beginning to end. Additionally, I would like to thank Hugo Ximenes for his assistance in the field, Dr. Jeff Vervoort and Dr. Garret Hart at Washington State University for their assistance with Hf/Lu and U/Pb age dating, Dr. Mike Dorais for assistance with microprobe analyses, and Dr. Bart Kowallis for help in apatite fission-track analyses.

TABLE OF CONTENTS

INTRODUCTION

The accretion of arcs to continents is one of the dominant processes of continental growth. (e.g. Taylor and McClennan, 1995). Most continents consist of at least some arc terranes or fragments of arc terranes that are far traveled. Most commonly, fragments mounted on subducting oceanic crust are carried to subduction zones where they are accreted to the upper plate. Arc fragments can also be transported by the formation of backarc and marginal basins (Jovlivet et al., 1999; Maillet et al., 1995). This process of suprasubduction zone extension has been well documented in various marginal and backarc basins of the west Pacific and Southeast Asia regions. Examples include the Lau, Izu-Bonin-Mariana, Banda Sea, Japan, and New Hebrides Basins (e.g. Hawkins, 1995; Harris, 2004; Jovlivet et al., 1999; Maillet et al., 1995). Eventually, with continued backarc extension, attenuated arc terranes may collide with continental plates and become allocthonous accreted nappes (Harris, 2006). One such far traveled accreted arc fragment in East Timor is the focus of this paper.

East Timor is the most fully-developed part of the Banda arc-continent collision (Harris, 1991). It is located on the eastern end of the Indonesian archipelago on the collisional boundary between the SE Asian plate and the NW Australian continental margin (Figure 1). The Australian plate is moving to the NNE and colliding with the SE Asian plate at a rate of 70 km per million years (Genrich et al., 1996; Nugroho, 2005). Collision initiated during the Late Miocene in the central Timor region, as the tip of the Australian plate made contact with and began subducting beneath the SE Asian plate (Carter et al., 1976). Not until the mid Pliocene (~3 Ma) did the accretionary wedge emerge above sea level as the continental edge of Australia entered the subduction zone

initiating a rapid phase of accretion and uplift in the forearc (Johnston and Bowin, 1981). Due to both the obliquity of the collision and the shape of the Australian continental margin, collision has propagated from central Timor to the southwest at the rate of 110 km/Ma (Harris, 1991). This subduction and eventual collision has formed a pair of mountainous ridges known as the Banda arc or Banda orogen. The inner (northern) arc of islands feature an active volcanic arc, and the outer arc an emergent forearc wedge and foreland fold and thrust belt. The two arcs are separated by a forearc basin which varies in width from 200 km near Savu to 5 km north of Timor where it has been closed off by both collision related shortening and vertical uplift (Harris, 1991).

This study focuses on the structurally highest portion of the accretionary outer arc comprised of medium grade metamorphic rocks overlain by Cretaceous to Pliocene sediments and volcanic units named the Banda Terrane (Audley-Charles and Harris, 1990). This terrane is exposed as eroded remnants of a larger thrust sheet throughout Timor and other islands of the Banda Sea region.

Many studies have focused on the composition and metamorphic history of similar rocks (Mutis Complex) found in West Timor (Lalan Asu massif, deWaard, 1957, 1954a, 1954b; Mutis massif, Sopaheluwaken, 1991, 1989, De Roever, 1940; Miomoffo massif, Sopaheluwaken, 1991, 1989, Van West, 1941; Booi massif, Earle 1981, 1980, Brown and Earle, 1983; Mollo massif, Earle, 1980; Usu massif, de Waard, 1959). Myriad studies since the early 1900's have documented the allocthonous tectonic origin of the Mutis Complex (Tappenbeck, 1939; de Roever, 1940; van West, 1941; van Bemmelen, 1949; de Waard, 1954a, 1954b, 1957; Audley-Charles, 1968; Audley-Charles and Carter, 1972; Barber and Audley-Charles, 1976; Earle, 1981; Brown and Earle,1983;

Sopaheluwaken et al., 1989; Harris, 1991, 1992, 2006; Harris and Long, 2000). Few investigators have looked closely at similar metamorphic rocks in East Timor known as the Lolotoi Complex (Audley-Charles, 1968; Barber and Audley-Charles, 1976). The lack of detailed studies has led some to contend that the metamorphic massifs of East Timor may represent autochtonous metamorphic basement blocks of Australian continental basement having been exposed either as upthrust basement blocks (Grady, 1975; Chamalaun and Grady, 1978) or as basement involved thrust slabs (Charlton, 2002). These conclusions regarding the origin, structure and tectonic history of the metamorphic rocks in East Timor have been made solely by either association with the Mutis Complex in West Timor or speculation. Several fundamental questions regarding the origin of the metamorphic rocks of East Timor and their sedimentary cover sequences remain unanswered. The debate over whether the Lolotoi Complex is allocthonous in nature and derived from the upper Asian plate as documented in West Timor, or is autocthonous with an Australian affinity is still unresolved. Most recently, Harris (2006) provides a synthesis of data collected throughout the Banda arc, including some results presented in this paper to demonstrate an Asian affinity for Banda Terrane rocks.

The purpose of this paper is to better constrain the tectonic affinity and structural evolution of the Lolotoi Complex of East Timor. Underlying issues to be addressed include composition of the protolith, peak metamorphic conditions, metamorphic and cooling ages, structural evolution, and the relationship to Mutis Complex rocks in West Timor.

The detailed investigation of the Lolotoi Complex involved: 1) detailed mapping of the Lolotoi and Bebe Susu massifs of East Timor, 2) petrographic studies of

metamorphic assemblages and microstructures, 3) geochemical whole rock and trace element analyses for provenance and protolith compositions, 4) geothermobarometry to determine limits of metamorphic conditions, 5) Lu-Hf age analysis of garnets to determine the age of peak metamorphic conditions, 6) apatite fission-track analysis to constrain low temperature thermal history and 7) structural analysis of outcrops and thin sections to explore the deformation history.

GEOLOGICAL SETTING

The Banda Terrane consists of up to 2000 km^2 isolated remnants of a metamorphic complex overlain by Cretaceous to Miocene age volcanic rocks, clastic sediments, carbonates and chert known as the Palelo Group (Figure 3). Stratigraphic columns shown in Figure 3 illustrate not only the generalized stacking order of East Timor units with the Banda Terrane as the uppermost structural unit, but also the difference in age and rock type between the Banda Terrane and units from the Australian slope and rise. Note the abundance of relatively young turbiditic sediments, arc affinity volcanic rocks, and felsic and mafic dikes in the Banda Terrane units compared to similar age Australian affinity units. Structurally underlying the Banda Terrane is a thick tectonic mélange that grades downward into fold and thrust sedimentary cover sequences of Australian affinity (Harris et al., 1998). These Australian continental margin units are comprised of Cretaceous-Pliocene passive margin deposits and underlying Permian-Jurassic Gondwana Sequence units. During the Pliocene collision of the Australian continental margin with the SE Asian plate, passive margin deposits known as the Kolbano Sequence were mostly accreted to the front of the Banda Terrane, while

Gondwana Sequence deposits were underthrust and subcreted beneath (Harris, 1991) (Figure 3). The thick, clay-rich Wailuli shale of the uppermost Gondwana Sequence acts as the decollemont at the base of the Kolbano Sequence and roof of the Gondwana Sequence thrust wedges. This shale also forms most of the matrix of the Bobonaro mélange scaly clay over which the Banda Terrane was tectonically emplaced (Harris et al., 1998). Continued underthrusting and duplex stacking of the Gondwana Sequence uplifted the Banda Terrane and overlying sediments to heights of nearly 3000 m (Harris, 1991). Subsequent erosion has removed most of the Palelo Group sedimentary and volcanic cover sequences leaving mostly isolated remnant metamorphic klippe of Banda Terrane. In East Timor these eroded metamorphic remnants are collectively known as the Lolotoi Complex, in West Timor they are known as the Mutis Complex. The principle massifs in East Timor, which are the focus of this study are, the Bebe Susu, Lolotoi, the Lacluta massifs, though data from other areas was also collected (Figure 2).

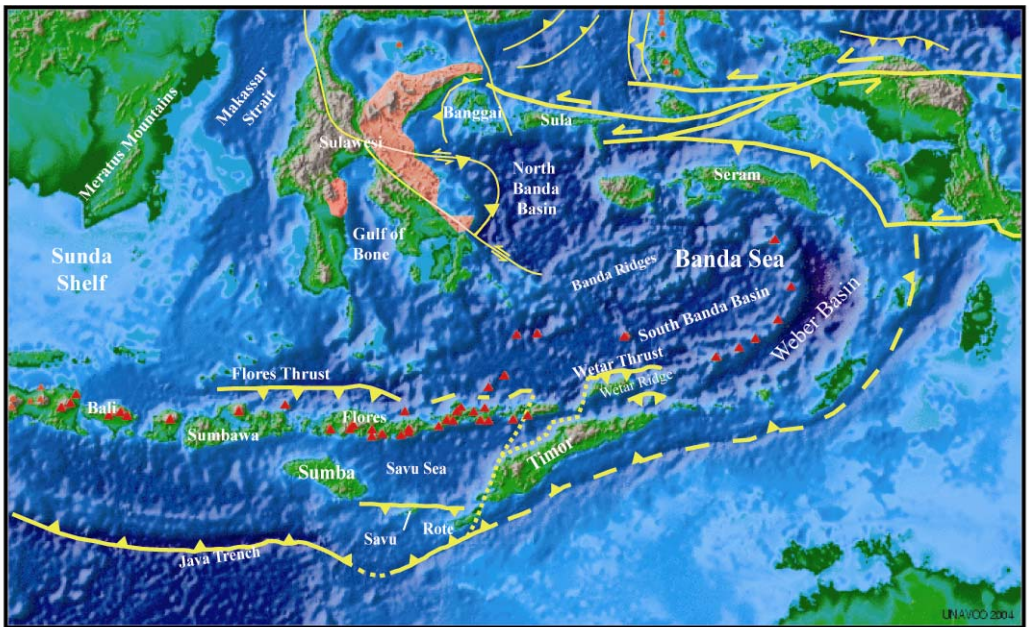

Figure 1. Digital elevation model of the Banda Arc region. Active faults are shown in yellow, active volcanoes are shown in red.

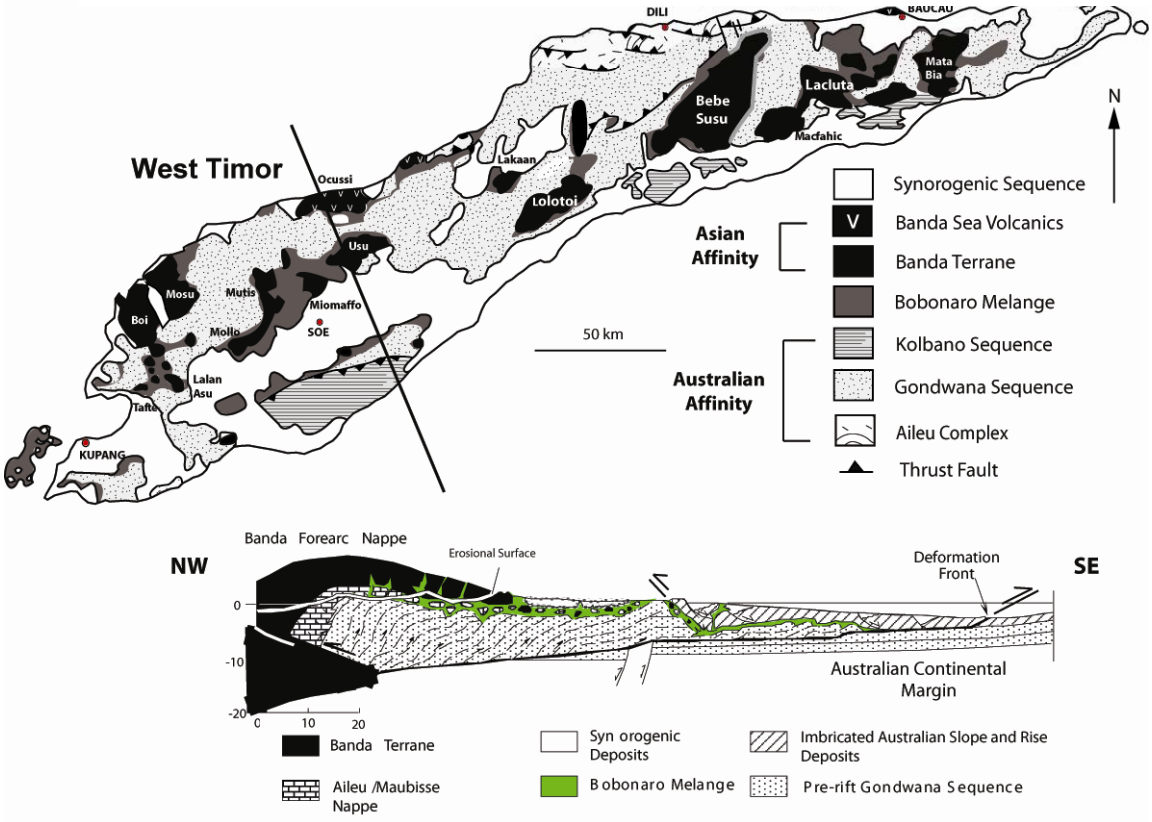

Figure 2. (Top) Generalized geologic map of Timor showing various Banda Terrane massifs that structurally overlie Australian affinity Gondwana Sequence units. (Bottom) Cross section from Harris et al., (1998) showing that Timor is essentially a young accretionary fold and thrust belt formed by underthrusting of the Australian continental margin beneath the Banda arc, due to the collision of the Australian and SE Asian plates.

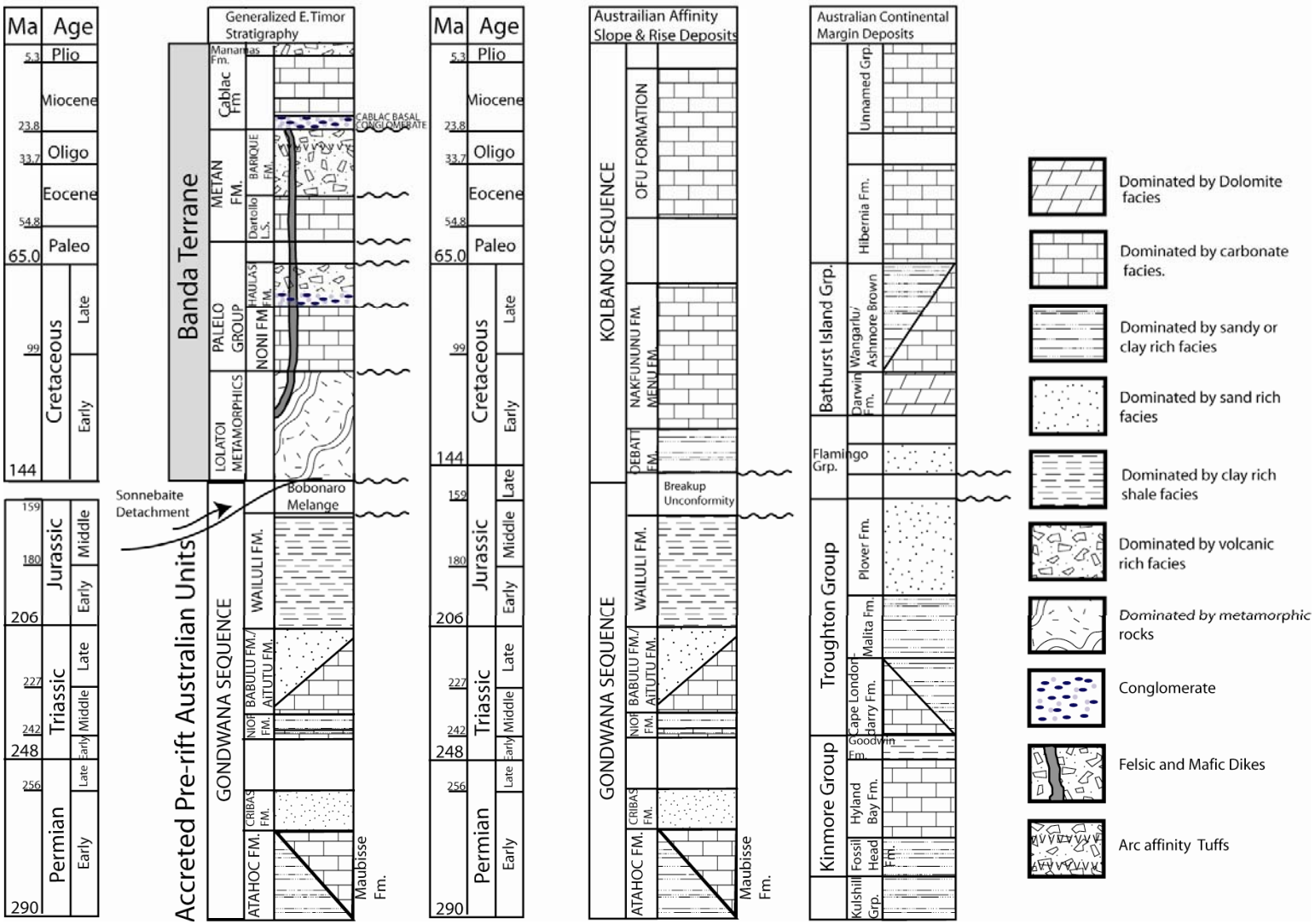

Figure 3. Stratigraphic columns of lithotectonic units in East Timor, Australian slope and rise deposits accreted to the Banda Terrane, and Australian continental margin deposits. In East Timor the Banda Terrane is interpreted to have been thrust over the Gondwana Sequence during Pliocene collision and emplacement. Notice the abundance of volcanic rich facies and felsic and mafic dikes in the Banda Terrane compared to a complete lack of these units in the Australian related passive margin sediments.

LOLOTOI COMPLEX METAMORPHIC ROCK TYPES AND DISTRIBUTION

There are two different metamorphic units in East Timor, the Aileu and Lolotoi Complexes. The Aileu Complex is found along the north coast and consists mostly of metapelites with associated amphibolitic mafic intrusions (Berry, 1986). The grade of metamorphism decreases rapidly to the south where the Aileu Complex becomes a slate belt that is transitional with the unmetamorphosed Permian to Triassic Maubisse formation (Praysetyadi and Harris, 1996). The Aileu Complex differs from the Lolotoi Complex in that is derived from a mostly psamitic protolith (Berry and Grady, 1981) with Early Proterozoic and Paleozoic detrital zircon ages (Harris, 2006). It is also gradational with Australian affinity units such as the Maubisse formation (Barber and Audley-Charles, 1976; Prasetyadi and Harris, 1996).

Metamorphic rock types found in the Lolotoi Complex of East Timor consist of medium pressure-temperature greenschist to amphibolite facies units and are dominated by (in order of decreasing abundance) greenschist, graphitic phyllite quartz-mica schist, amphibolite gneiss and schist and garnet bearing pelitic gneiss and schists. Greenschists and amphibolites are metabasic with protolith compositions consistent with basalts and basaltic andesites. Quartz-mica schists and garnet bearing schists are metapelites with a protolith likely resembling shale or greywacke (Earle, 1981). A complete discussion of provenance and petrology of each metamorphic rock type is provided in the section that follows.

Metamorphic rock types in the Lolotoi Complex alternate at multiple scales, commonly several times at outcrop scale. The scale of these heterogeneities and lack of

exposure outside of stream beds renders most individual units unmappable. Yet significant compositional relationships are observed in the general distribution of dominant rock types. Figures 5 and 6 show dominant metamorphic rock type distributions in portions of the Bebe Susu and Lolotoi massifs.

Maps show graphitic phyllite is interbedded with all other rock types present; however, it is relatively more abundant on the fringes of the nappes. Alternating greenschist and quartz-mica schist dominate the majority of the interior of the nappes, though they are commonly interfingered with graphitic phyllite. Garnet-mica schists, and mica schists interfinger with greenshists and graphitic phyllite in outcrops of isolated, deeply eroded areas of the central part of the Bebe Susu massif. Workers in West Timor (deWaard, 1959; Earle, 1981) have also noted a similar frequent alternation of rock types in the Usu, Lalan Asu, and Mutis massifs, which suggests a sedimentary origin for much of the crystalline schists. Amphibolite also only outcrops in the central part of the Bebe Susu massif, though is widespread in float. Locally, brecciated greenstone is found at the highest structural levels in the thin northern portion of the Bebe Susu nappe and also is found extensively on the southern edge of the Bebe Susu nappe. Harzburgite, lherzolite, serpentinite, and altered gabbro and diorite are found locally in float throughout the Lolotoi Complex. Mafic and felsic igneous dikes are also found locally within all massifs investigated.

The vertical stacking sequence of metamorphic units in the Lolotoi Complex is more difficult to determine than for thicker massifs with reportedly steeper metamorphic gradients in the Mutis Complex . However, it is apparent from field relations that lower grade greenstone, greenstone breccia and graphitic phyllite dominate at shallower

structural levels. Greenschist, quartz-mica schist, and graphitic phyllite are more prolific at intermediate levels. Higher grade amphibolite and pelitic schist are found only in outcrop at the deepest structural levels. This general stacking relationship also holds true for most massifs of the Mutis Complex. In the Boi massif of West Timor, Earle (1980) identifies the main lithologies from structural top to bottom as 1) serpentinite, tremolite schist, 2) monometamorphic metagabbro (greenschist) and amphibolite, and 3) polymetamorphic amphibolite and pelitic gneisses. In the Usu massif, de Waard (1954b) identified basic crystalline schists comprised of greenschists and amphibolites and pelitic crystalline schists consisting of phyllites, mica-schists and gneisses. In the Mutis and Miomoffo massifs, Sopaheluwaken, (1989) identifies peridotite, metabasites (amphibolite, greenschist, and metatuff) and metapelites with recognized biotite, garnet and staurolite zones. Also identified were loose blocks of granulite found at the uppermost structural levels of the Mutis massif (Sopaheluwaken (1989). Sopaheluwaken (1991) suggests this represents an inverted metamorphic gradient in the Mutis massif as a result of hot peridotite emplacement. Other workers investigating this same massif have concluded ophiolite sole metamorphism could not have heated such a thick package of rocks and that the stacking order of rock types in other massifs is different (Earle, 1981). Harris (2006) suggests the apparent inversion of the metamorphic package is more likely a result of late low angle normal faulting.

Comparison of the Lolotoi Complex rocks with those found in the Mutis Complex shows no significant difference exists in rock type, grade, or stacking relationships. Some minor differences in abundances and grade do merit mention: 1) the amount of peridotite and serpentinite is higher in some Mutis Complex massifs, 2)

amphiboles in the Lolotoi Complex are mostly hornblende rich, with little actinolite found, 3) granulite was not found anywhere in the Lolotoi Complex, and 4) no evidence of an inverted metamorphic gradient was found in East Timor, although lack of thick sections mostly preclude adequately testing this relationship. In comparing major metamorphic rock types from West and East Timor no major differences exist in composition, grade, or stacking relationships, and based on these parameters alone, both complexes most likely share similar depositional and metamorphic histories.

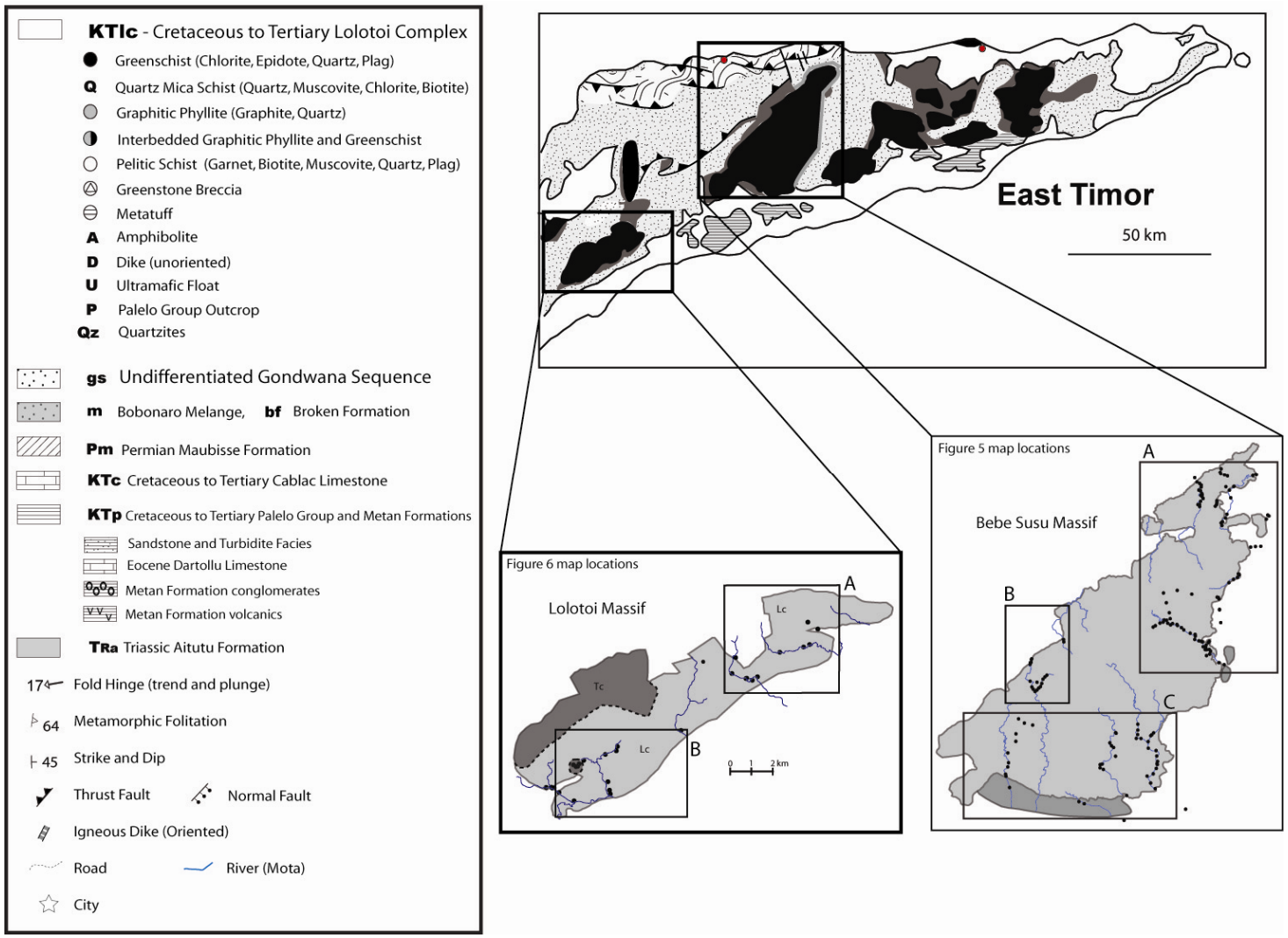

Figure 4. Locations of outcrops and sample locations in the Lolotoi and Bebe Susu massifs (black dots). Key applies to detailed maps of enclosed areas shown in Figures 5 and 6.

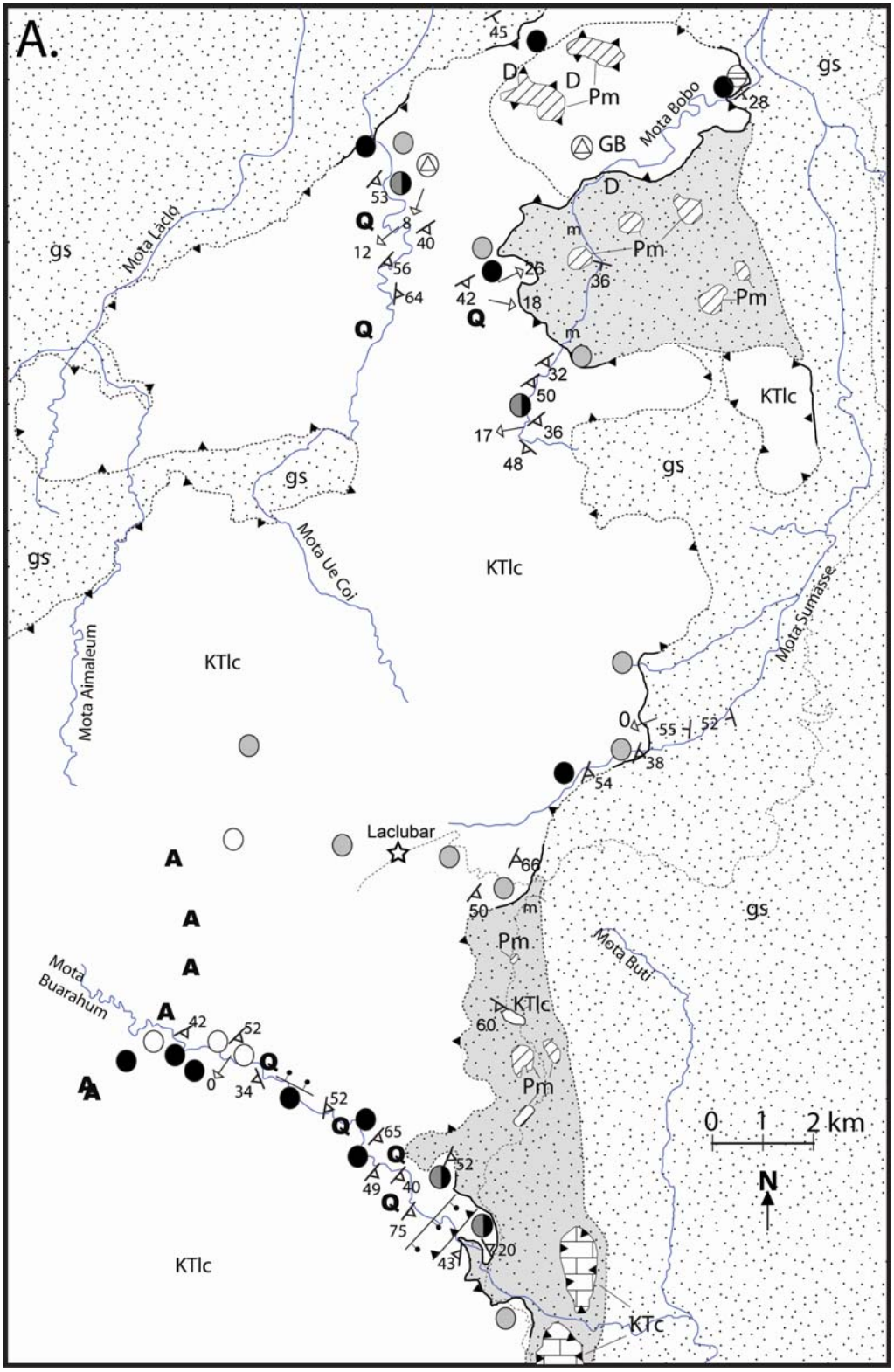
A.
gs
Mota Lacló
Mota Bobo
Mota Ue Coi
Mota Aimaleum
Mota Sumasse
Mota Buti
Mota Buarahum
Laclubar
KTlc
KTc
Pm
D
GB
0 1 2 km
N

Figure 5A.

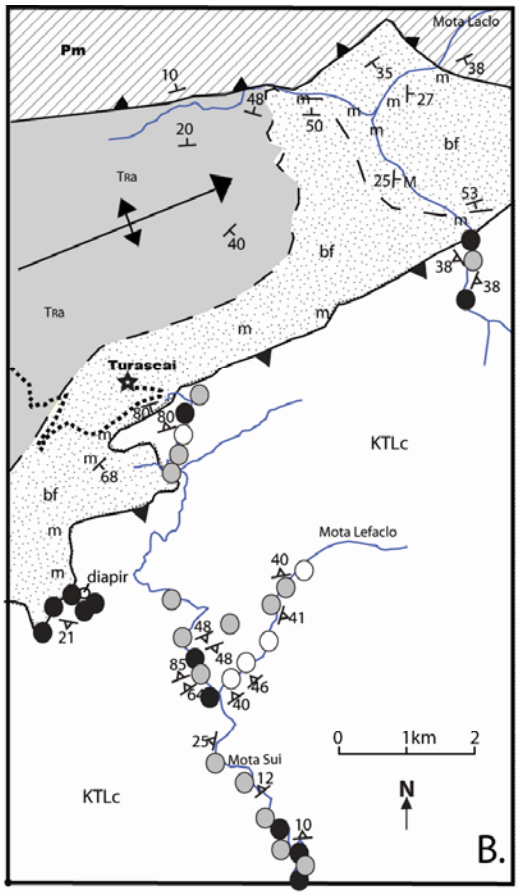

Figure 5. Detailed geologic maps of the Lolotoi Complex. See Figure 4 for locations and key to rock types. Lateral extents of these units could not be mapped due to outcrop scale interlayering of rock types and heavy vegetation. Dominant metamorphic lithologies are shown. A) NE Portion of the Bebe Susu massif. Note the presence of Permian Maubisse limestone only on the fringes and in fensters in the thin northern portion of the nappe. Foliations dip mainly to the SE and NW. Gondwana Sequence units were not differentiated during field mapping. Notice the mélange on the NE and SE portions of the map area, which reflect the thrust contact between the Lolotoi Complex and underlying Australian affinity units (Harris et al., 1998). B) NW part of the Bebe Susu massif on the southern flank of the Aitutu anticline. Most blocks in mélange are composed of broken parts of a Maubisse thrust sheet that structurally underlies the Bebe Susu Massif. C) SW part of the Bebe Susu nappe. Notice Asian affinity cover units found in normal fault contact with Lolotoi metamorphics. Breccia along the sourthern portion of the nappe is likely associated with this faulting.

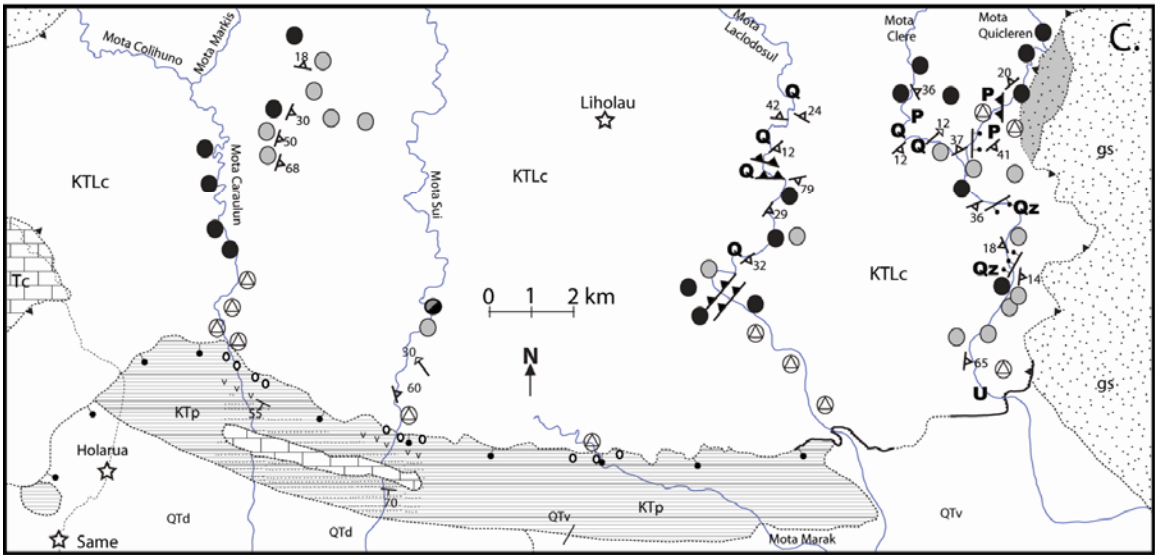

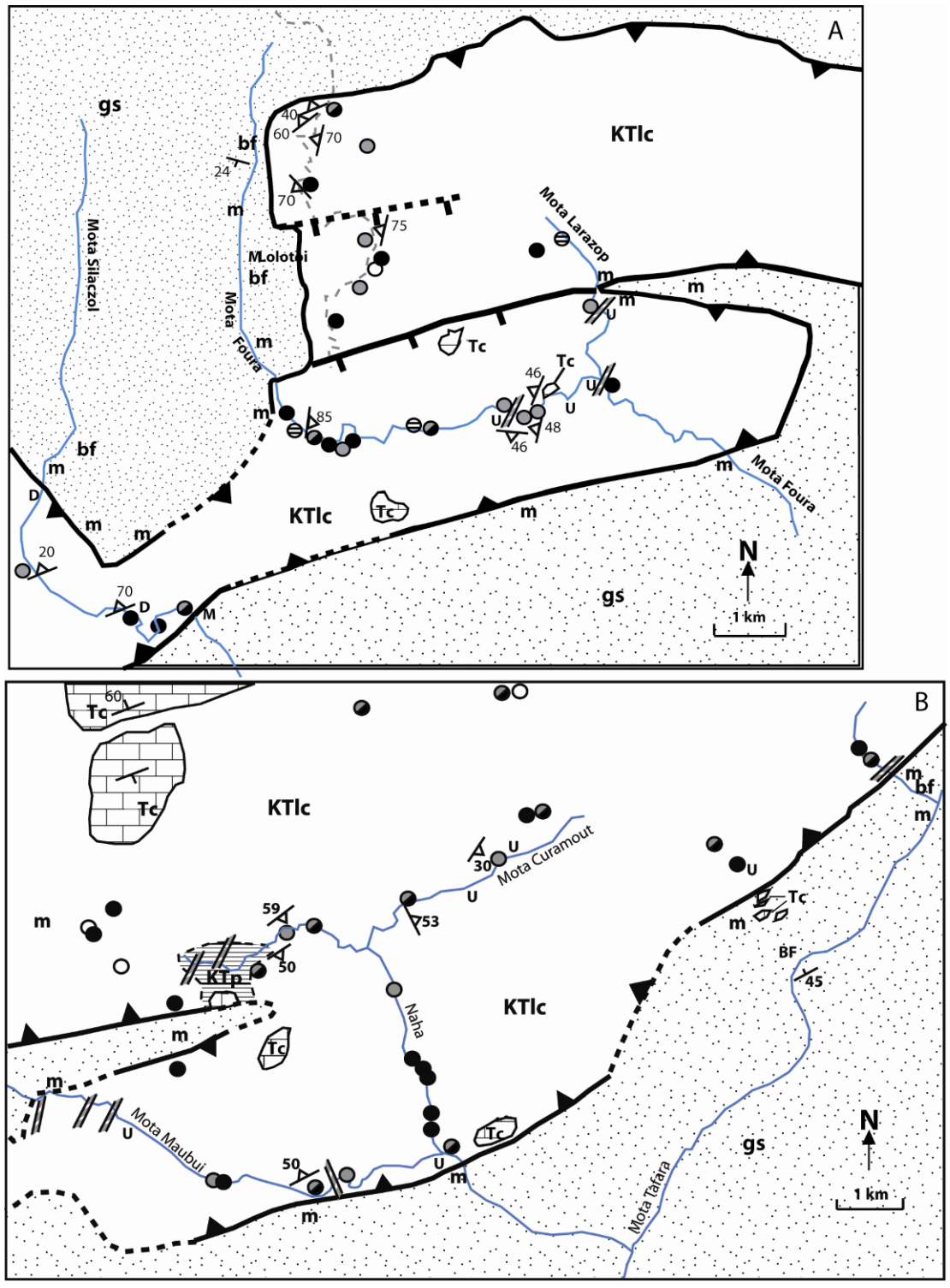

Figure 6. Geologic maps of northern (A) and southern (B) portions of the Lolotoi massif showing distribution of metamorphic rock types and large scale structures. Notice in (B) the presence of Palelo Group units intruded by dikes, and Cablac Limestone overlying the Lolotoi metamorphics.

PETROLOGY

Thin sections and hand samples were evaluated to determine mineral assemblages, textural relationships, alteration effects and variation within rock types. In addition, pre-, syn-, and post-kinematic indicators were observed to determine relative timing of mineral growth episodes and further constrain timing of metamorphic processes. In order to fully compare Mutis and Lolotoi Complex rocks, thin sections and hand samples from the Mutis Complex were also examined, however are not reported on here. In order of decreasing abundance, the Lolotoi Complex consists of greenschist, graphitic phyllite, quartz-mica schist, amphibolite and pelitic schist. Petrologic information for several representative samples are shown in Table 1, additional sample descriptions are provided in Appendix I.

Lolotoi Complex greenshists have a mineral assemblage of chlorite + quartz + plagioclase ± epidote ± muscovite ± minor apatite and sphene (Table 1). Samples are typically dominated by quartz or chlorite, with modal percentages of quartz ranging from 20 to 40 % and amounts of chlorite from 40 to 50 %. They commonly exhibit well aligned chlorite grains and distinct chlorite-rich and quartz-rich domains on the mm to cm scale, though relatively homogenous non-gneissic textures are also common. Nearly complete retrograde alteration of plagioclase, muscovite, and biotite to fine grained chlorite is common. Quartz and especially carbonate veining is prolific in most greenschist samples. Some carbonate-rich greenschist may be better classified as reported by deWaard (1957) as a calcarenous series of impure marbles consisting of quartz-calc schist and epidote-albite-calc schist.

Quartz-mica schists contain a main assemblage of quartz + muscovite ± biotite ± chlorite ± amphibole. Micas are very well foliated and quartz-rich and mica-rich domains appear to be related to original depositional layering of clay-rich and sand-rich layers (Figure 7b). Quartz domains dominate most samples, occupying from 40% up to 80% of the sample volume. Muscovite is typically very fine-grained with common alteration of original banding by fold transposition. Localized folding forms assymetrical microfolds which indicate vergence principally in a southerly direction, though western and northern vergence was also documented. Some samples exhibit well defined S-C mylonitic fabrics (Figure 7d).

Graphitic phyllites are composed exclusively of layers of graphite and quartz. The higher the abundance of graphite, the more fissile and less resistant the phyllites become. Many of the areas within the nappes with little to no exposure are most likely rich in graphitic phyllite.

Amphibolites contain mostly green amphibole (hornblende), rare blue amphibole (tschermakite and ferro-tschermakite), + quartz ± plagioclase ± opaques ± muscovite, ± biotite, ± chlorite ± epidote ± garnet. Apatite and sphene are abundant accessory minerals. Samples are typically amphibole-rich relative to quartz, with modal percentages of amphibole ranging from 50 to 80 percent (Figure 7c). Textures, grain size and degree of foliation vary from sample to sample. Amphibole grain size varies from very fine (<.05 mm) to coarse (>5.0 mm). Most samples, though not all, are gneissic, having well aligned amphibole blades with alternating amphibole-rich and quartz-rich bands. Schistose samples have relatively homogenous textures and tend to be more quartz-poor. Few samples have a relict igneous texture with blebs of quartz and

amphibole. Virtually no microscale folding is present though some brittle deformation is observed in gneissic samples. Secondary calcite veins are rarely present.

Garnet mica schists are characterized by biotite + muscovite + quartz + garnet + plagioclase ± staurolite ± kyanite ± chlorite ± sillamanite. Garnet porphyroblasts are typically hybidioblastic with few unaltered idioblastic grains remaining, and range in size from 2 mm to ~1 cm (Figure 7a.). More completely resorbed xenoblastic garnets are present in some samples. Many garnets have abundant inclusions of quartz, epidote, ilmenite, biotite and/or plagioclase. Textural relationships in one float sample collected in the southern Bebe Susu nappe show multiple generations of garnet growth, with inclusion free garnets preserved as cores inside inclusion laden overgrowths. Microprobe X-ray dot maps of Mn and Fe also confirm the occurrence to two growth intervals. Inclusion trails present in most garnets indicate little rotation has occurred. Inclusion trails also show evidence of pre-, syn-, and post-kinematic garnet growth (Figure 8a-f). Some alteration of garnets has occurred with micas at grain boundaries through net transfer reactions with micas as evidenced by spessartine rich garnet rims (Kohn and Spear, 2000). Kyanite porphyroblasts are up to 5 mm in size and always are hybidioblastic to xenoblastic. Plagioclase compositions are principally andesine and labradorite. Compositions range from An_{20} to An_{67} along the albite-anorthite solid solution. No potassium feldspars were identified in thin section. Multiple generations of biotite growth have occurred as indicated by both syn- and post-kinematic indicators and by differences in extent of foliation. Retrogradational alteration of micas, garnet and plagioclase to chlorite is common on grain boundaries, but for the most part samples appear well preserved. Calcite veins are rarely found in this rock type.

Earle (1981) describes retrogression and veining as the main metamorphic phenomena operating on Mutis Complex rocks after the peak of metamorphism. This also is the case for the Lolotoi Complex, as retrogression of garnets, amphiboles, and plagioclase to micas and chlorite is widespread. Veining in the Lolotoi Complex is far more common in greenschists than in amphibolites or pelitic schists.

Additional minor occurrences of various rock types are associated with the Lolotoi metamorphics. Altered peridotite is found sparsely in float. The peridotite consisits of lherzolite and harzburgite, which has been largely altered to serpentine and chlorite. The peridotite is commonly heavily veined with calcite (Figure 9c) Clasts from overlying cover sequences found throughout the Lolotoi Complex include altered igneous rocks (Figure 9d), clastic carbonates, fossiliferous limestone (Figure 9a), and fault breccias containing both metamorphic and carbonate clasts (Figure 9b).

DISCUSSION

One of the defining characteristics of Banda Terrane metamorphic rocks in West Timor is the occurrence of polymetamorphic rocks (i.e. Brown and Earle, 1983); however, limited petrologic or textural evidence is found in the pelitic rocks of the Lolotoi Complex for the occurrence of multiple metamorphic events. Multiple episodes of garnet growth found in one Lolotoi Complex float sample does indicate polymetamorphism, however all garnet-mica schist samples collected from outcrop in the Bebe Susu massif exhibit just a single generation of garnet growth. No textural or compositional characteristics of amphibolites indicate a polymetamorphic history, and their close proximity to outcrops of monometamorphic pelitic schists suggests an

identical metamorphic history. Brown and Earle (1983) note in their investigation of polymetamorphic schists and amphibolites in the Boi and Mutis massifs, an early high pressure assemblage of garnet (preserved as homogenous core areas in now retrograded garnet porphyroclasts) + Al silicate + biotite + plagioclase + quartz + opaques. They document a later lower pressure assemblage of cordierite + biotite + plagioclase + sillimanite + quartz ± hercynite ± opaques, with retrograde garnet and relict plagioclase. Brown and Earle, (1983) use these assemblages in addition to geothermobarometric calculations to conclude that the early assemblage was a result of high P-T (pressures ~ 10 kbar and temperatures >750 °C) metamorphism, which was followed by decompression during rifting and resulted in the latter intermediate temperature (600-700 °C), low pressure (3-4 kbar) phase of metamorphism. These two overlapping assemblages are not observed in any of the Lolotoi Complex samples. However, very limited occurrences of metapelitic rocks in the Lolotoi Complex limit observations of early and late assemblages. It is important to note that polymetamorphic pelitic units in West Timor are limited in extent and occur only in a small number of massifs. Descriptions of monometamorphic assemblages in West Timor are consistent with observations presented here for the Lolotoi Complex.

While petrologic characteristics of Mutis and Lolotoi Complex rocks are for the most part in agreement, minor differences are apparent, the greatest of which is the paucity of polymetamorphic indicators in East Timor compared to those locally documented in the west. This difference could be an indication of a metamorphic gradient from east to west, with western Mutis rocks experiencing a more extensive late stage of metamorphism, producing low pressure assemblages containing cordierite and

sillimanite. Perhaps this late stage of metamorphism is expressed in eastern rocks only as a partial retrogradation of the initial higher P-T metamorphic assemblage.

Table 1. Modal percentages of minerals for representative samples of each metamorphic unit.

	Metabasites							Metapelites						
	Amphibolites				Greenschists			Garnet bearing schists				Quartz-mica schists		
Minerals	8-3-9	8-4-2	8-3-5	8-4-4	Bobo-2	04-WS2	04T-ML6	8-3-5	F1-1	SF-3	04T-MLO	Clere	7-26-7	7-17-4
Quartz	15%	20%	40%	40%	20%	40%	30%	40%	50%	30%	40%	40%	80%	60%
Biotite									20%	20%	35%	10%	10%	
Muscovite									10%	8%	15%	20%	10%	35%
Chlorite			20%		50%	40%	40%	20%	5%			20%		
Plagioclase				5%					5%	10%	2%			
Garnet			5%						10%	30%	5%			
Epidote					5%	2%	10%							
Opaques	4%	2%	5%	5%	<1%	3%	<1%	5%	1%	<1%	3%	10%		5%
Hornblende	80%	75%	20%	50%				20%						
Calcite					20%	15%	20%							
Pyrite			10%					10%						
Staurolite									<1%					
Kyanite									5%	2%				
Zircon														
Apatite	<1%	1%	<1%	<1%				<1%						
Sphene	<1%	1%	<1%	<1%				<1%						

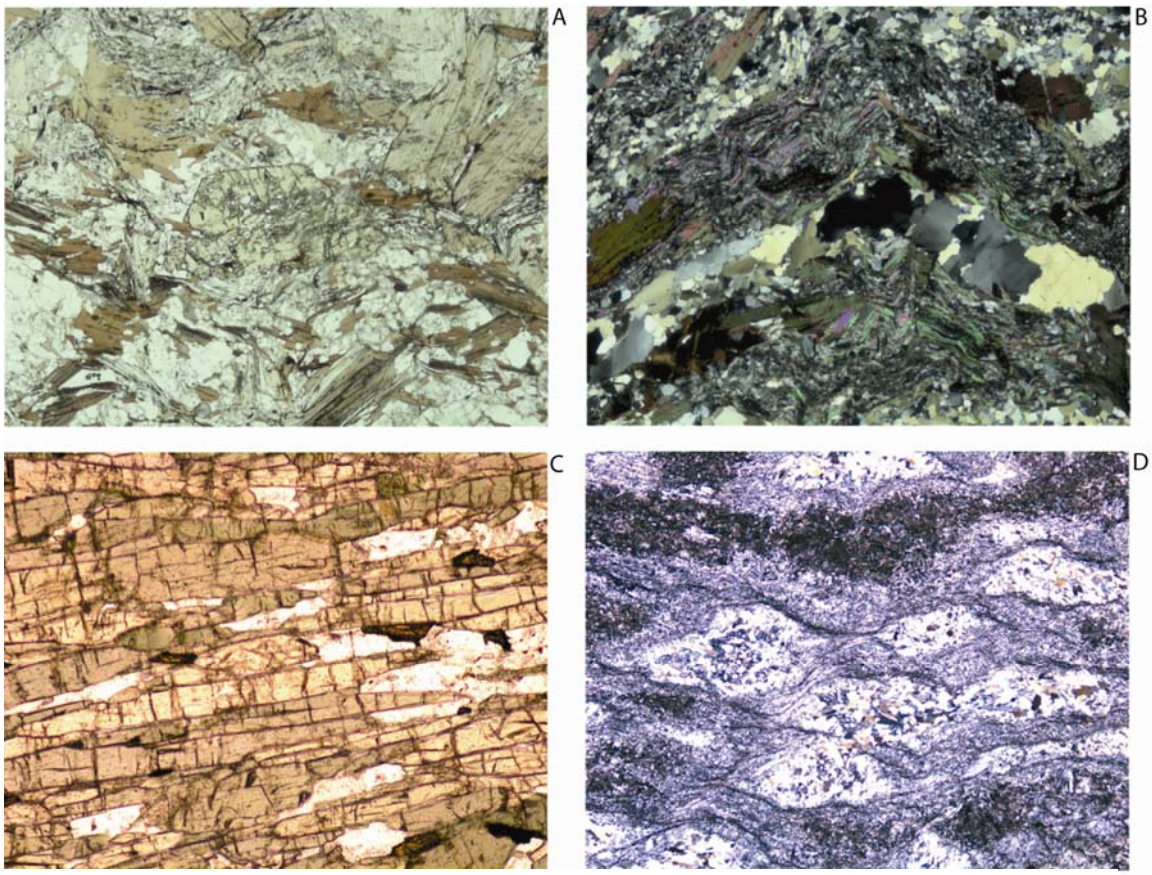

Figure 7. Photomicrographs of representative Lolotoi Complex samples. A. Garnet-mica schist with disrupted foliations and two possible episodes of biotite growth. B. Quartz-mica schist with bands of quartz and fine grained muscovite. Muscovite rich domains exhibit two generations of folding. C. Hornblende amphibolite. Amphiboles are well aligned and well preserved, modally they comprise the majority of the rock. D. Mylonitc quartz-mica schist. Extensive grain size reduction has occurred and a weak S-C fabric is visible.

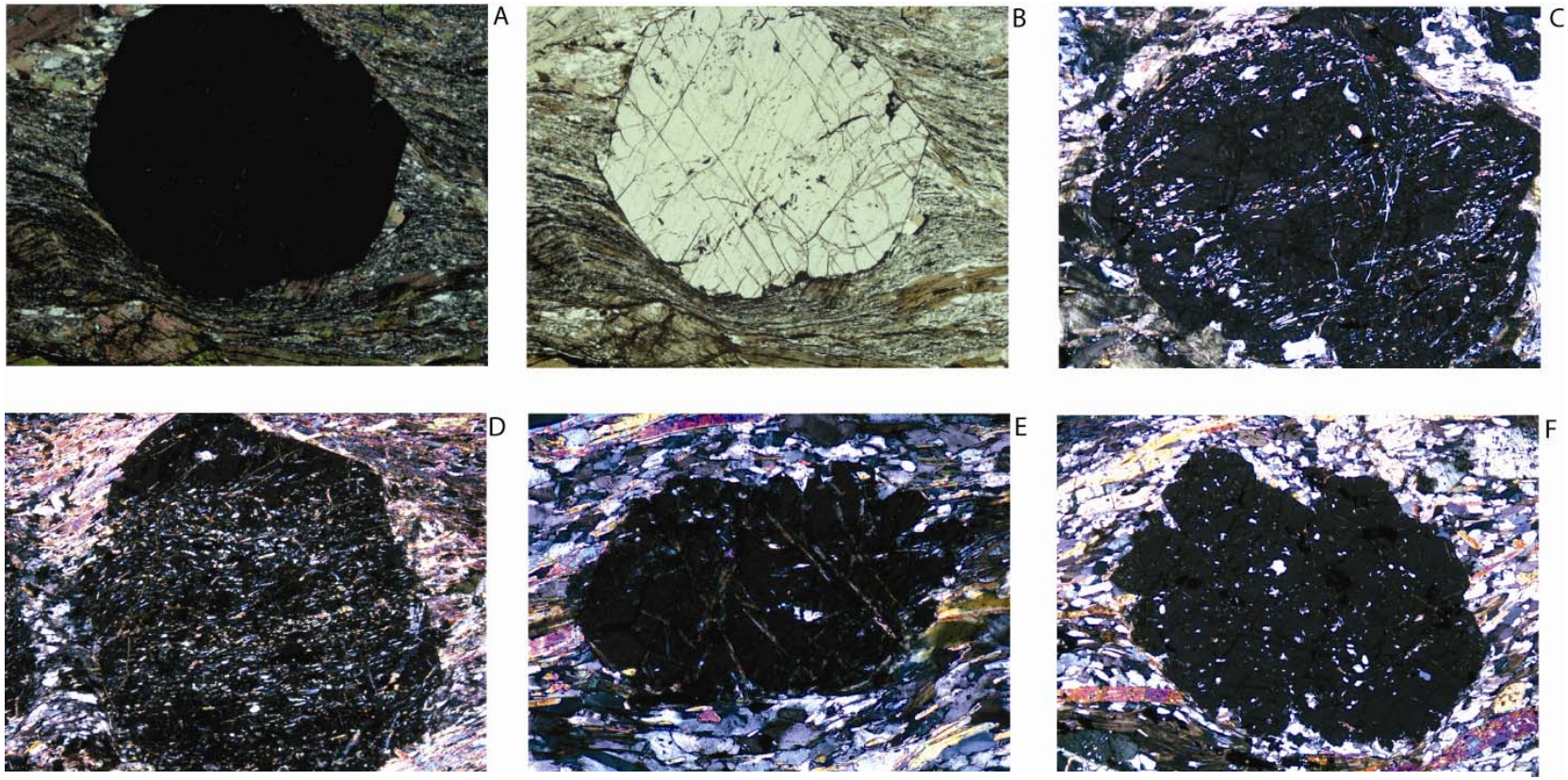

Figure 8. A and B show a nearly idioblastic garnet with strait inclusion trails indicating prekinematic growth. C. shows two episodes of garnet growth, the first comprises the core of the grain and is relatively inclusion free, the second growth episode comprises the outer portion and is inclusion rich. D. shows postkinematic growth as evidenced by the constant undulation pattern through the garnet and matrix. E and F show significantly resorbed garnets with poorly defined inclusion trails.

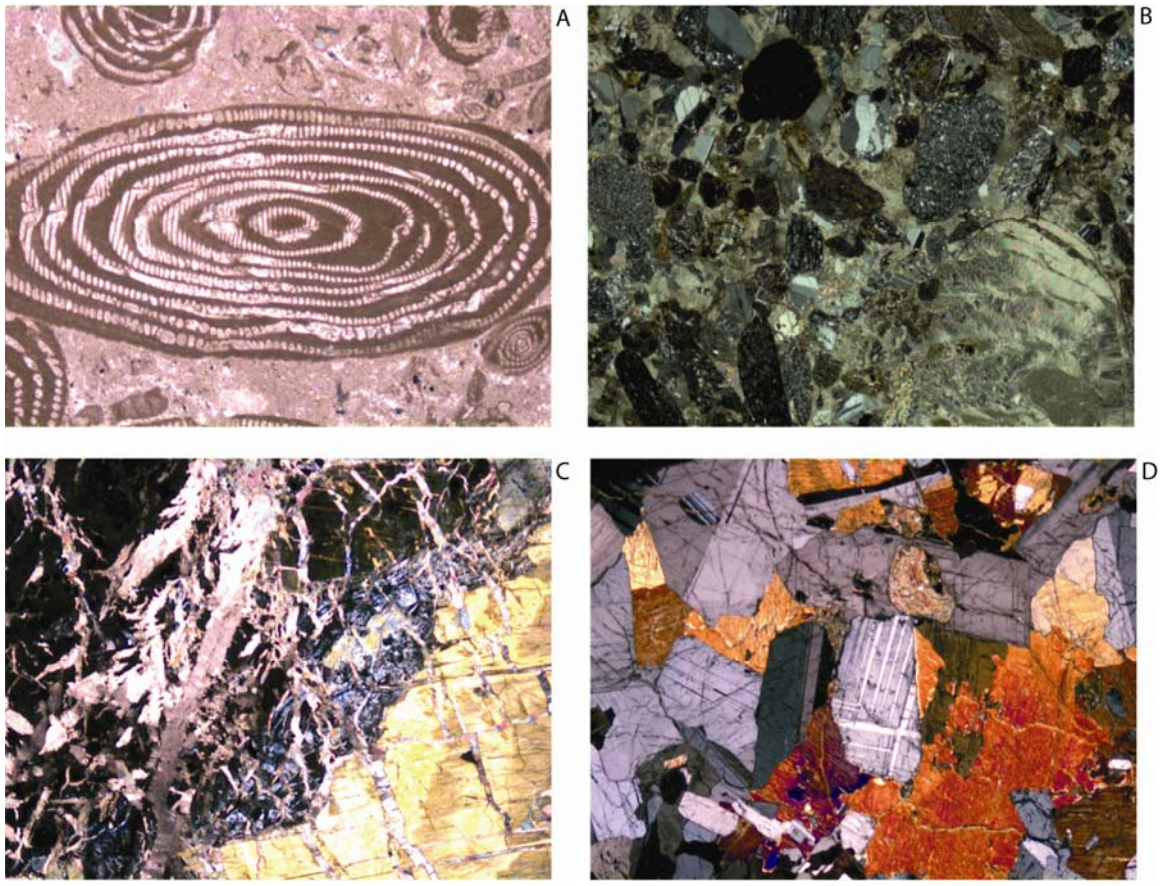

Figure 9. Photomicrographs of additional rock types associated with the Lolotoi Complex. A. Foraminifera packstone of Eocene age found locally to overlie Lolotoi metamorphics. B. Conglomerate found at the base of the Palelo Group, just overlying the metamorphics. Clasts of amphibolite, quartz-mica schist and Palelo Group carbonates are found in the conglomerate. C. Altered peridotite. Pyroxene has been extensively altered to chlorite and serpentine with only portions of large grains remaining unaltered. Extensive carbonate veining is also present. D. Gabbro. Sparse float of unmetamorphosed igneous rocks are found throughout the Lolotoi Complex.

PROVENANCE DETERMINATION FROM WHOLE ROCK GEOCHEMISTRY

Whole rock, major, and trace element analyses were performed using X-ray fluorescence of fused glass disks and pressed powder pellets. A summary of whole rock and trace element data is presented in Appendix II. 59 samples were analyzed, including all metamorphic rock types as well as volcanic, mantle derived and dike rocks.

Primitive mantle normalized multi-element spider diagrams showing abundances of REE and other relevant trace elements for several rock types are shown in Figure 10 (normalization is based on McDonough and Sun, 1995). Elements are ordered with incompatibility increasing from right to left. Metamorphic samples and relatively unaltered igneous samples both show similar patterns, indicating metamorphism has not significantly altered trace element concentrations. Negative niobium anomalies present in all samples suggest igneous provenance from a subduction zone related source, rather than a continental, ocean island or mid ocean ridge setting (e.g. Tatsumi and Tetsu, 2003).

Discriminant diagrams based on whole rock and trace element proportions were employed to determine igneous provenance. All of the discriminant diagrams used require compositions of basalt to basaltic andesite (Rollinson, 1993), thus, other more mafic and felsic samples were not plotted. Figure 11 shows a graph of total alkalis vs. silica indicating that metabasic rocks cluster within the basalt and basaltic andesite fields. Many authors of tectonic discrimination studies indicate that care must be taken when dealing with hydrothermally altered basalts or basalts metamorphosed up through greenschist facies conditions due to the mobility of certain elements. Strontium (Pearce and Cann, 1973), phosphorus (Winchester and Floyd, 1976), potassium (Pearce et al.

1975), magneisum, barium, and sodium (Pearce, 1996) tend to be more mobile during alteration processes, thus diagrams that use these elements were avoided. Pearce and Cann (1971, 1973) determined that the elements Ti, Zr, Y, Nb and Cr are generally immobile during alteration up through greenschist facies metamorphism and are the most effective elements for basalt discrimination. Figures 12, 13, and 14 show several discrimination diagrams used for amphibolite and greenschist samples. Figure 12 shows that sample compositions are not consistent with within plate basalt, but cluster in mid-ocean ridge basalt (MORB) and volcanic arc basalt (VAB) fields. Figure 13 indicates that samples are tholeiitic, and although the oceanic and continental fields overlap, figure 12 confirms that most samples are indeed oceanic. Figure 14 shows samples are from a plate margin rather than an intraoceanic, island arc or continental setting. Figure 14 also indicates dominant MORB and island arc provenance. In total, nineteen discrimination diagrams from various authors were used to determine the tectonomagmatic setting of meta-mafic units in the Lolotoi Complex (Table 2). A small number of discriminant diagrams were inconclusive due to the fact that analyses were so widespread that no trend or cluster of points could be determined.

In summary, discriminant analysis results indicate provenance that is transitional between MORB and VAB, which is found most commonly in marginal and back arc basins. Pearce (1996) states:

" Many marginal basins have compositions similar to those of normal MORB. However, VAB and VAB/MORB transitions have also been identified in most back-arc basins. Volcanic arc basalt compositions characterize parts of the marginal basin ridge system close to the subduction zone, such as the Valu Fa Ridge, Tonga (Jenner et al.,

1987) and the southern part of the East Scotia Sea (Saunders and Tarney, 1979). Volcanic arc basalt/MORB transitions characterized ridges at intermediate distances to the subduction zones (such as the Eastern Lau Spreading Centre, Tonga: Pearce et al., 1994) and the strongly attenuated arc terranes that often border back-arc crust (such as the Lau Basin: Hawkins and Allen, 1994)".

In terms of petrogenetic evolution, these chemical signatures most likely represent "melting at shallow levels of MORB mantle containing a variable subduction component, or by mixing of MORB-mantle and mantle wedge sources" (Pearce, 1996). Also, the occurrence of turbidites found throughout the Palelo Group, shallow water carbonates, and ignimbrite deposits indicate that the arc was likely mounted partially on continental basement (Earle, 1981; Harris, 2006). This could also explain why meager continental arc signatures were obtained from some discriminant diagrams.

Discriminant diagrams for pelitic rocks show mostly mafic to intermediate compositions, which originated from continental to oceanic island arcs (Figures 15 and 16, Table 3).

The above provenance findings further support the interpretation made by Harris (2006) that these metamorphosed fragments represent portions of the Great Indonesian arc, which collapsed and rifted apart during Eocene to Miocene supra-subduction zone seafloor spreading caused by slab rollback of the Australian plate to the south and east. Furthermore, the presence of abundant pelitic deep marine sedimentary units interbedded with volcanic units and abundant igneous intrusions without large plutons, indicates the original position of Banda Terrane metamorphics was near, but off axis of a magmatic belt, likely in a proximal forearc position.

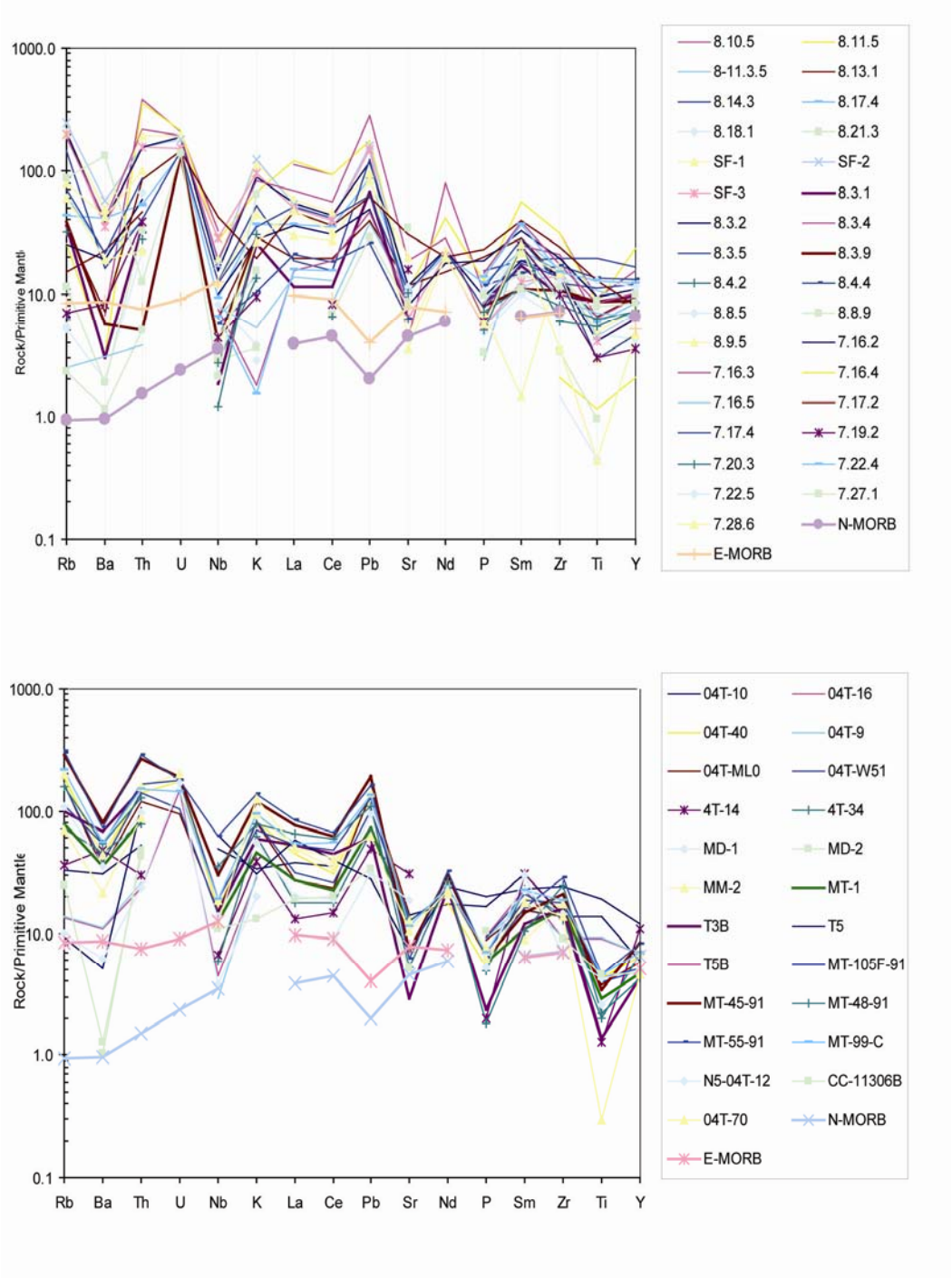

Figure 10. Primitive mantle normalized multi-element spider diagrams for samples from the Bebe Susu (top) and Lacluta and Lolotoi (bottom) massifs. Included in the plots are analyses from greenschists, amphibolites, quartz-mica schists, garnet-mica schists, and relatively unaltered igneous rocks. Notice the negative niobium anomalies present in most samples, indicating a subduction related origin. Analyses follow a trend typical of volcanic arc basalts. N-MORB and E-MORB are also plotted (from Sun and Mcdonough, 1989).

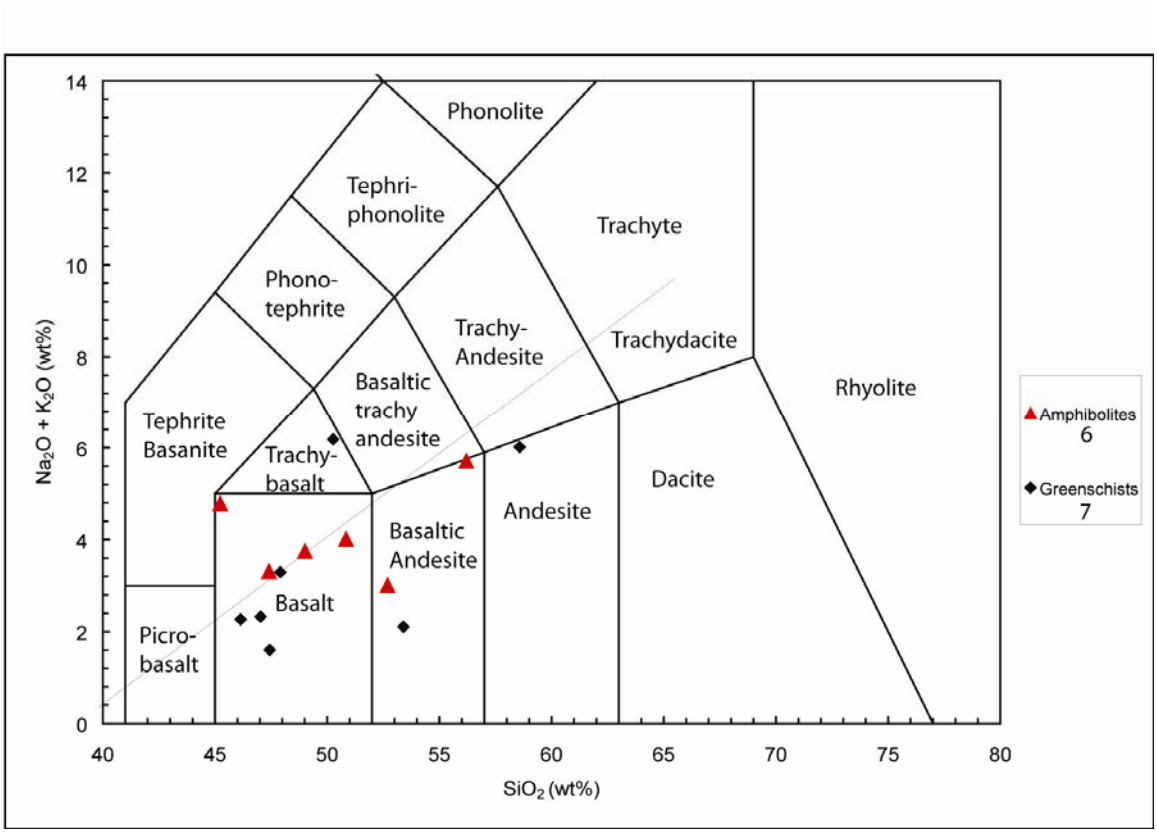

Figure 11. Total alkalis vs. silica diagram showing nearly all analyses of amphibolites and greenschists fall within the basalt and basalic andesite fields. (Whole rock geochemical data has been normalized to 100%). (Classification after LeBas et al.,1986)

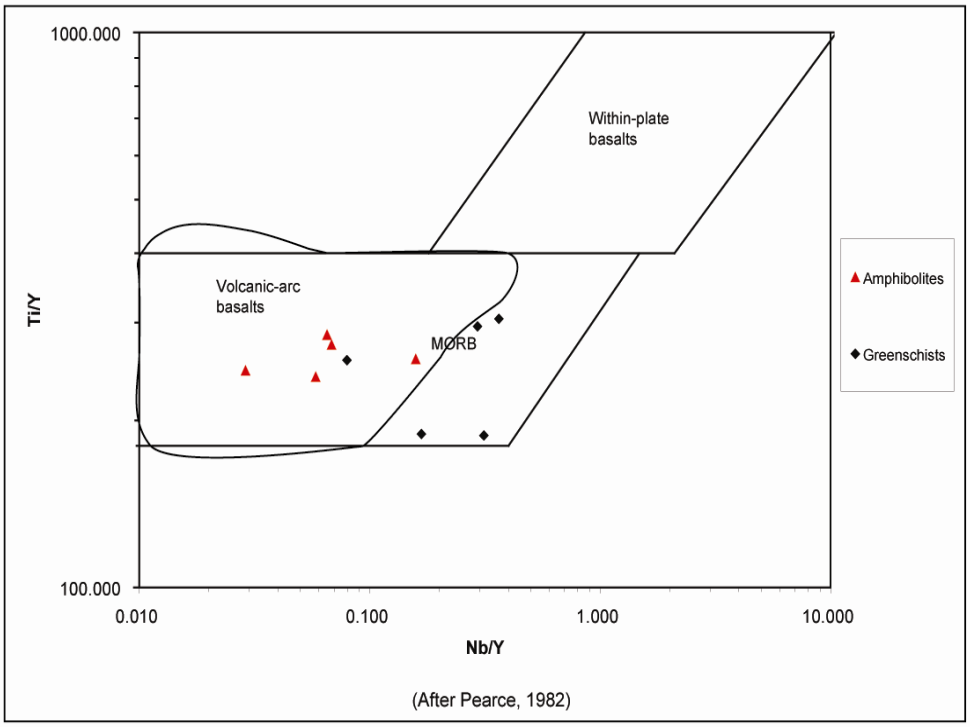

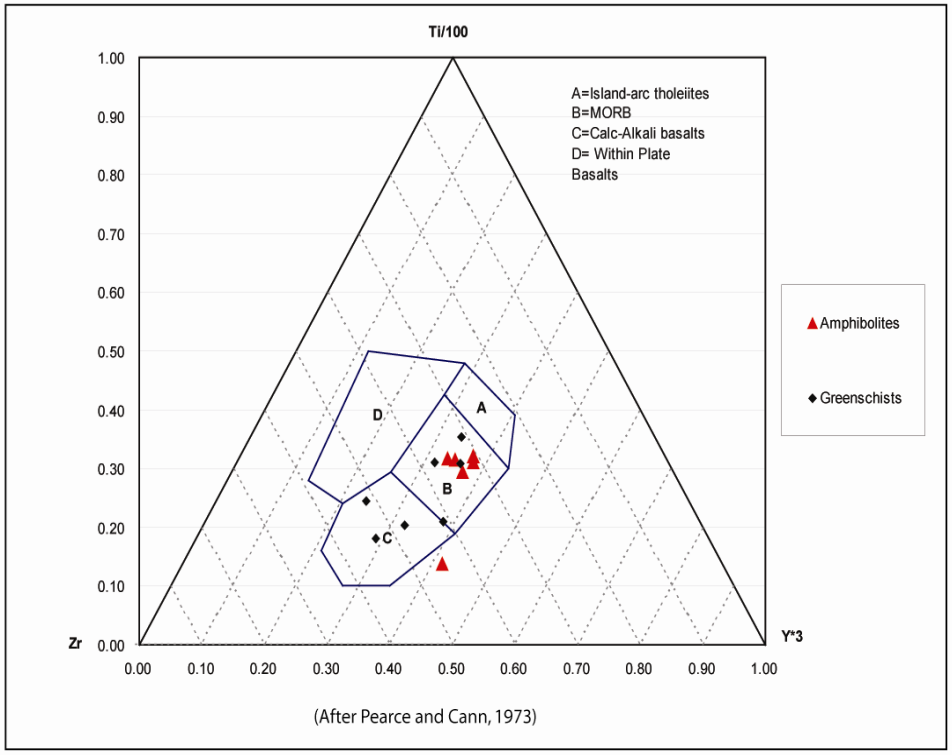

Figure 12. Tectonic discriminant diagrams for metabasites. Both diagrams show MORB and volcanic arc signatures. Notice no analyses fall within the within-plate basalt fields in either diagram.

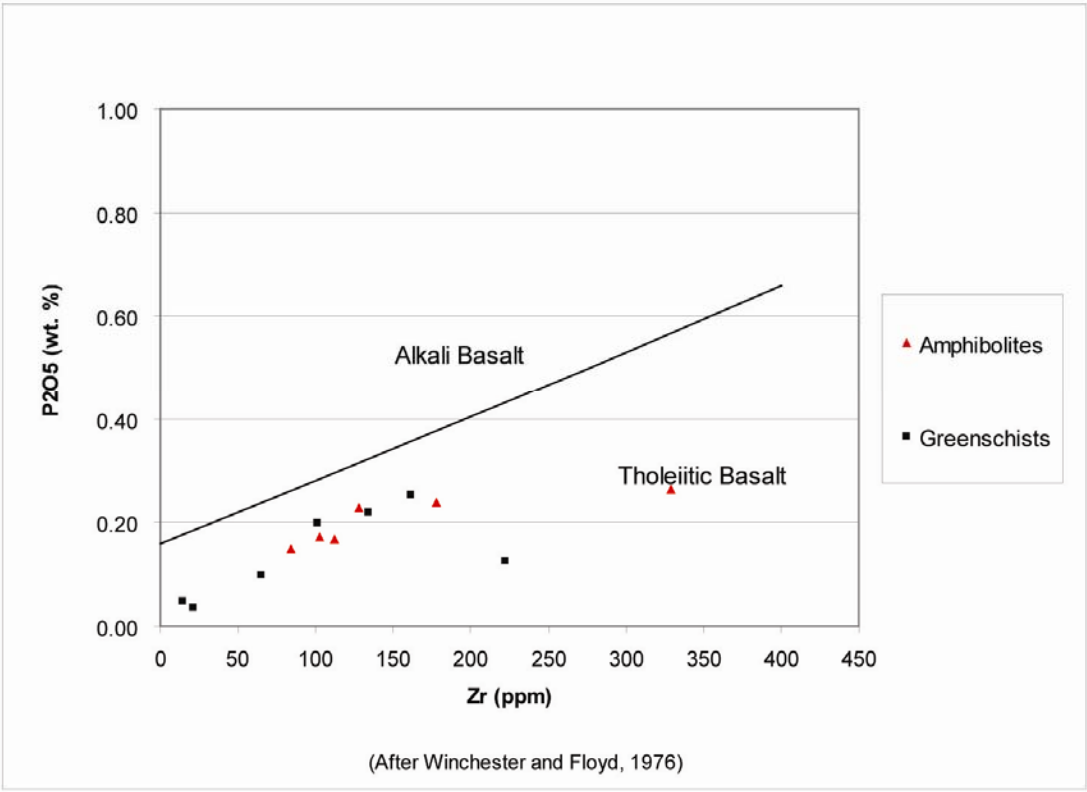

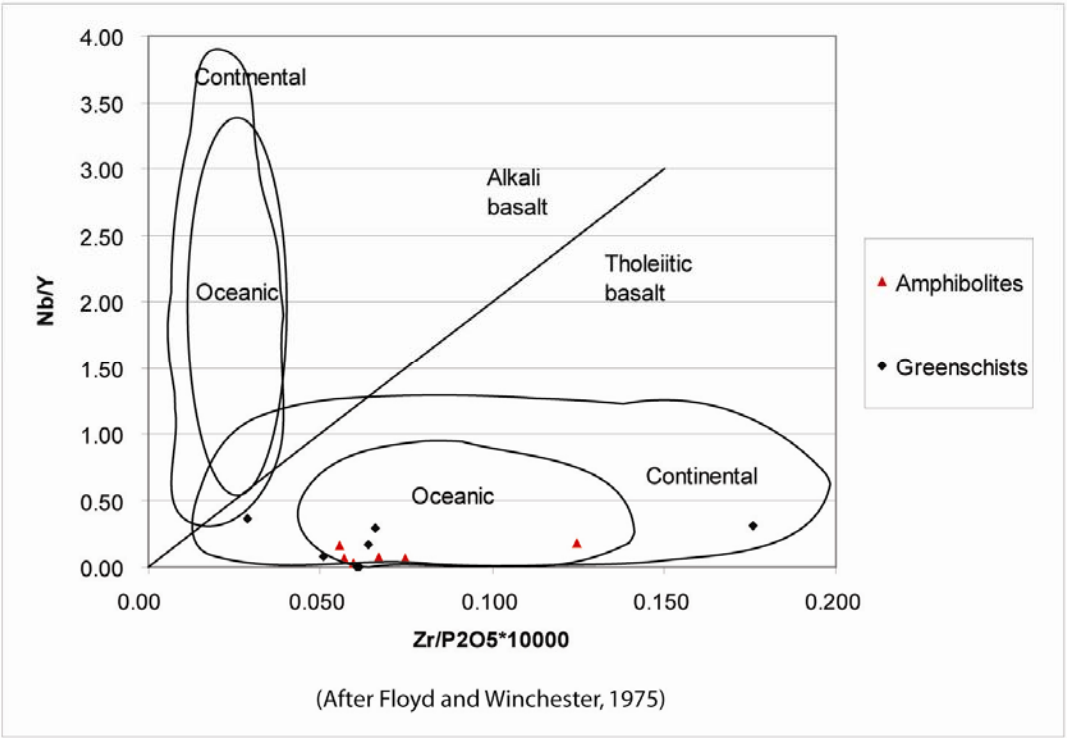

Figure 13. Tectonic discriminant diagrams for metabasites. Above, showing definite tholeiitic compositions. Below, again showing tholeiitic signatures, but also indicating an oceanic rather than continental origin.

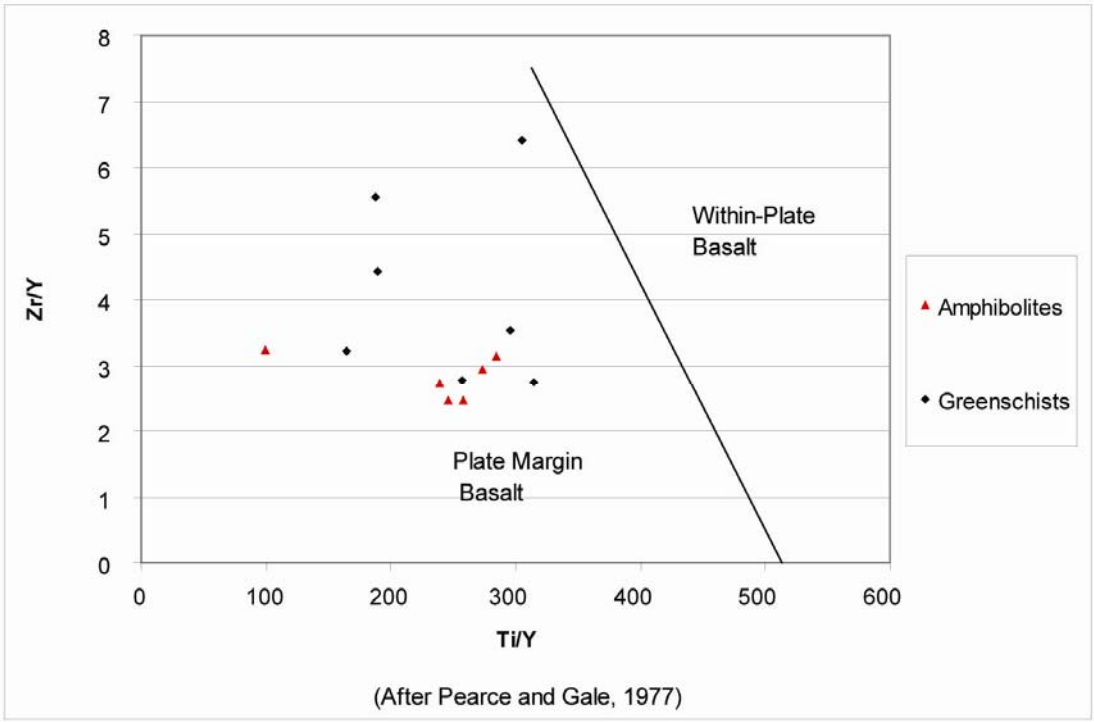

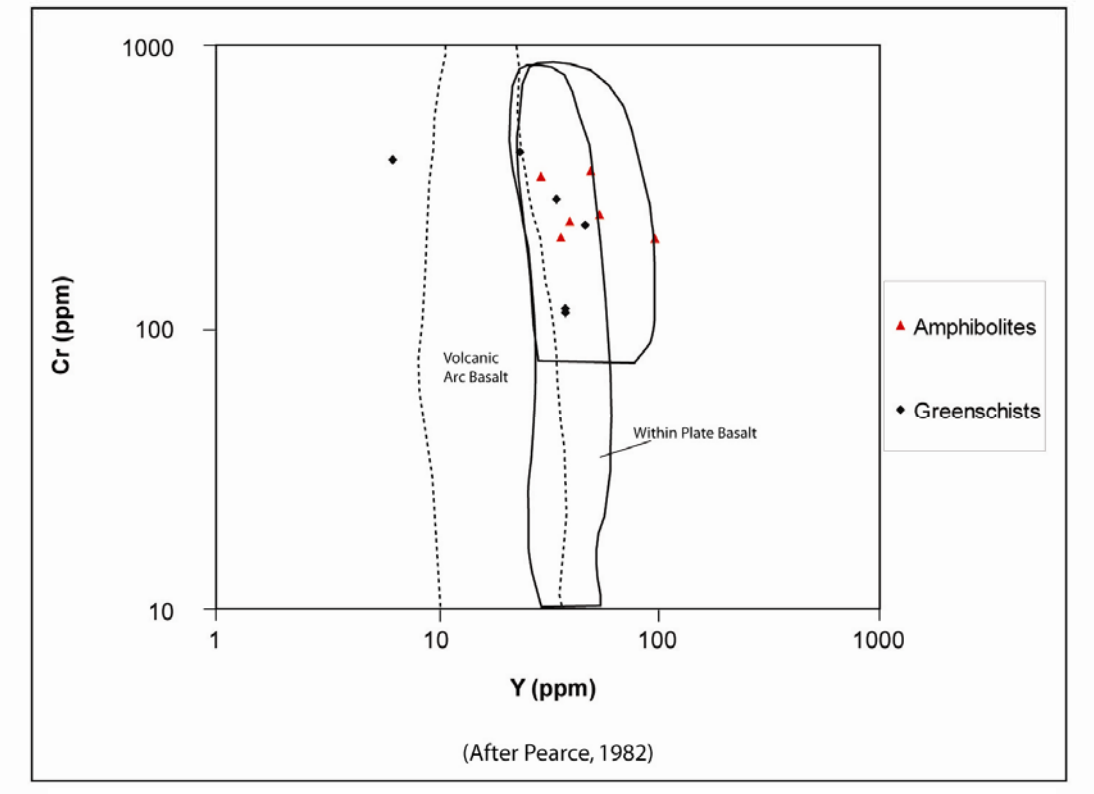

Figure 14. Tectonic discriminant diagrams for metabasites. Above, showing a plate margin origin rather than within plate. Below, compositions fall within both MORB and the overlapping within plate basalt field. However, other diagrams indicate the analyses are more consistent with MORB origin.

Table 2. Summary of 19 discriminant diagrams of tectonic environments for Lolotoi Complex metabasites.

Discriminants	Source	Amphibolites	Greenschists
Zr-Ti/100-Y*3	(Pearce and Cann, 1973)	MORB	Calc-Alkali Basalts, MORB
Ti-Zr	(Pearce and Cann, 1973)	MORB	Island Arc Tholeiites, MORB
Ti-Zr	(Pearce, 1982)	MORB, Volcanic Arc	MORB, Volcanic Arc
Zr/Y-Zr	(Pearce and Norry,1979)	MORB, Volcanic Arc	MORB, Within Plate Basalt
Zr/Y-Zr	(Pearce, 1983)	Inconclusive	Inconclusive
Zr/Y-Ti/Y	(Pearce and Gale, 1977)	Plate Margin Basalt (Not within plate)	Plate Margin Basalt (Not within plate)
Ti/Y-Nb/Y	(Pearce, 1982)	MORB, Volcanic Arc	MORB, Volcanic Arc
Zr/4-2Nb-Y	(Meschede, 1986)	N type MORB, Volcanic Arc	Within Plate Tholeiites, N type MORB, Volcanic Arc
V-Ti/1000	(Shervais, 1982)	MORB, Back Arc Basin	MORB, Back Arc Basin, Arc Tholeiite
La/10-Y/15-Nb/8)	(Cabanis and Lecolle, 1989	N type MORB, Volcanic Arc, Back Arc Basin	MORB, Volcanic Arc
Cr-Y	(Pearce, 1982)	MORB	MORB, Volcanic Arc
Cr-Ce/Sr	(Pearce, 1982)	Volcanic Arc Basalt, MORB	Volcanic Arc Basalt, MORB
Y/Nb-TiO2	(Floyd and Winchester, 1975)	MORB	MORB, Continental Tholeiite
P2O5-Zr	(Winchester and Floyd, 1976)	Tholeiitic Basalt	Tholeiitic Basalt
TiO2-Zr/P2O5*10000	(Winchester and Floyd, 1976)	Oceanic Tholeiitic Basalt	Oceanic Tholeiitic Basalt
Na2O+K20-SiO2	(Macdonald, 1968)	Subalkaliine	Subalkaline
MgO-FeO-Al2O3	(Pearce et al., 1977)	Inconclusive	Inconclusive
K2O-TiO2-P2O5	(Pearce et al., 1975)	Inconclusive	Inconclusive
MnO*10-TiO2-P2O5*10	(Mullen, 1983)	MORB, Island Arc Tholeiites	MORB, Island Arc Tholeiites, Calc Alkali Basalts

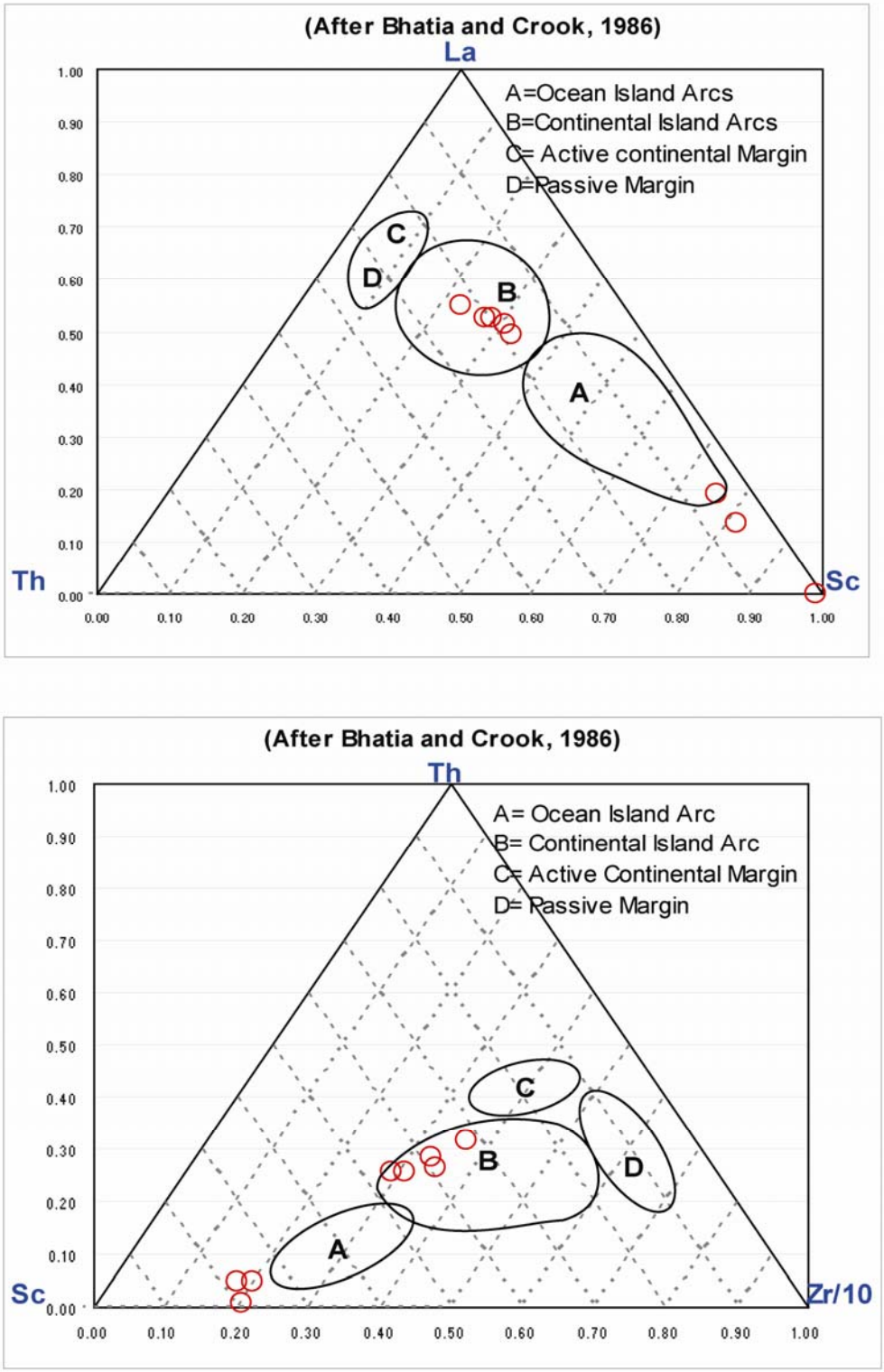

Figure 15. Tectonic discriminant diagrams for pelitic rocks. Above, shows a mainly continental island arc provenance with scattered oceanic arc related compositions. Below, shows a very similar result.

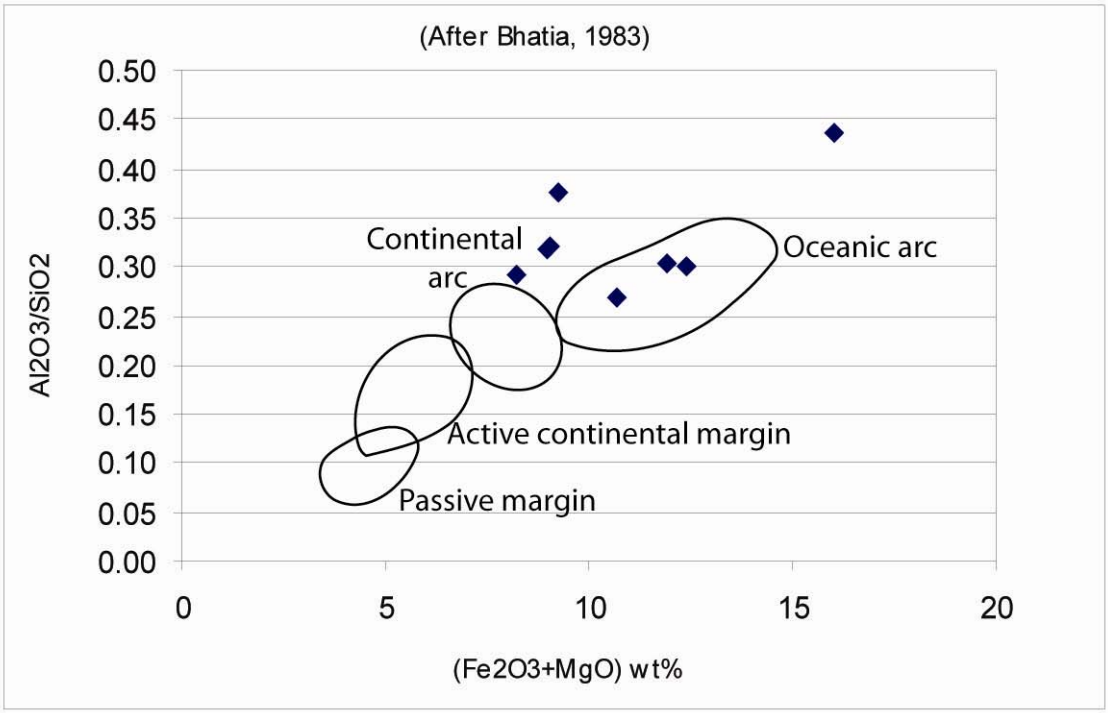

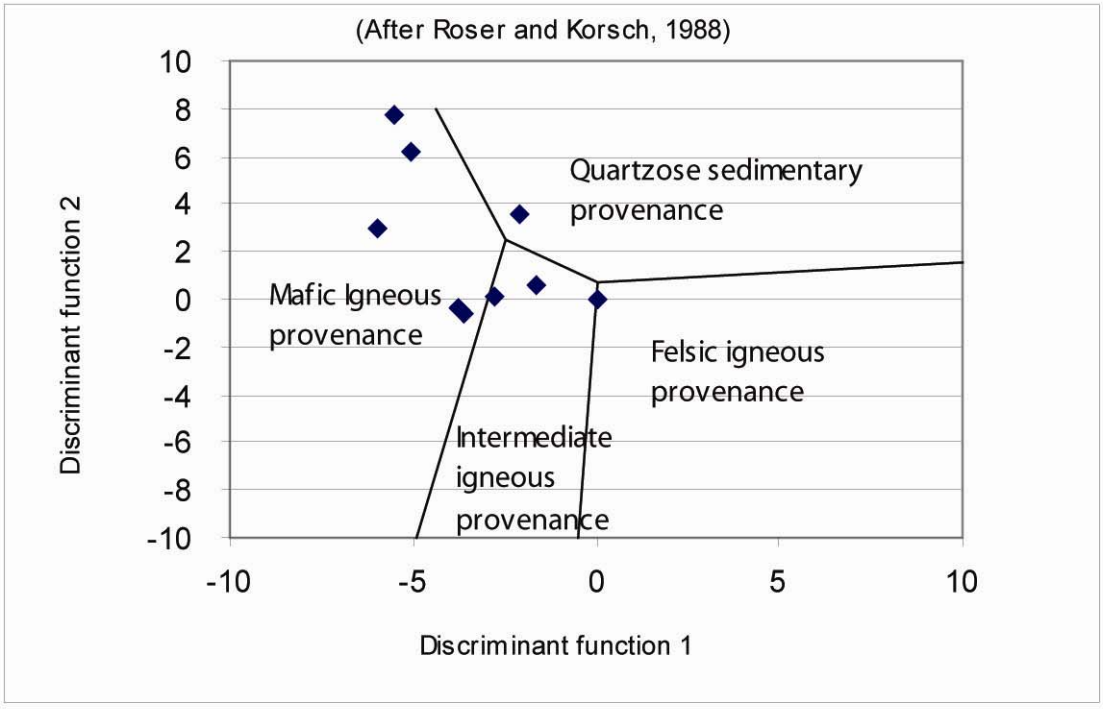

Figure 16. Tectonic discriminant diagrams for pelitic rocks. Above, shows mainly .oceanic arc signatures with some analyses scattered near the continental arc field. Notice that no analyses fall near the passive margin or active continental margin fields. Below, shows composition are consistent with mainly mafic to intermediate igneous provenance.

Table 3. Summary of seven tectonic discriminant diagrams for pelitic rocks.

Discriminants	Source	Garnet bearing schists	Quartz-mica schists
Fe2O3+MgO-TiO2	Bhatia, 1983		Active Continental Margin, Contienental Arc
Al2O3/SiO2-Fe2O3+MgO	Bhatia, 1983	Active Continental Margin	Active Continental Margin
Log(K2O/Na2O)-SiO2	Roser and Korsch 1986	Island Arc	Island Arc
Discriminants 1 vs 2	Roser and Korsch 1988	Intermediate to Mafic Ignous provenance	Felsic Ignous provenance
Discriminants 1 vs 2	Roser and Korsch 1988	Intermediate to Mafic Ignous provenance	Intermediate Igneous provenance
Th-La-Sc	Bhatia and Crook, 1986	Continental Island Arc	Continental Island Arc
Sc-Th-Zr/10	Bhatia and Crook, 1986	Continental Island Arc	Continental Island Arc

MINERAL GEOCHEMISTRY

Mineral chemistry data was collected using a Cameca SX-50 Electron Microprobe in order to determine the pressure-temperature conditions of metamorphism. Minerals analyzed include garnet, amphibole, plagioclase, biotite, and muscovite. Garnet analyses were performed using an acceleration voltage of 15 Kv, a minimum beam size of 1-2 microns and a beam current of 30 to 40 nA. Beam size was increased to 10 microns during garnet X-ray dot map scans. Amphiboles, Biotite, muscovite, and feldspars were all analyzed using an acceleration voltage of 15 Kv, a beam size of 10 microns, and a beam current of 10 nA. In addition, the electron microprobe was used qualitatively to confirm petrographic microscope observations and mineral identification.

Microprobe analyses were performed on garnet grains in garnet mica schists, garnet amphibolites and garnet bearing greenschists from both outcrop and float samples collected in the Lucluta and central to southern portions of the Bebe Susu massifs. Eight different samples were studied to determine growth episodes, zoning profiles, retrograde effects, and geothermobarometric conditions.

Microprobe X-ray dot maps show zoning profiles in seven samples that are indicative of one single episode of garnet growth (Figure 17, samples O4T-MLO, 8-3-5, SF-2). Zoning profiles of Mg, Mn, Fe, and Ca in the seven samples are typical of normal growth zoning during prograde metamorphism (Banno et al., 1986). Mn and Ca decrease in abundance from core to rim and Mg and Fe increase in abundance from core to rim. Only one sample (8-11-5), found in stream float, appears to have two generations of garnet growth. This is most easily observed in the Mn map in Figure 17, which shows the second generation of growth as a distinct concentric increase occurring around the

original garnet core. Zoning anomalies due to retrograde reactions do occur in many samples, mostly at grain boundaries and around large inclusions. Spessartine (Mn) spikes near grains edges in conjunction with irregular grain boundaries indicate some retrograde net transfer reactions have taken place (Figure 17, samples 8-3-2 and F1-1) (Kohn and Spear, 2000). Inclusions in garnet grains are common, with ilmenite, epidote, and biotite quartz and plagioclase being the most abundant.

Biotite analyses showed some grains have undergone retrograde chloritization reactions as indicated by their low potassium levels. Analyses with potassium values below 9 wt.% were not used in geothermometry calculations, due to likely chloritization. Biotite compostions are fairly consistent across grains, except where alteration to chlorite has occurred. Biotite grains in contact with garnets and matrix grains were both analyzed. Compositions are generally consistent with standard values, indicating reliable results were obtained. Analytical results are shown in Appendix III.

Plagioclase was also analyzed for use in calculations of peak pressures. Plagioclase compositions varied significantly from sample to sample as shown in Figure 18. All analyses lie along the Ca-Na solid solution, with compositions consistent with andesine and labradorite. No potassium-rich plagioclases were found during microprobe analysis.

METAMORPHIC CONDITIONS

Garnets were paired with neighboring biotites to obtain estimates of peak metamorphic temperatures. Care was taken during pairing of mineral analyses to use unaltered compositions characteristic of peak conditions. In samples having undergone

retrograde net transfer reactions, garnets with the highest Mg/Fe ratios and the biotites with the lowest Fe/Mg ratios were used (Kohn and Spear, 2000). In samples with evidence of retrograde exchange reactions, peak conditions are represented by garnets with the highest Mg/Fe ratios and biotites with the highest Fe/Mg ratios (Kohn and Spear. 2000). These compositions correspond spatially in garnets to rim areas, just inside of any alteration halos. It is important to note however that where retrograde reactions have occurred, these analyses represent minimum estimates of peak conditions, as possible higher conditions may have been represented by now resorbed rim areas.

Wu and Cheng (2005) evaluated multiple garnet-biotite thermometers and garnet-alumino silicate-quartz-plagioclase barometers, concluding that the Kleeman and Reinhardt (1994) thermometer and the Newton and Haselton (1981) barometers are the most valid and reliable. The Kleiman and Reinhardt garnet-biotite thermometer yielded temperatures ranging from 530°C to 600 °C. Garnet-aluminosilicate-quartz-plagioclase pairings yielded pressures ranging from 6 to 8 kbars, using the Newton and Haselton barometer. Temperature-pressure plots of six individual samples are shown in Figure 19. Notice that intra sample values are very consistent but greater variation exists from sample to sample. This is evident in Figure 20 which shows the range of all calculated temperatures and pressures.

Amphibole samples analyzed include 10 samples from the Bebe Susu and Lacluta massifs. Select amphibole microprobe data is summarized in Appendix III. Figure 21 shows that most of the amphibole compositions fall into the hornblende and magnesio-hornblende compositional fields, with the exception of one blue amphibole which straddles the tschermakite and ferro-tschermakite fields (amphibole classification based

Leake et al., 1997). Amphiboles were probed at rims, cores, and intermediate positions to determine the range of temperatures through which the grains grew. Temperatures and pressures were calculated using single mineral amphibole geothermobarometry based on calculations by Gerya et al. (1997). Results for 9 samples range from 6 to 7.5 kbar and 580 °C to °650 C with an error of absolute error of ±1.2 kbar and ± 37 °C. Only one sample of ferro-tchermakite from float was analyzed, it was found to have a pressure of 9 to 10 Kbar and 650 °C to 680 °C. Pressure-temperature plots for several individual samples are shown in Figure 22.

Traverses across grains show some variation in compositions, which provide differences in P and T through time. However the variation is within the error range and thus apparent P-T variations with time may be artificial. In general, amphibole grain cores tend to exhibit higher pressures and temperatures indicating nucleation initiated near peak conditions and amphibole growth proceeded through a range of conditions as pressure and temperature both decreased. This suggests a clockwise P-T-t path with both pressure and temperature decreasing after attainment of peak conditions.

DISCUSSION

P-T estimates obtained from mineral chemistry analyses of Mutis massif rocks in West Timor have been interpreted to show a steep inverse metamorphic gradient (Sopaheluwaken, 1990). No data was found in this study of the Lolotoi Complex to support this interpretation. Pressure-temperature data from garnet bearing pelitic rocks is very consistent with that from amphibolite samples. P-T ranges for both rock types

overlap, however amphibolites indicate slightly higher peak temperatures, while garnet bearing pelites exhibit slightly higher peak pressures.

Similar geothermobarametric results have been obtained in West Timor, where Sopaheluwaken (1990) reports garnet-biotite temperatures of 550 °C to 750 °C based on six different geothermometers. Also reported are GASP pressures of 6.0 to 8.6 kbar based on five different barometers. Various other mineral pairings of metapelitic rocks performed by Sopaheluwaken resulted in very similar P-T estimates. Metabasic rocks were also evaluated by amphibole-plagioclase, garnet-amphibole and amphibole mineral pairings. Temperatures and pressures reported for these samples range from 510 °C to 580 °C and 6.2 to 8.2 kbar. This temperature range is significantly lower than that of the metapelites, even though pressures estimated for both rock types are nearly identical. Sopaheluwaken (1990) noted the presence of granulite float at the highest structural levels of the Mutis massif. These yielded temperatures up to 950 degrees and pressures up to 10.7 kbar. No similar granulite facies rocks were found in the Lolotoi Complex.

No large differences in metamorphic conditions exist between metapelitic and metabasic rocks of the Mutis and Lolotoi Complexes. Small differences between the two massifs are all within the error limits of the analyses.

These intermediate temperatures and pressures, in conjunction with previously discussed igneous provenance, indicates that these Lolotoi Complex rocks were altered during tectonic and depositional burial. This most likely occurred along the southeastern margin of Asia prior to the late Eocene to early Oligocene extensional collapse of the Great Indonesian arc (Harris, 2006).

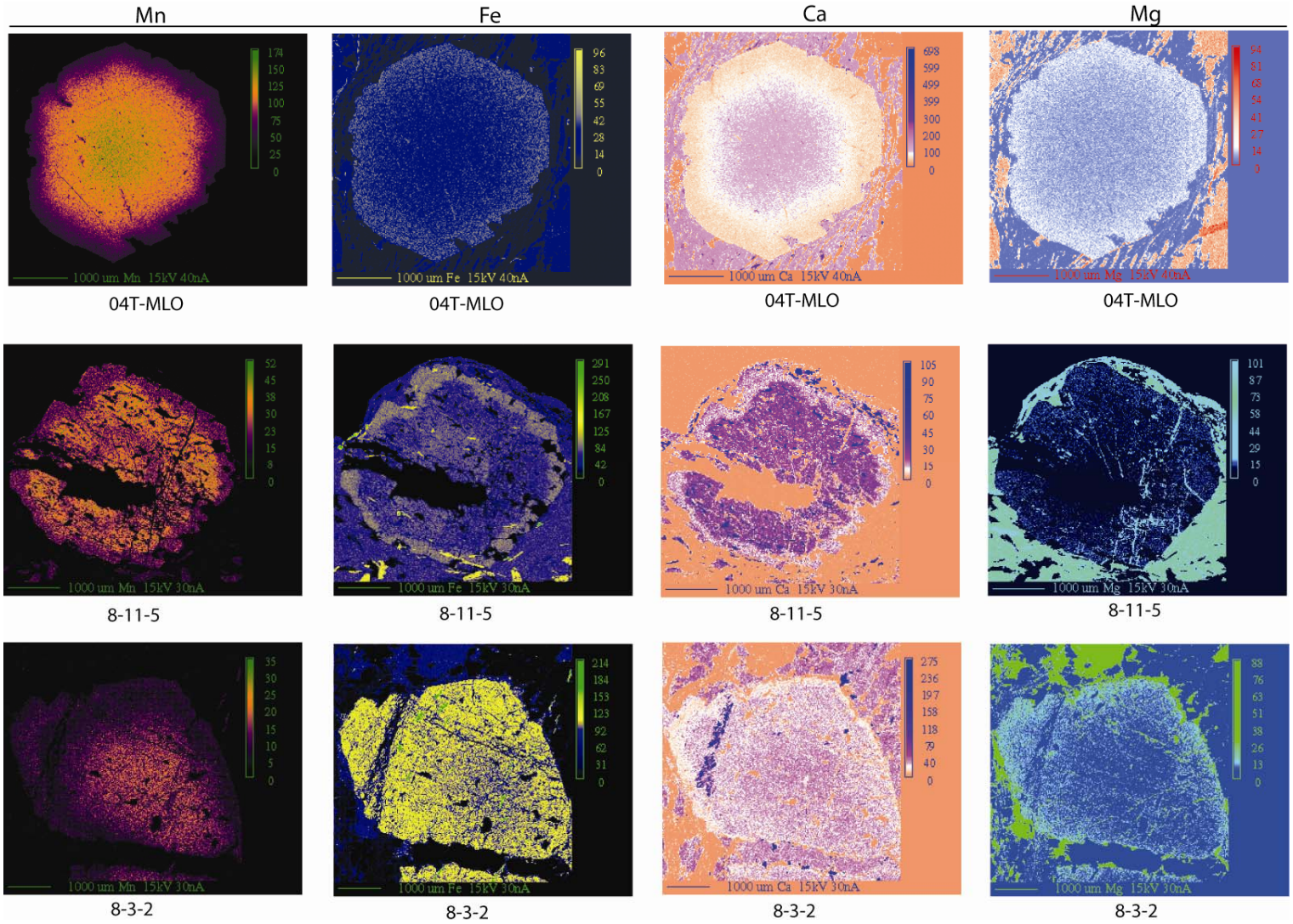

Figure 17. Microprobe X-ray dot maps showing Mn, Fe, Ca, and Mg zoning in garnets from garnet-mica schists and garnet amphibolites. Most garnets show a single generation of growth with normal patters of Mn and Ca decreasing in abundance from core to rim, and Fe and Mg increasing from core to rim. Sample 8-11-5 exhibits two episodes of garnet growth as is most apparent in the Mn zoing profile. Several samples (8-3-2, F1-1) show Mn rich rims which are indicative of retrograde net transfer reactions.

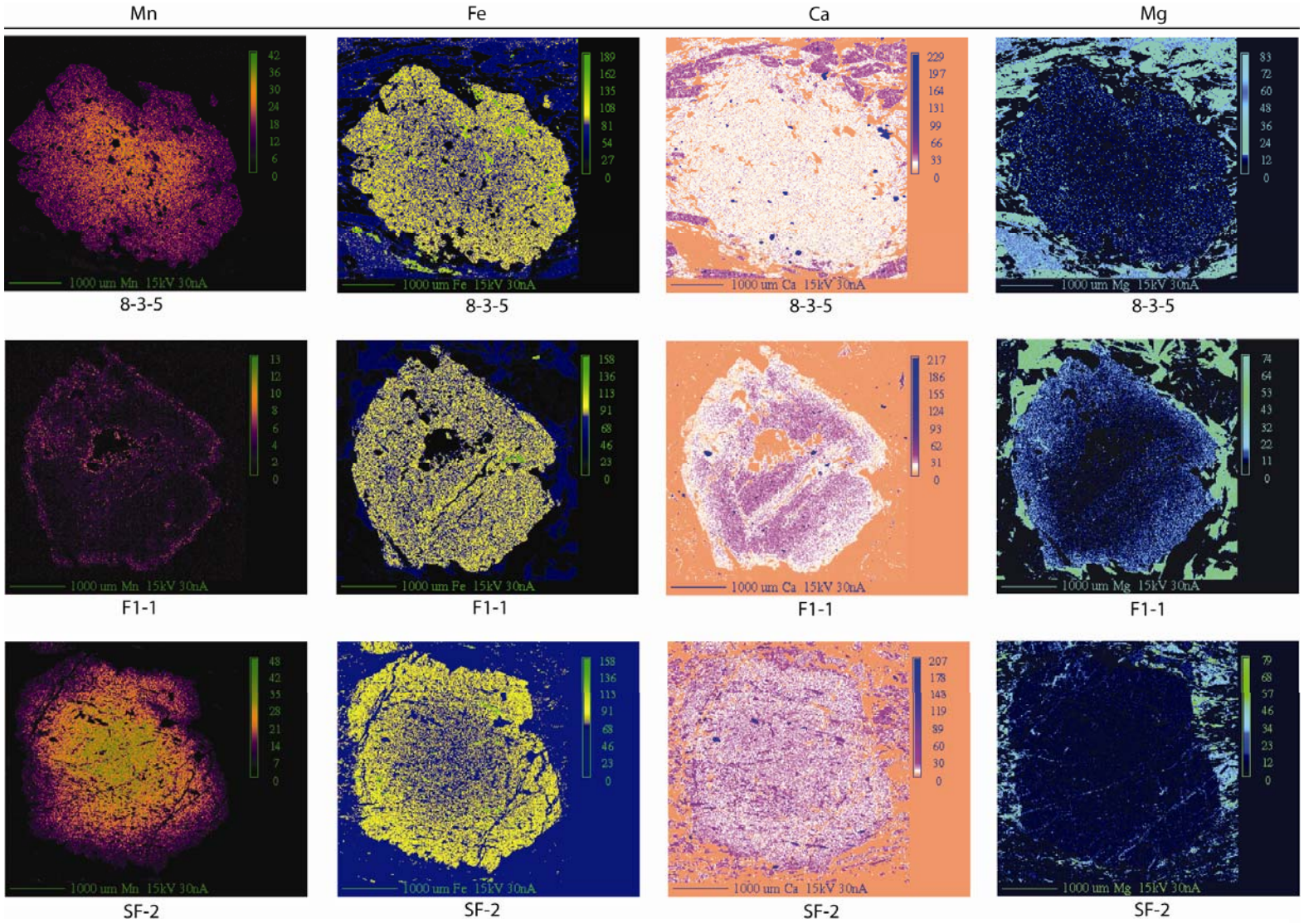

Figure 17. (continued) Additional microprobe X-ray dot maps. 8-3-5, and SF-2 show a normally zoned partially resorbed grain profiles. F1-1 exhibits a Mn spike on the outer rim and Ca zoning hints of multiple episodes of growth, but this is not confirmed in the Mn profile.

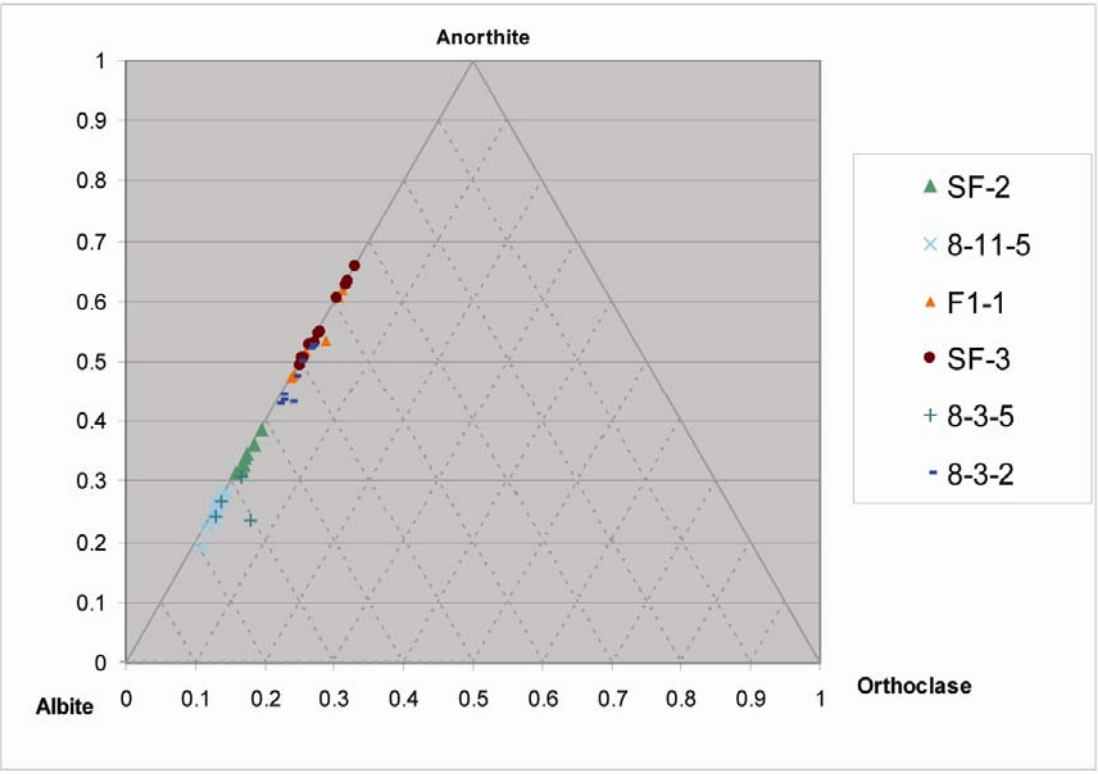

Figure 18. Feldspar compositions range from An_{20} to An_{67} along the solid solution between anorthite and albite. Most compositions have very little potassium, with no sample containing more than 7% K.

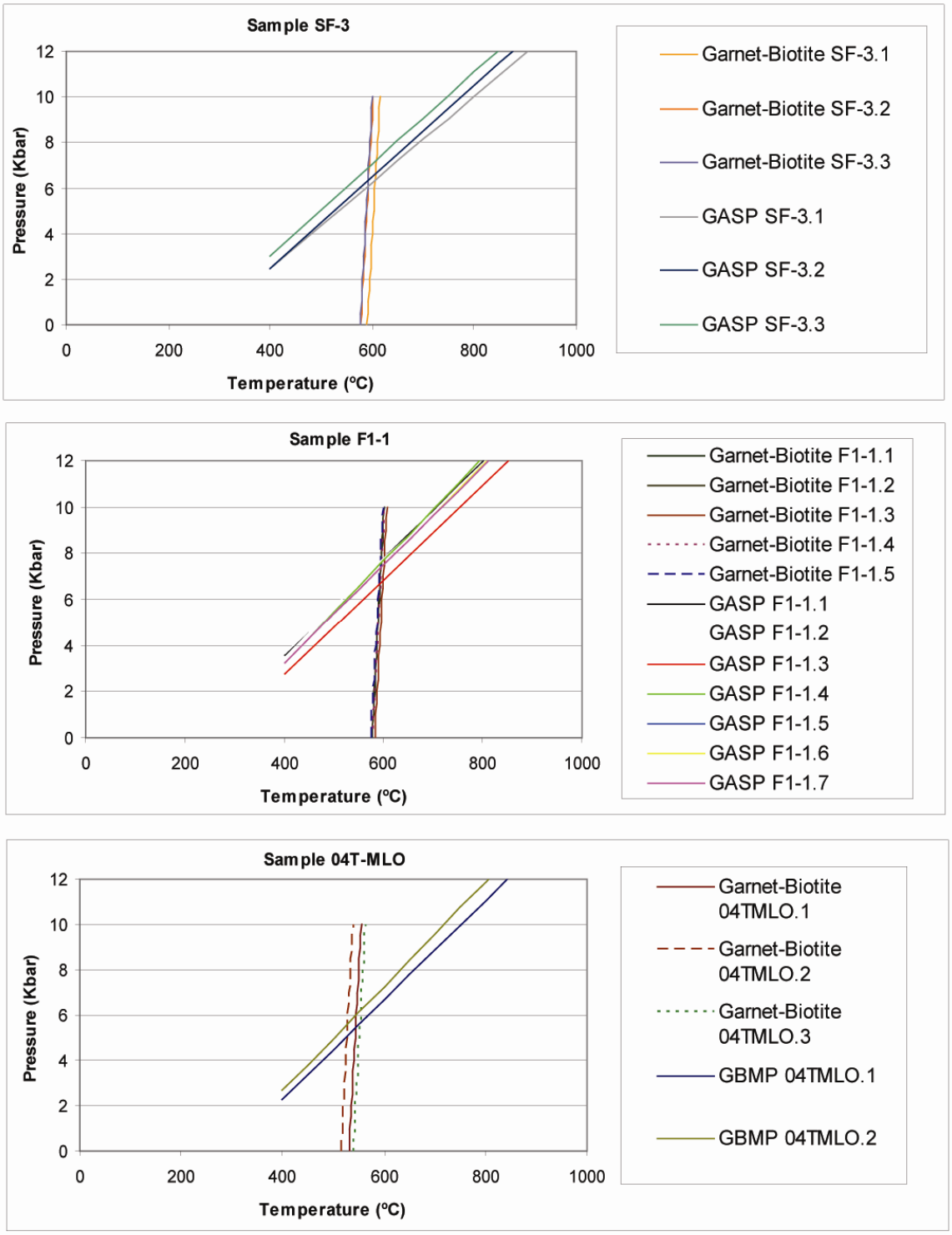

Figure 19. Geothermobarometric plots of garnet-biotite thermometers (Kleiman and Reinhardt, 1994) and garnet-aluminosilicate-quartz-plagioclase (GASP) barometers (Newton and Haselton, 1981). Most individual samples show closely spaced results for individual grain analyses, which are well within the range of error of barometers and thermometers used.

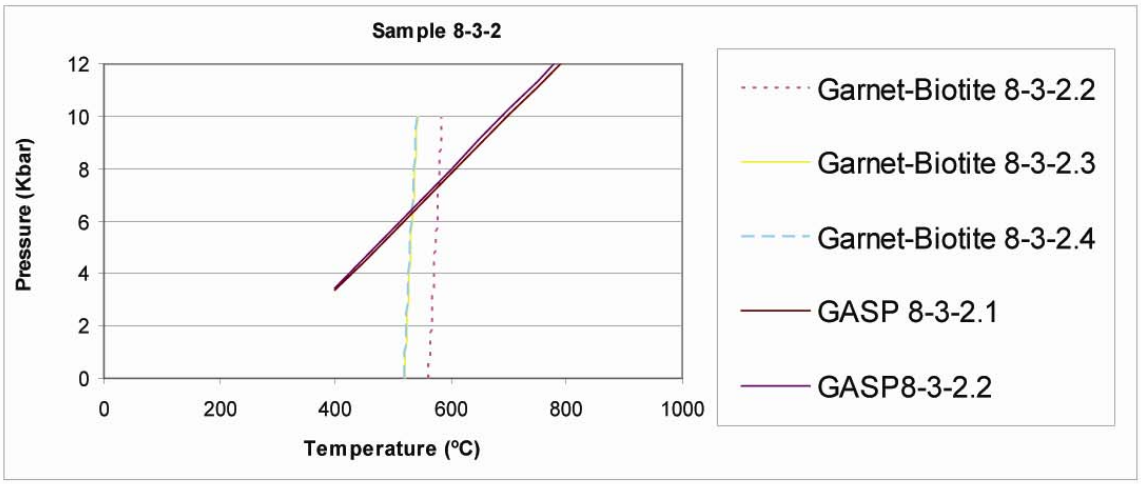

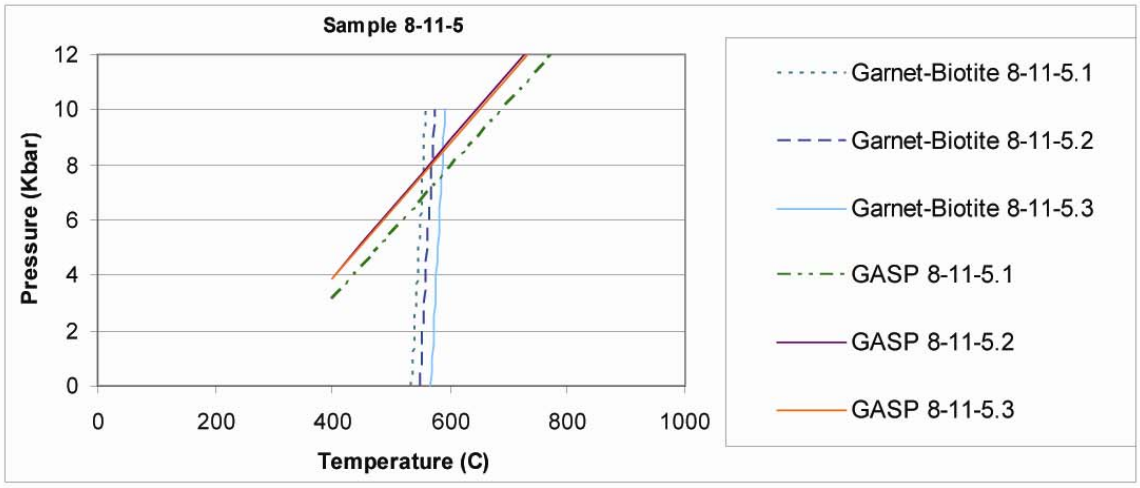

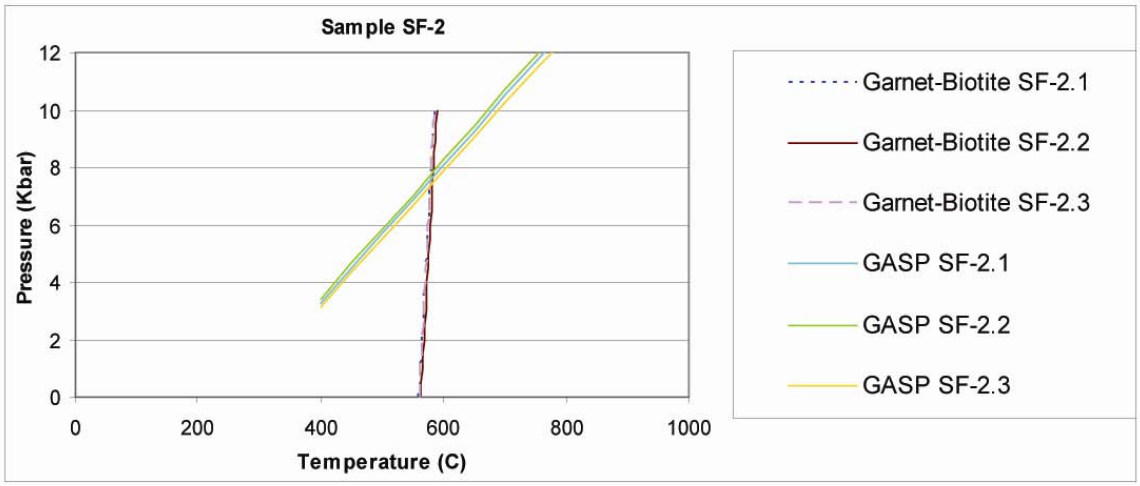

Figure 19. (continued)

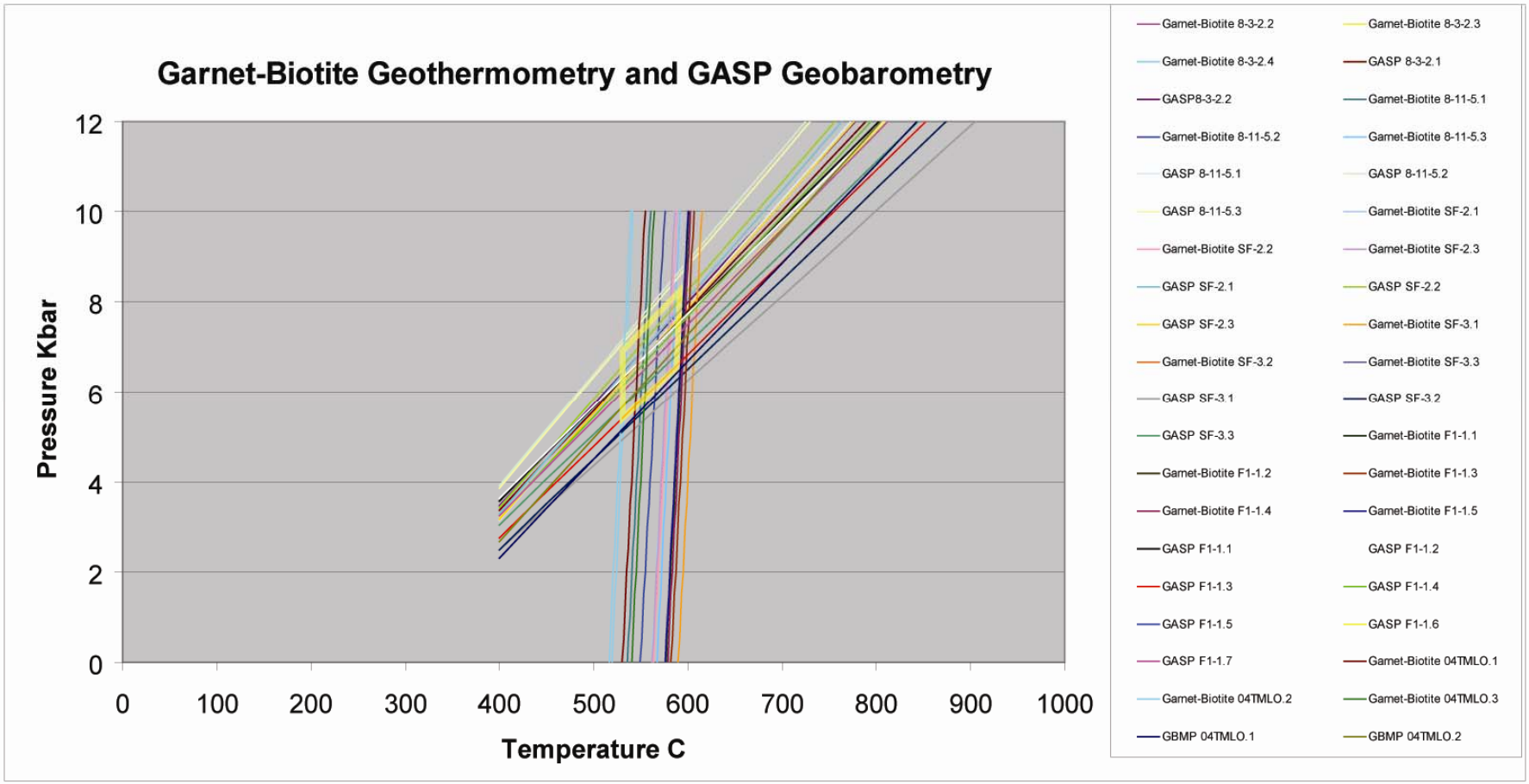

Figure 20. Geothermobarometric results for all pelitic samples analyzed. The range of calculated P-T conditions is highlighted above. Temperatures range from around 530 °C to 600 °C and pressures range mostly from 6 to 8 kbar.

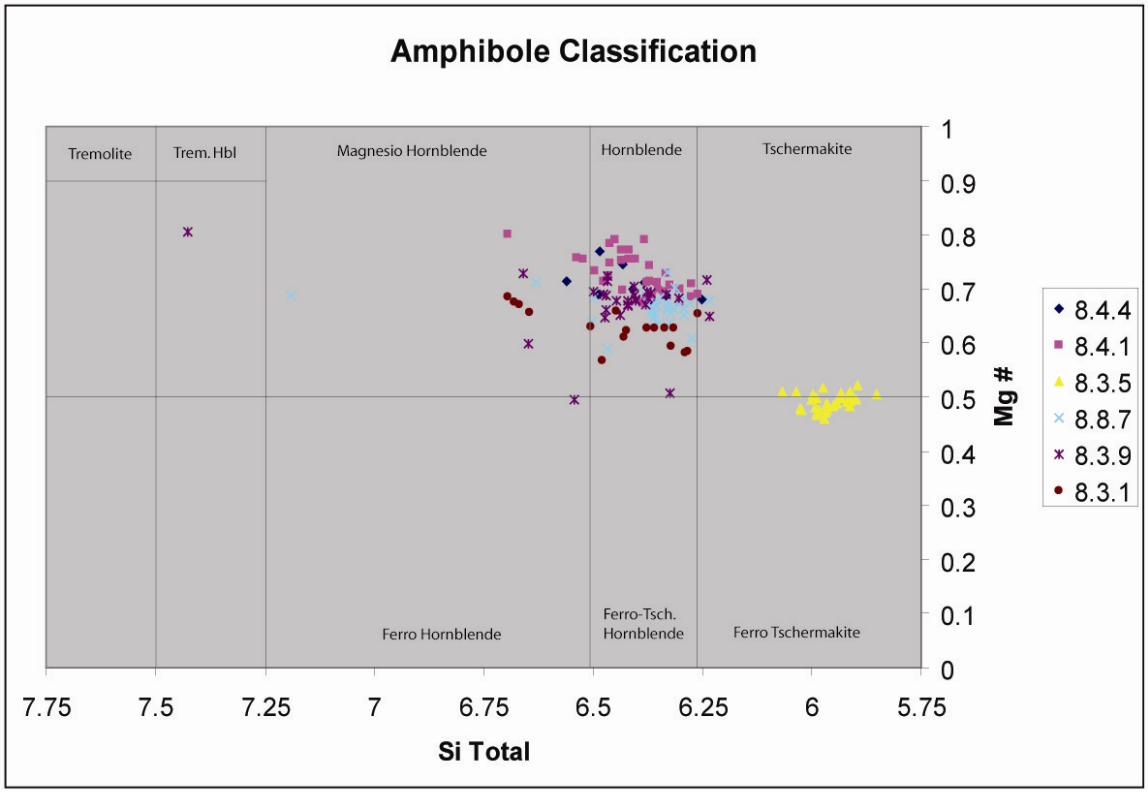

Figure 21. Amphibole classification (based on Leake et al., 1997) showing most compositions cluster within the hornblende and magnesio hornblende compositional fields. Only one sample has a tschermakite to ferro tschermakite composition.

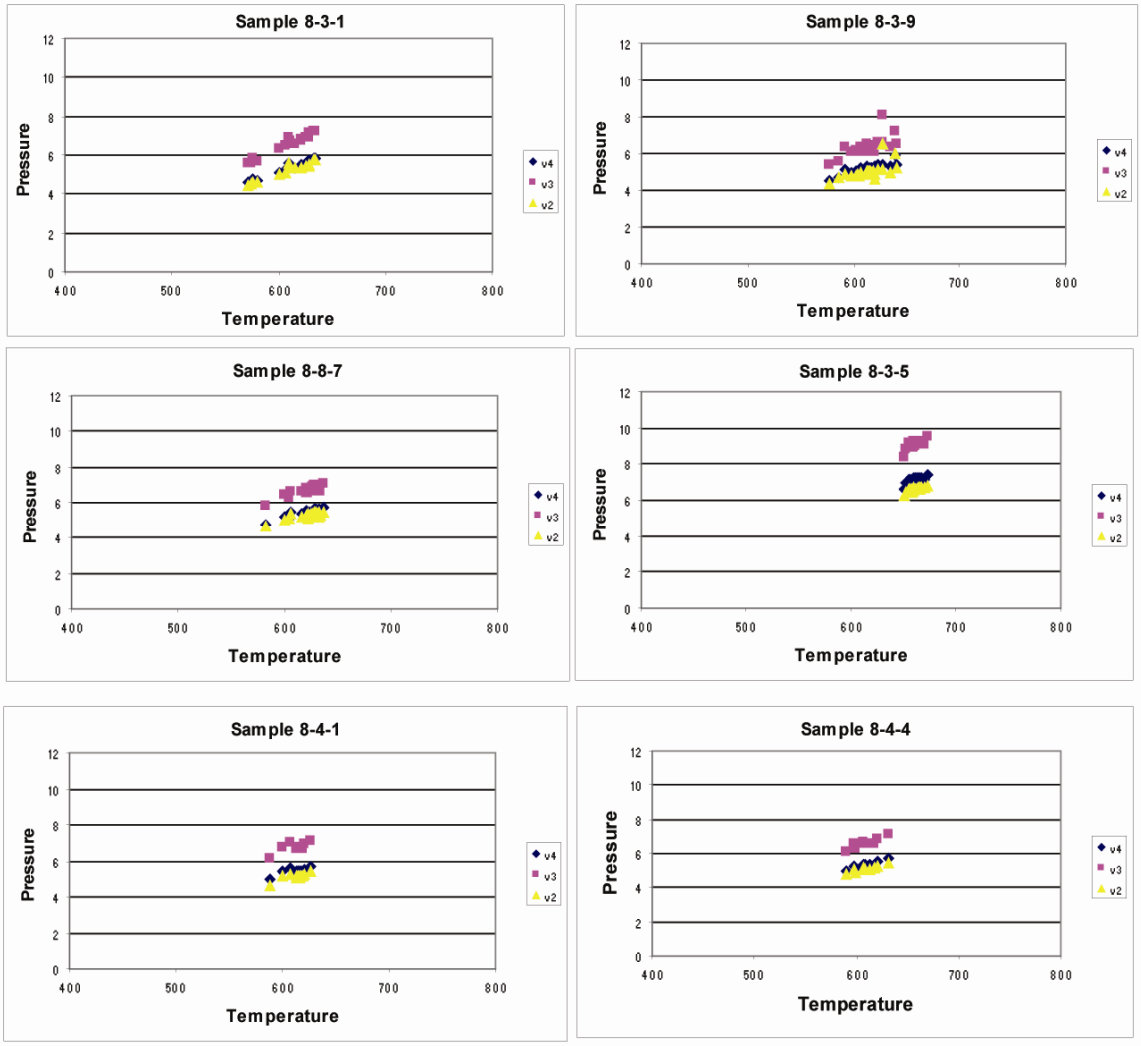

Figure 22. Geothermobarometry of amphibole grains (based on Gerya et al.). V3 which is based on natural data is determined to be the most accurate P-T estimate. V2 and V4 are estimates based on experimentally derived data and tend to provide pressures which are too low. Most samples have temperatures ranging from 580 C to 640 C, though some are slightly higher. Pressures range mainly from 6-8 kbar.

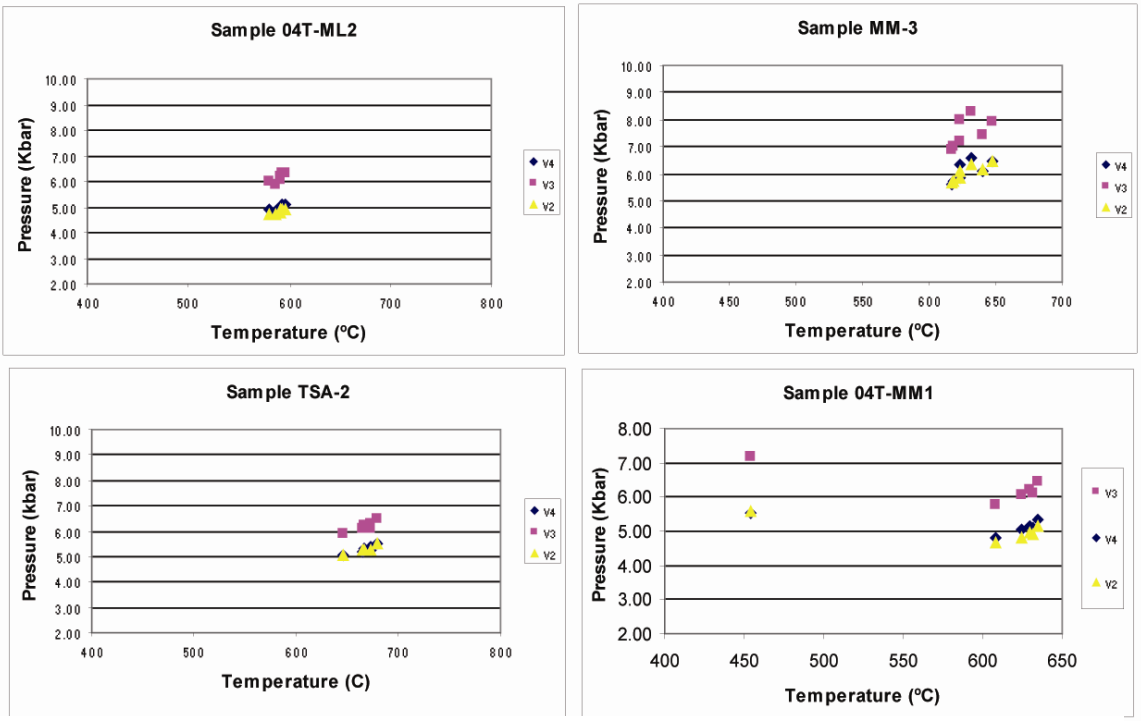

Figure 22 (continued)

AGE ANALYSES

Multiple techniques of age analyses were employed to determine the timing of key tectonic events. Uranium-lead age analyses of detrital zircons are used to constrain provenance. Lutetium-Hafnium age analyses of garnet are used to determine timing of peak metamorphism. Apatite fission-track ages are used to examine the low temperature thermal and exhumation histories of the Lolotoi Complex.

U-Pb AGE ANALYSIS OF ZIRCONS

U-Pb age analysis was performed on detrital zircon from one sample of Lolotoi Complex amphibolite. Eleven other samples were prepared, but no zircon was found. These included samples from garnet-mica schists, amphibolites, greenschists and quartz mica schists. The scarcity of zircons in most samples is possibly due to the commonly Zr undersaturated nature of arcs fringing continents, which is the most likely source for these units. Trace element analysis shows zirconium concentrations range from 15 ppm to 326 ppm, thus some zirconium is present, but must be taken up in other mineral phases. In sample 8-3-9 from the central Bebe Susu Massif two distinct zircon types were found, small extremely rounded and pitted zircons and subhedral lightly abraded zircons with preserved crystal terminations (Figure 23).

U/Pb analysis was conducted using ThermoFinnigan Element2 Laser Ablation-ICP-MS at Washington State University. Analytical procedures for U/Pb analysis at WSU are described in Appendix IV. Initial analyses show a bimodal distribution of ages, one of Late Precambrian (560 Ma), the other of Late Cretaceous age (80 Ma). The Late Precambrian zircons are easily recognizable as the highly rounded, abraded and pitted

detrital grains (Figure 23). The younger Cretaceous ages are consistent with euhedral zircon grains, though they are still somewhat pitted and abraded, but to a far lesser extent than the older grains. The detrital nature of these grains shows that they are not in situ metamorphic zircons and indicates that the protolith was likely a volcanogenic sediment. Since the sample came from an amphibolite collected from deep structural levels in the Lolotoi Complex, deposition of overlying rocks then, must have taken place after the 80 Ma closure of the zircon grains.

LUTETIUM-HAFNIUM AGE ANALYSIS OF GARNETS

^{176} Hf is the daughter product of ^{176}Lu decay, which has a halflife of about 39 Ga (Sguigna et al., 1982). The Lutetium-Hafnium system is well suited for a wide spectrum of dating purposes including deciphering metamorphic P-T-t paths for young mountain belts (Blichert-Toft, 2001). Lu and Hf concentrations in garnet are high compared to most of the major silicate rock forming minerals, thus garnet is an ideal phase for age analysis using the Lu-Hf chronometer (Blichert-Toft, 2001).

These samples are the first Lu-Hf age analyses reported from Timor. They were performed on garnet mica schists, three from the Bebe Susu massif and one from the Lacluta massif. Samples with relatively inclusion free garnets were chosen to minimize the effects of other Lu-Hf bearing mineral phases. The four samples chosen were 04T-MLO (Al_{65-75}, Gr_{10-15}, Py_{6-10}, Sp_{5-10}), SF-2 (Al_{60-70}, Gr_{10-13}, Py_{6-13}, Sp_{15-20}), 8-3-5 (Al_{60-67}, Gr_{12-14}, Py_{7-10}, Sp_{10-20}), and 8-3-2 (Al_{60-70}, Gr_{10-20}, Py_{3-13}, Sp_{3-13}). Sample 04T-MLO shows clear pre-kinematic indicators while the other three samples show ambiguous evidence of either pre- or syn-kinematic growth. Garnets were hand picked from

coarsely crushed samples, then crushed again and hand separated into cleaner and less clean fractions. Garnet-free whole rock samples were separated by removing all garnet fragments by hand picking. Both garnet and whole rock samples averaged about 250 mg, an amount containing more Lu and Hf than needed for an analysis, but enough to ensure a representative sample (Vervoort et al., 2004). Dissolution of whole rock samples was carried out using HF-HNO_3 mixtures in steel jacketed PTFE dissolution vessels for 5 days (Patchett and Ruiz, 1987; Vervoort and Pachett, 1996). Garnet fractions were dissolved using a tabletop dissolution procedure described in Appendix IV.

Separation of Hf and Lu from each other and other constituents was performed using multiple stages of column chemistry as outline by several authors (Patchett and Tatsumoto, 1980; Vervoort and Patchett, 1996; Vervoort and Blitchert-Toft, 1999). Fully separated Hf and Lu samples were dissolved in HCl and spiked with mixed ^{176}Lu-^{180}Hf tracer solutions to determine Lu concentrations and ^{176}Lu/^{177}Hf ratios (Vervoort et al., 2004). Samples were then analyzed using a ThermoFinnigan Neptune ICP-MS multi-collector (see Appendix IV for analytical details). Lu-Hf concentrations, ratios and age determinations are summarized in Table 4. Isochrons for the four samples give ages of 46.5 ± 1.2, 45.20 ± 0.4, 45.4 ± 3.3, and 46.4 ± 0.7 (errors are 2 σ) with a weighted mean age of 45.4 ± 0.7 Ma. MSWD (mean squares of weighted deviates) values for the four isochrons are 0.7, 1.3, 3.6 and 8.3 (Figure 24). MSWD values less than 2.5 are considered to represent valid isochrons, which are within the limits of analytical error (Rollinson, 1993). Values above 2.5 indicate that the scatter of points cannot be explained only by analytical error (Rollinson, 1993). Despite the high MSWD values for two of the samples, the ages obtained are within error of the other two samples. Textural

evidence shows garnets analyzed have undergone only one generation of growth and thus have not been heated above the blocking temperature of Lu-Hf during any subsequent alteration. Thus, this age is interpreted to represent peak metamorphism.

While Lu-Hf analyses of West Timor rocks have not previously been performed, K/Ar and $^{39}Ar/^{40}Ar$ analyses of various mineral phases from five different massifs in West Timor (Mosu, Boi, Mollo, Mutis, and Usu) have been performed by other workers. K-Ar ages reported by Earle (1980) and Sopaheluwaken (1990) range from 31 to 38 Ma. Ar/Ar ages for hornblende separates published by Harris (2006) range between 34.00 ± .03 to 38.60 ± 2.20 Ma. Considering that the blocking temperature of the Ar/Ar system in hornblende is approximately 480 °C (Mezger, 1990), these ages likely correspond to post peak metamorphic cooling conditions. These high temperatures of 480 °C persisting for approximately 10 Ma after peak metamorphism likely indicate Mutis rocks probably started cooling several million years after the Lolotoi Complex. This temporal gradient in cooling may be related to the closer proximity of Mutis units to the Great Indonesian arc as evidenced by abundant volcanic rocks found throughout the complex.

APATITE FISSION-TRACK ANALYSIS

Apatite fission-track analyses were performed to determine the low temperature thermal history of Banda Terrane metamorphic rocks. Twelve samples from Banda Terrane massifs in East Timor, West Timor, and Aileau Complex units in Kisar were examined. Mounted apatites were polished, exposed to Californium-252 radiation and chemically etched to expose horizontal tracks just below the surface. Only 2 samples contained sufficient track densities to produce viable horizontal track length information.

Histograms of horizontal tack length measurements show no long 16 to 18 micron tracks, indicating uplift from the partial annealing zone must have taken place in the last few million years (Figure 25). Apatite fission-track ages were determined using the fission-track population method described by Naeser (1976, 1979) and more recently by Naeser et al. (1989) and Donnelick et al. (2005). In the population method track counts from many grains are pooled to obtain a single age for the entire sample, rather than an age for each individual grain as in the external detector method (Fleischer et al., 1964; Naeser and Dodge, 1969). This is the preferred method for dating apatites that contain abundant defects and have low track densities. Spontaneous track densities, induced track densities, mica detector track densities, and etch pit diameters (dpar) were measured using a petrographic microscope, automated stage, digitizing tablet and apatite fission-track stage software. Four samples and two standards provided viable ages. Eight samples were not reliable for several reasons: 1) scarcity of fossil tracks due to apparent low uranium values (Figure 26), 2) lack of apatite grains, and 3) inconveniently high numbers of induced tracks that made accurate determination of track densities impossible (Figure 26). These types of problems are inherent limitations in apatite fission-track analysis and are documented by Donnelick et al. (2005).

Ages were calculated for the remaining samples using the equation:

$$t_{pooled} = (1/\lambda_d) \{ \ln [1 + \lambda_d \zeta g \rho_d (\Sigma N_s/\Sigma N_i)]\}$$

where t_{pooled} is the AFT age of a pooled population of apatite grains, λ_d is a decay constant of ^{238}U (1.55125×10^{-10}), ζ is a laboratory calibration factor based on the external detection method of fission-track standards, g is a geometry factor, ρ_d is an

induced fission-track density for a uruanium standard, ΣN_s is the sum of spontaneous fission tracks over area Ω, and ΣN_i is the sum of induced fission-tracks over area Ω (Donnelick et al., 2005).

One age of 41 ± 13 Ma was obtained for a Mutis Complex sample, and three ages of 20 ± 2Ma, 18 ± 2 Ma and 12 ± 1 Ma obtained from Aileu Complex metamorphic rocks collected on the island of Kisar, just east of Timor. No track length distribution data is available for the Kisar samples and their metamorphic and thermal history in this region have not been investigated.

Calculated errors are one standard deviation and were obtained using the equation:

$$\sigma_{pooled} = [(1/\Sigma N_s) + (1/\Sigma N_i) + (1/N_d) + (\sigma_\zeta/\zeta)^2]^{1/2}$$

where σ_{pooled} is the 1σ error, σ_ζ is the 1σ uncertainty of the calibration factor, and other variables are described above (Donnelick et al., 2005).

The Mutis sample has a relatively high error due to relatively low numbers of both fossil and induced tracks. In addition, frequent blemishes and irregularities in the apatite grains reduce the accuracy of track counts and produce an inflated age. (Figure 26).

It should be emphasized that this age was obtained from a Mutis Complex sample. However, based on the data heretofore presented it does not seem unreasonable to apply it as a proxy in evaluation of the Lolotoi Complex evolution. A maximum fission-track age of 41 Ma could be consistent with peak metamorphism at 46 Ma followed by rapid exhumation out of the fission-track annealing zone occurring in 5 million years.

Assuming a temperature gradient of 25 °C per km and peak temperature conditions near 600 °C, this would have resulted in uplift from depths of approximately 24 km to a depth of ~5 km and temperatures of ~125 °C. This corresponds to uplift rates of roughly 3.8 mm/year. If the large error is taken into account, fission-track ages may be much younger and uplift rates could be significantly slower. In addition, samples from several Banda Terrane massifs yield Ar/Ar cooling ages and K/Ar ages that range from 39-34 Ma (Harris, 2006). These results would favor a much younger apatite fission-track age, unless the Mutis massif consists of units with slightly different ages that were juxtaposed after cooling.

An apatite fission-track thermal history model was determined from track length measurements, calculated ages, etch pit diameters (dpar) and user defined time-temperature constraints. Modeling was performed using AFTsolve 0.8.3 designed by Ray Donelick and Richard Ketcham (1998). The program allows both forward and inverse modeling of data to determine what time-temperature history best fits measured track length and age data.

Only one sample (MT112-91) provided sufficient data to perform thermal modeling. Major time-temperature constraints used in inverse modeling for this sample include: 1) 45.6 Ma age of peak metamorphism, which corresponds to temperatures of approximately 600 ºC; 2) a 28 Ma unconformity age of overlying unmetamorphosed cherts, sandstone, and carbonate rocks (Haile et al., 1979) indicating low temperatures near 20 ºC; and 3) current exposure at the surface at 20 ºC. Measured fission-track lengths closely match the calculated length distribution based on these time-temperature constraints.

Several possible non-unique thermal models are shown in Figure 27. Models A and C, which statistically best fit measured data are consistent with rapid post metamorphism exhumation and cooling followed by shallow burial beneath accumulating sediments. Models also indicate rapid uplift from 3 Ma to the present, which likely represent collision and nappe emplacement. Model B only takes beginning and end constraints into account and provides a poorer fit of measured and calculated data. The minimum fission-track age predicted by the best-fit model is 23 Ma. This age is significantly lower than the age provided by the population track counting method and indicates that the 41 Ma age is probably not viable due to abundant apparent tracks. Despite the ambiguity and errors of ages obtained, the modeled thermal history based on track length measurements and known time-temperature constraints still provides a possible low temperature thermal history.

DISSCUSSION

Age dating techniques constrain the tectonic history of the Lolotoi Complex by indicating that: 1) deposition occurred mainly after 80 Ma as evidenced by detrital zircon grains found in deep structural levels of the metamorphic Complex; 2) peak metamorphic conditions were reached near 46 Ma as indicated by Lu-Hf dating of garnets; 3) from around 46 to 28 Ma rapid exhumation and cooling occurred as suggested by a maximum fission-track age of 41 Ma and a later 28 Ma unconformity age with overlying Palelo Group rocks; 4) shallow heating and burial beneath accumulating Palelo Group and Cablac sediments occurred from 28 Ma to 3 Ma and temperatures from 120 to 140 °C

were reached; and 5) uplift to the surface occurred from 3 Ma to the present due to collision with the Australian continental margin.

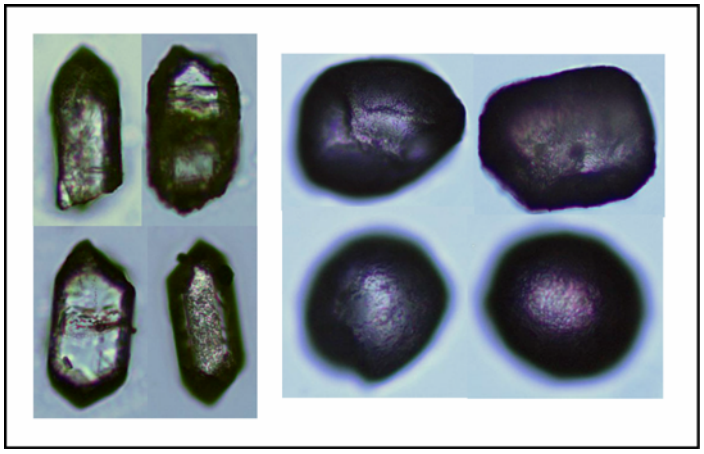

Figure 23. Detrital zircons of Late Cretaceous age (Left) and Late Precambrian age (right). Notice the older zircons are extremely eroded and pitted while the younger zircons are nearly euhedral with preserved crystal terminations.

Table 4. Lu-Hf Analytical results for garnet and whole rock samples obtained using an ICP-MS multicollector.

Sample	Type	$^{176}Lu/^{177}Hf$	2 σ abs	$^{176}Hf/^{177}Hf$	2 σ abs	Lu ppm	Hf ppm
8-3-2							
8-3-2 C.1	Garnet clean	3.52123	0.00704	0.285853	0.000009	5.610	0.226
8-3-2 U1.1	Garnet less clean	3.57296	0.00715	0.285868	0.000010	4.573	0.182
8-3-2 U2.1	Garnet less clean	2.84393	0.00569	0.285315	0.000007	5.208	0.260
8-3-2 U3.2	Garnet less clean	1.48191	0.00296	0.284101	0.000006	4.717	0.452
8-3-2 WR.1	Sav whole rock	0.02499	0.00005	0.282811	0.000006	0.198	1.124
8-3-2 WRB.1	Bomb whole rock	0.00792	0.00002	0.282807	0.000006	0.262	4.697
8-3-5							
8-3-5 C.1	Garnet clean	4.03088	0.00806	0.286517	0.000021	3.084	0.109
8-3-5 U1.1	Garnet less clean	4.09187	0.00818	0.286610	0.000034	2.859	0.099
8-3-5 U2.1	Garnet less clean	4.41653	0.00883	0.286845	0.000018	3.004	0.097
8-3-2 WR.1	Sav whole rock	0.12201	0.00024	0.283206	0.000008	0.339	0.394
8-3-2 WR.B1	Bomb whole rock	0.02282	0.00005	0.283146	0.000006	0.383	2.379
04TMLO							
04TMLO C.1	Garnet clean	20.21426	0.04050	0.301189	0.000054	17.899	0.126
04TMLO U1.1	Garnet less clean	15.84595	0.03175	0.300938	0.000072	13.479	0.121
04TMLO U2.1	Garnet less clean	11.42500	0.02300	0.292602	0.000030	12.306	0.153
04TMLO WR1.1	Sav whole rock	0.01828	0.00004	0.282750	0.000019	0.011	0.086
04TMLO WR2.1	Sav whole rock	0.01598	0.00003	0.281818	0.000043	0.015	0.134
04TMLO WRB2.1	Bomb whole rock	0.00522	0.00001	0.282681	0.000006	0.025	0.041
SF-2							
SF-2 C.1	Garnet clean	3.76012	0.00752	0.286398	0.000048	3.246	0.123
SF-2 U1.1	Garnet less clean	3.52681	0.00705	0.286546	0.000179	1.958	0.079
SF-2 U2.1	Garnet less clean	2.99564	0.00599	0.285383	0.000024	3.779	0.179
SF-2 WR.1	Sav whole rock	0.01951	0.00004	0.282848	0.000006	0.186	1.351
SF-2 WRB.1	Bomb whole rock	0.00941	0.00002	0.282862	0.000006	0.270	4.065

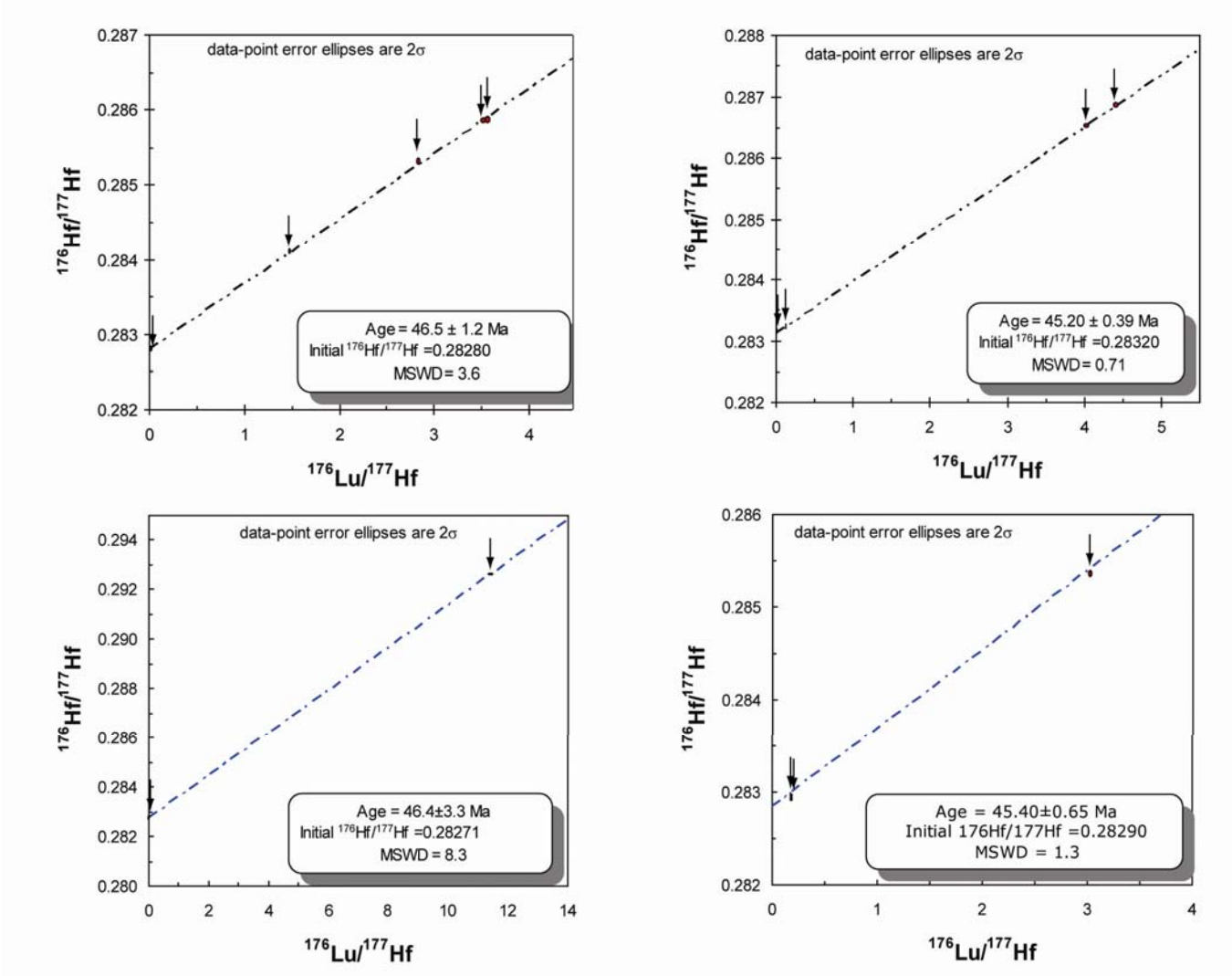

Figure 24. Hafnium-Lutetium isochrons for four samples. Multiples points on the isochron were obtained by analyzing clean garnet, unclean garnet, and whole rock fractions. Data point error ellipses are 2σ.

Table 5. Apatite Etch pit diameter data (Dpar)

dpar	Angle with C-	dpar	Angle with C-	dpar	Angle with C-axis
2.61	2°	2.85	6°	3.06	3°
2.77	1°	2.32	10°	2.94	2°
2.84	0°	2.75	3°	2.58	2°
2.61	2°	2.75	2°	2.60	1°
3.41	14°	2.66	0°	3.30	6°
3.27	4°	2.58	2°	2.32	1°
2.98	7°	3.43	0°	2.63	5°
3.08	3°	3.18	7°	3.60	0°
2.82	2°	2.89	1°	2.99	1°
2.89	3°	3.65	0°	3.10	5°
3.96	8°	2.89	4°	3.27	5°
3.75	0°	3.10	9°		
3.70	2°	3.37	9°	**3.18**	**Mean dpar**
3.81	4°	3.10	1°		
4.10	7°	2.70	4°		
3.86	9°	3.17	9°		
3.69	1°	2.94	2°		
4.05	13°	3.01	10°		
3.98	19°	3.06	14°		
4.78	1°	3.32	14°		
4.20	0°	3.20	21°		
4.17	10°	3.53	18°		
3.65	2°	3.22	5°		
2.34	4°	2.89	2°		
2.73	0°	2.91	3°		

Table 6. Summary of track counts, ages, and errors.

Sample	Fossil Tracks	Induced Tracks	Total Mica Counts	Age (Ma)	Error (1st std dev.)	Notes
FC	270	685	2667	**34.62**	2.58	Standard
LC	97	630	2667	**13.54**	1.50	Standard
Kisar 43	178	779	2667	**20.08**	1.71	From Kisar Island
MT-44	177	859	2667	**18.12**	1.54	
MT45-1	109	760	2667	**12.62**	1.32	
MT-112-91	16	34	2667	**41.32**	12.55	Very low track density
MT105-91	No data	---	---	---	---	
04T-2G	No data	---	---	---	---	No Tracks
04T-67	No data	---	---	---	---	<30% Apatite, no tracks
MT111-91	No data	---	---	---	---	Very few apatite grains
MT-53A	No data	---	---	---	---	Not apatite, no tracks
MT106-91	No data	---	---	---	---	<1% apatite, no tracks
MT64-91	No data	---	---	---	---	<5% apatite, no tracks
MT43-5	No data					Too many Induced tracks

Table 7. Measurements of apatite fission-track lengths.

Sample	MT 112-91		MT105F-91		04T-2G	04T-67	MT111-91	MT-53A	MT106-91	MT64-91
	Track Length (µm)	Angle with C axis	Track Length (µm)	Angle with C axis	Track Length (µm)	Track Length (µm)	Track Length (µm)	Track Length (µm)	Track Length (µm)	Track Length (µm)
	10.27	12º	9.48	9º	5.82	none	none	none	none	none
	9.29	77º	8.99	25º						
	8.80	54º	10.97	2º						
	10.62	77º	9.99	4º						
	10.40	80º	10.63	13º						
	9.29	87º	10.97	5º						
	11.46	34º								
	10.64	73º								
	10.06	4º								
	9.90	74º								
	9.83	59º								
	10.58	2º								
	11.17	47º								
	10.32	43º								
	10.53	58º								
	12.05	39º								
	12.72	57º								
	11.14	73º								
	11.61	56º								
Mean	**10.56**		**10.17**		**5.82**					

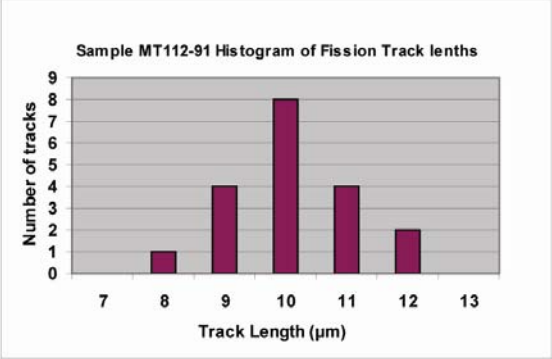

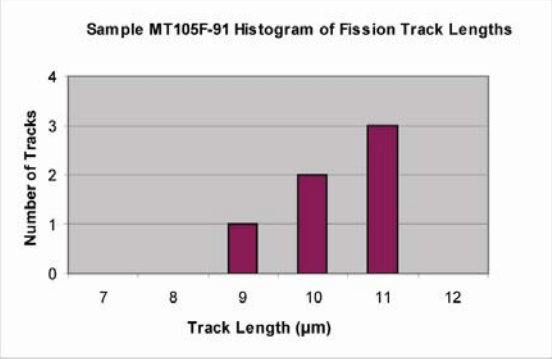

Figure 25. Histograms of horizontal apatite fission-track lengths. Both histograms show no long 16-18 micron tracks, which indicates some annealing has occurred and samples have been exhumed from the partial annealing zone recently enough that no new long tracks could be detected.

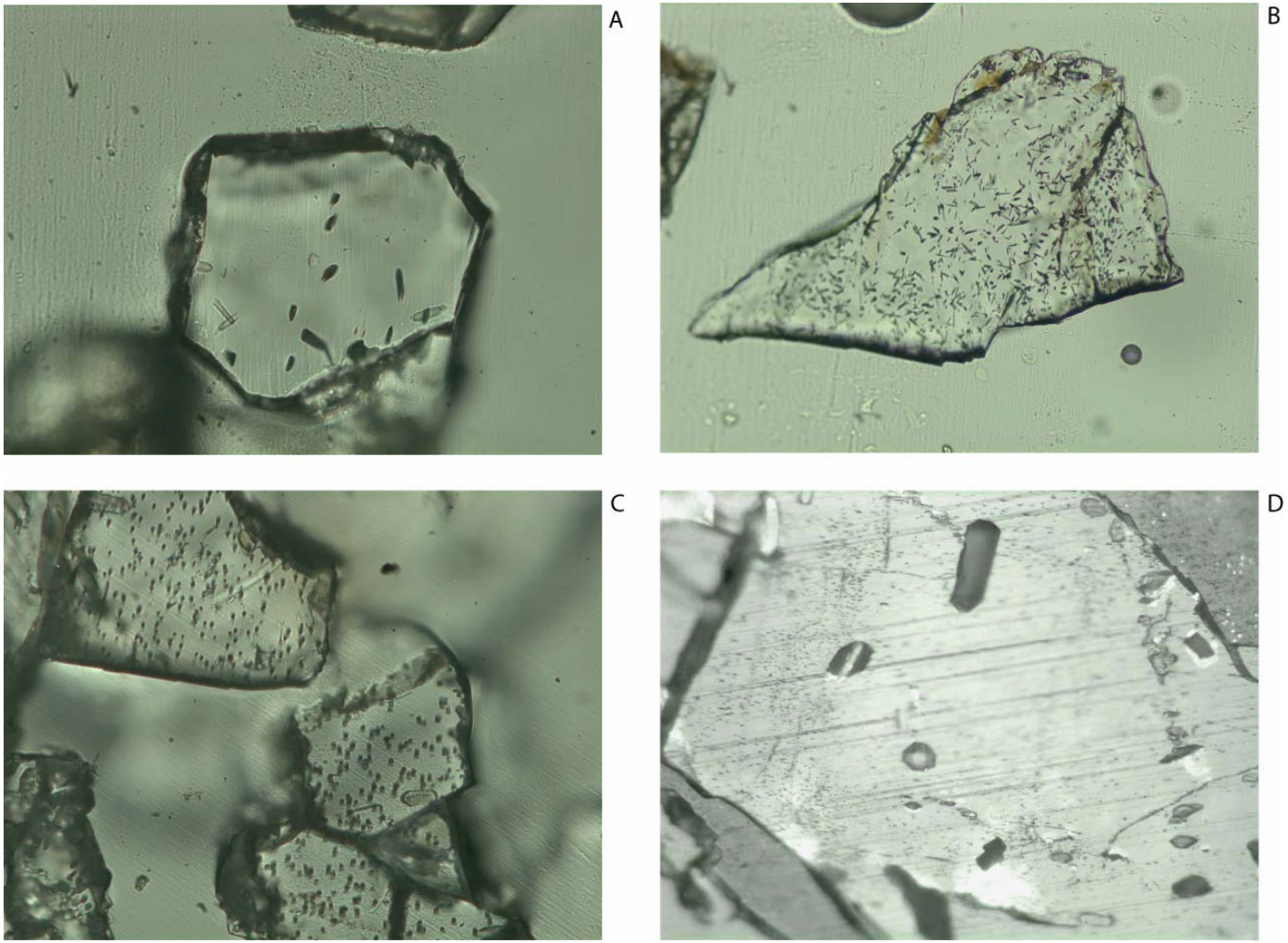

Figure 26. Photomicrographs of apatite grains. A. Induced tracks with low track density. B. Induced tracks with high fission-track density. C. Californium irradiated sample MT-112-91 showing very sparse fossil tracks. D. Sample MT-112-91 showing abundant flaws and inclusion arrays which complicate accurate determination of track densities.

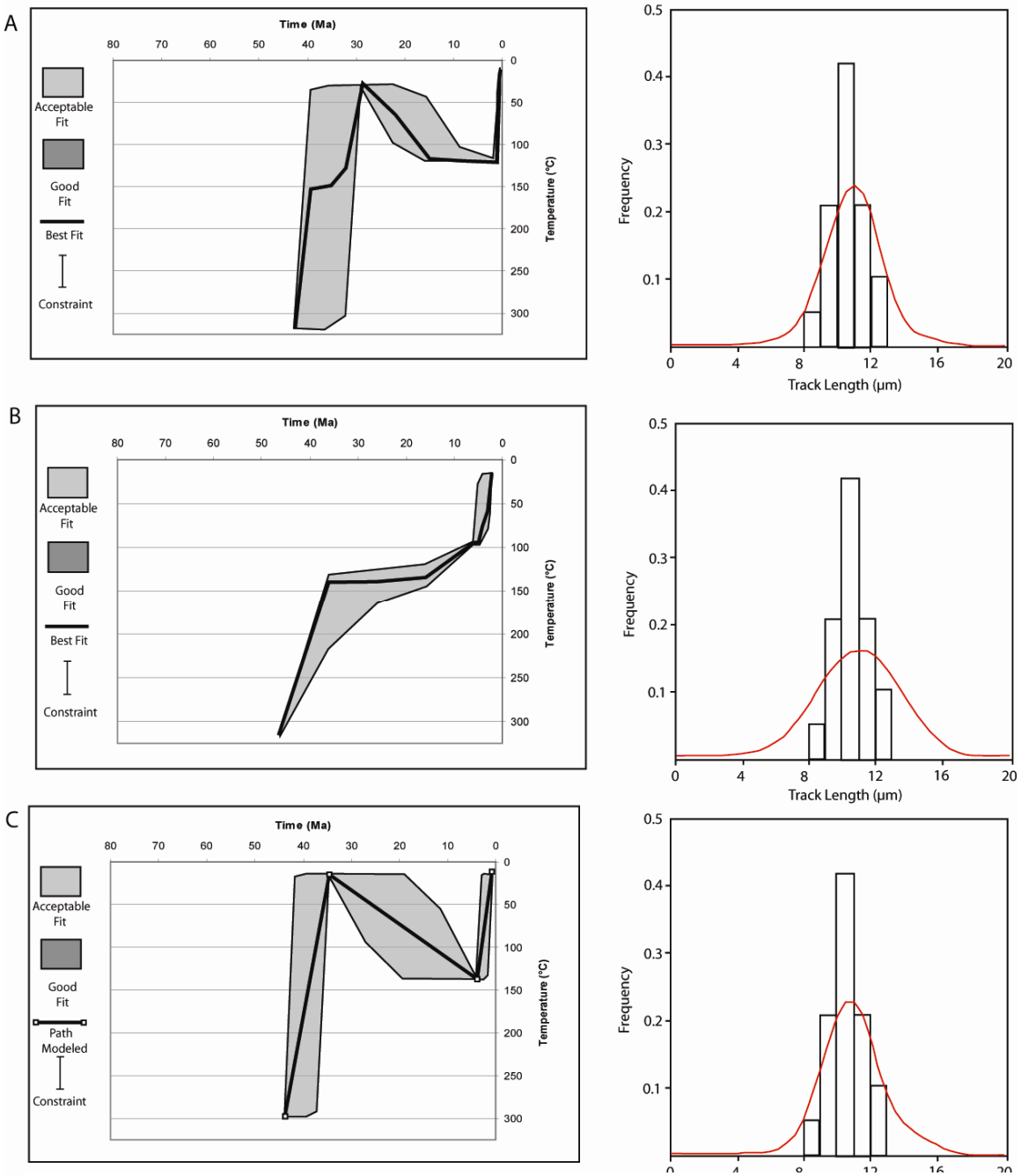

Figure 27. Apatite fission-track thermal history modeling based on AFTsolve 0.8.3 (Donnelick and Ketcham, 1998). A) time-temperature plot of an inverse model that produced statistically the best fit to measured track length data. Geological constraints used in inverse modeling include a 45.36 Ma age of peak metamorphism at around 600 °C, a 28 Ma depositional age of overlying unmetamorphosed carbonates near 20 °C, and a recent collision related exhumation. B) Inverse model that only uses beginning and end constraints and results in a statistically poor fit. C) Forward modeled path that closely resembles the inverse model shown in A.

STRUCTURAL ANALYSIS

Several workers have investigated the various phases of deformation recorded in Banda Terrane rocks of the Mutis Complex (e.g. Earle, 1980; Sopaheluwaken, 1990). However, no structural analyses have previously been performed on Lolotoi Complex rocks. Faults, foliations, fractures and folds were measured to determine both the ductile and brittle deformation histories.

VEINS

Vein orientations were recorded from 28 localities, at each location; a mean was taken of all veins with a similar orientation. Results show prevailing σ_1 directions were NW-SE. (Figure 28). Other minor vein sets may be explained by rotations of the rocks through a constant stress field, or slight changes in the principle stress orientations through time. Other structural features discussed below also show evidence of multiple principle stress orientations. Veins observed in outcrop and thin section cut through all other structures.

FOLIATIONS AND FOLDING

Detailed maps of the Bebe Susu and Lolotoi massifs show variation in S_1 orientations in geographical space on most traverses (Figures 5 and 6). However in Geometric space, S_1 poles to planes cluster along a NW-SE band that predicts folding of S_1 along a NE-SW axis from a NW-SE σ_1 (Figure 29). S_1 foliation planes are parallel to original layering (S_0). Foliations in broken and faulted graphite rich zones, mostly on the periphery of the nappes, are not included in data. Localized, mesoscale, open (interlimb

angle 60°-120°), asymmetric folds likely associated with larger scale F_1 folds, also cause variations in foliation orientations. Most fold limbs verge dominantly to the southeast, have axes oriented NE-SW, and plunge less than 20 degrees (Figure 31 b-e). Broad scale F_1 folds could not be directly measured, but are inferred from variations in homoclinal foliation orientations at the outcrop scale. A second shistosity that is axial planar to tight isoclinal folds of S_1 is locally developed and poorly defined (Figure 30).

FAULTING

In the Bebe Susu nappe internal faulting increases towards the south and central parts of the massif. Thrust faults exhibit two dominant orientations, one strikes NE-SW with thrusting both to the SE and NW, the other set strikes NW-SE with thrusting both to the SW and NE (Figure 32). Normal faults have mainly top down to the SW, S and SE sense of shear, indicating extensional stresses were mostly normal to the strike of the orogen (Figure 32). Some faults dipping to the east and west are only found along the edges of the massif and are attributed to local relaxation at the edges of the nappes. No strike slip faults were identified in outcrop. Damage zones for faults average around 1 m, though larger zones up to 1.5m were found (Figure 33). Offsets up to several meters were detected on most faults, though smaller faults were also found. Faults are traceable up to 50m across stream beds, but heavy vegetation restricts further field or aerial photo mapping. In many cases graphite layers act as detachment horizons and forms a large portion of the damage zones. Only one thrust fault with offset overlying river gravel showed evidence of recent movement. (Figure 33a).

SEQUENCE OF DEFORMATION

At least 3 main phases of deformation are recorded in the Lolotoi Complex, though not all phases are found in all rock types.

D_1) S_1 foliation formed parallel to S_0 under a layer-normal maximum principle stress prior to the onset of peak metamorphic conditions. S_0 consists of original interlayers of lesser amounts of pelitic and quartz-rich sediments and greater amounts of volcaniclastic sediments. This early S_1 foliation is recorded in nearly all metamorphic rock types with the exception of metatuff and greenstone breccia. (Figure 30 a-d).

D_2) In many samples a second foliation (S_2) is developed axial-planar to small scale isoclinal folds of S_1 (Figure 30c). S_2 foliations are poorly defined in outcrop. Some quartz-mica schists exhibit partially transposed S_1 foliations that are near vertical due to layer parallel stresses. Asymmetic microfolds associated with D_2 show mostly southward and eastward vergence. S_1 and S_2 are also broadly folded into mostly long wavelength SE verging folds with axes oriented approximately NE-SW, though it cannot be determined if this folding is related to D_2 or D_3.

D_3) Late stage brittle deformation in the form of normal and thrust faults, and vein filled fractures that cut across all earlier ductile structures in all pre-Oligocene rock types of the Banda Terrane (Figure 33).

DISCUSSION

Structural measurements throughout the Lolotoi Complex indicate an initial vertical maximum principle stress formed S_1 parallel to S_0. A later phase of deformation

characterized by small (cm to m) scale isoclinal folding and formation of an axial-planar S_2 foliation is attributed to horizontal NW-SE directed σ_1 stresses during peak metamorphism. F_1 compressional stresses were oriented principally NW-SE as indicated by parallelism between poles to thrust faults and fold axial planes, and the prevailing fracture sets. Fold asymmetry indicates mostly SE vergence. Underlying Gondwana sequence rocks exhibit similar compressional stress orientations and vergence (Harris et al., 2000). This suggests that either both the Gondwana Sequence and the Lolotoi Complex were deformed at the same time during emplacement of Lolotoi Complex metamorphics, or they both experienced similar stress conditions just prior to emplacement. However, this does not imply that they share a similar long term tectonic evolution.

Structural data from Mutis Complex massifs in West Timor vary from massif to massif. However, the series of deformation is similar among all the massifs. Earle, (1980) shows that structural orientations in different massifs become equivalent if they are rotated slightly relative to each other. Based upon this observation, Earle claims that the present mismatch in structure orientation between massifs may be due to syn- or post-emplacement rotation, either caused by refolding, or by strike-slip faulting. Overall, the Banda Terrane massifs across Timor show consistent NE-SE striking foliations and fold axes, which implies little to no rotation has occurred. This explanation may also apply to small differences between structural orientations of Lolotoi and Mutis Complex massifs.

CONTACT RELATIONSHIPS

Contact relationships between Lolotoi Complex rocks with underlying Gondwana Sequence rocks and overlying Cretaceous to Miocene cover units provide valuable information for constraining its tectonic evolution. Harris et al. (1998) reported the presence of mélange consisting of block in clay facies and broken formation at the base of flat lying Banda Terrane nappes. This was again verified in several locations on the fringes of the Lolotoi and Bebe Susu nappes (Figure 34b). The mélange is interpreted to result mostly from simple-shear along the thrust contact between Banda Terrane nappes and underlying Gondwana sequence rocks, which is also the suture between Asian and Australian affinity rock types. The suture formed as the Australian continental margin was pulled into the subduction zone underlying the Banda Terrane. The mélange in essence represents deformation in an over-stuffed subduction channel (Harris et al., 1998). Workers, who support an upthrust basement model (Charlton, 2002; Grady, 1975; Chamalaun and Grady, 1978) and interpret the Lolotoi Complex to be conformably resting on underlying rocks, failed to note the significance of this mélange.

In the northen portion of the Bebe Susu nappe, occurrences of pink, crinoidal Maubisse Limestone protrude from low-lying hills surrounding Lolotoi metamorphic rocks (Figure 5a). This relationship was interpreted by Chamalaun and Grady (1978) and later by Charlton (2002) to indicate a pre-Permian age for the Lolotoi Complex. However, close examination reveals these resistant limestones actually protrude through non-resistant greenstones at the thin edge of the Bebe Susu nappe, and represent exposures within fensters through the metamorphic rocks. Melange surrounding the limestone knobs and deeply insized erosional patterns indicate the basal contact of the

Maubisse formation is beneath the metamorphic rocks. Similar Maubisse units directly to the southeast are conformable with Gondwana Sequence units.

Late Cretaceous through Early Oligocene age unmetamorphosed sedimentary and volcanic cover units of the Palelo Group, Metan Formation, and Cablac Formation are present locally on the fringes of the Lolotoi nappe, central and southern portions of the Bebe Susu nappe, eastern finge of the Lacluta nappe, and extensively in the Mata Bia nappe. At the southern edge of the Bebe Susu nappe, Palelo Group and Metan Formation units are in normal fault contact with Lolotoi Complex metamorphics along a chlorite rich breccia zone. Similar contact relations are reported in West Timor between the Mutis Complex and overlying Palelo group sediments, which are characterized by de Waard, (1957) and van West, (1941) as a crush zone of brecciated chlorite schist.

In the Banda Terrane, the age of peak metamorphism is younger than the age of most overlying sedimentary and volcanic cover units, thus the contact between the two is not a depositional unconformity as previously reported (e.g. Earle, 1980). Large sections of missing units in the Palelo Group and Metan Formation indicates attenuation by extension has occurred. The juxtaposition of metamorphic units with older overlying sediments and volcanics likely involved extensional exhumation with metamorphic rocks in the footwall and structurally thinned cover units in the hanging wall.

Figure 34 shows a panoramic of the southern edge of the Bebe Susu massif with steeply dipping Eocene limestone and adjacent Metan Formation volcanics and carbonates juxtaposed against Lolotoi metamorphics. Traverses through these Metan Formation rocks reveals shallow water sandstones and shale, bedded tuffs, and nummulitic and stylolytic Dartollu Limestones followed down-section by veined and

pressure-solved turbidite seccessions (Figure 35 and 36). Further down-section near the contact between the Palelo Group and the Lolotoi Complex, abundant coarse conglomerates and sandstones of the Haulasi Formation are found (Figure 36). The basal portion of the Palelo Group, the Noni Formation, is poorly represented in this area. Though it is well exposed near the Mata Bia massif farther to the east (Figure 36). Younger Oligocene to early Miocene Cablac limestone is also found overlying portions of the Lolotoi Complex, particularly in the Lolotoi massif (Figure 6). The faunal assemblages found throughout the Metan Formation, Palelo Group and Cablac Limestones are characteristic of a low latitude shallow marine environment and differ greatly from any Australian affinity faunas of similar age found in Timor (Audley-Charles and Carter, 1972; Carter et al., 1976).

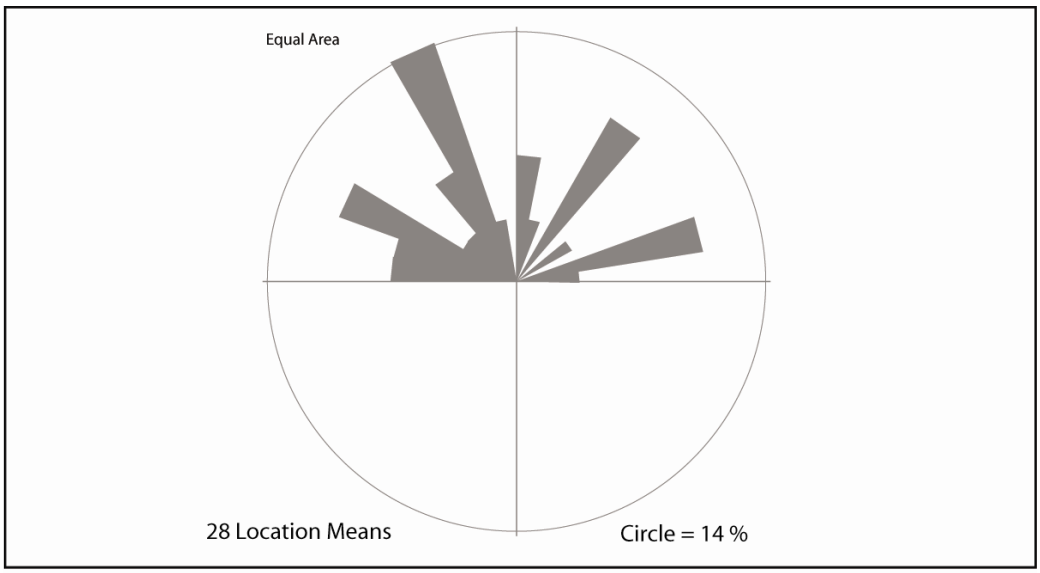

Figures 28. Vein orientations. The dominant NW trending petal is consistent with a maximum principle stress oriented NW-SE. Other petal orientations are somewhat dispersed and could reflect either changes in sigma 1, or rotations of rocks through a constant stress field.

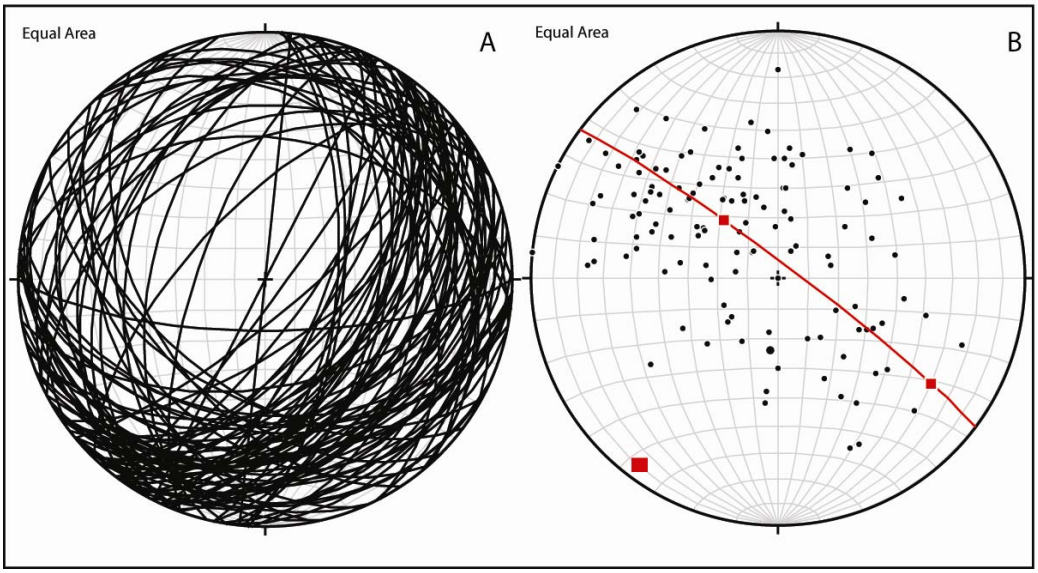

Figure 29. A. S_1 Foliation orientations for the Bebe Susu massif showing the dominant foliation dips to the southwest. B. Poles to foliation planes with a cylindrical best fit showing the pi girdle and pi axis. The pi axis likely represents a regional large scale fold axis oriented NE-SW, about which S_1 and S_2 foliations have been deformed.

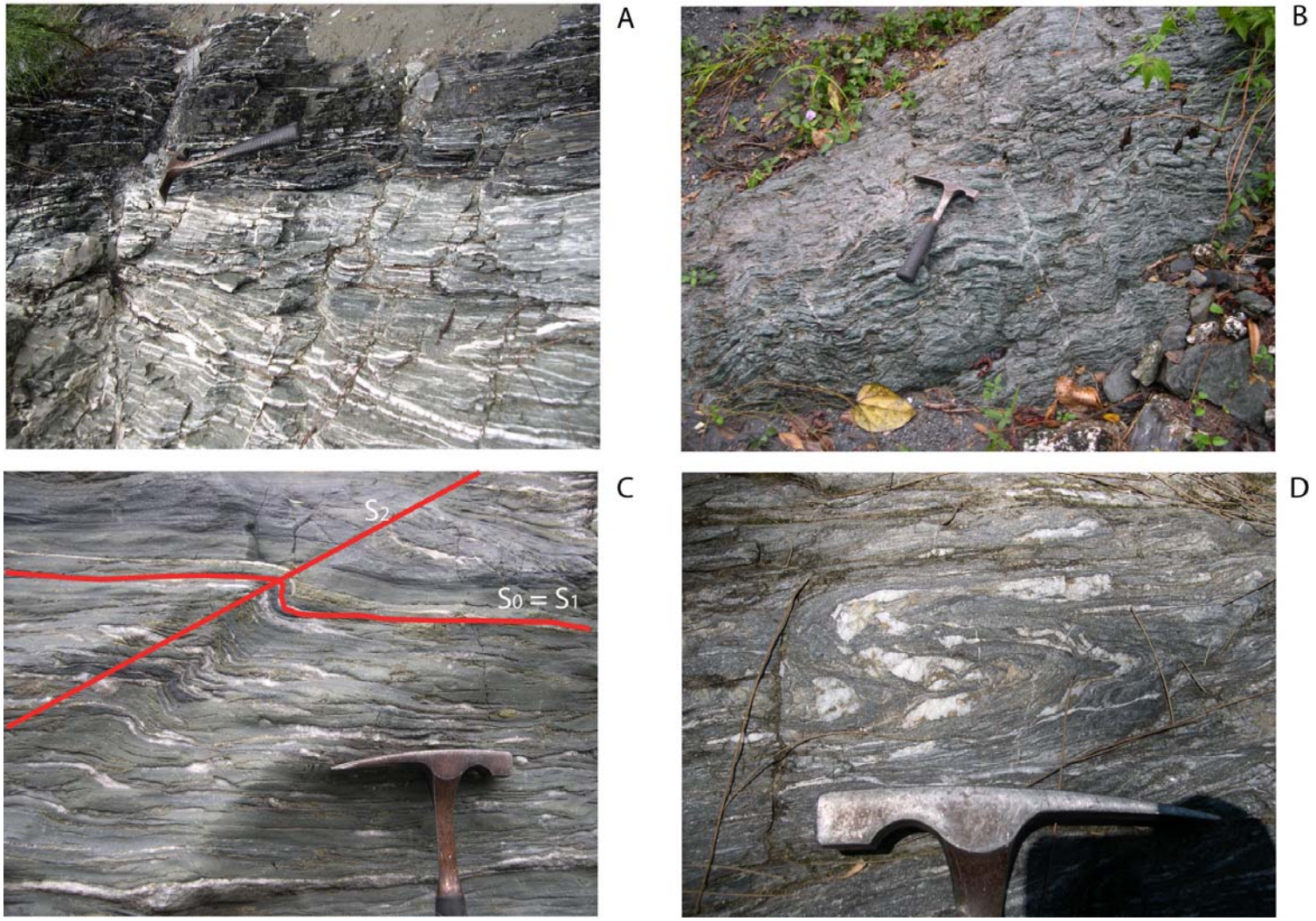

Figure 30. A. relatively undeformed S_1 foliations in graphitic phyllite and underlying greenschist white bands are quartz rich layers. B. Deformed S_1 foliations forming small scale crenulation-like folds. C. Small scale open fold deforming S_1 foliations in greenschist with weakly developed S_2 foliations axial planar to folding, folds verge eastward. D. Isoclinal folds of S_1 formed during D_2 deformation.

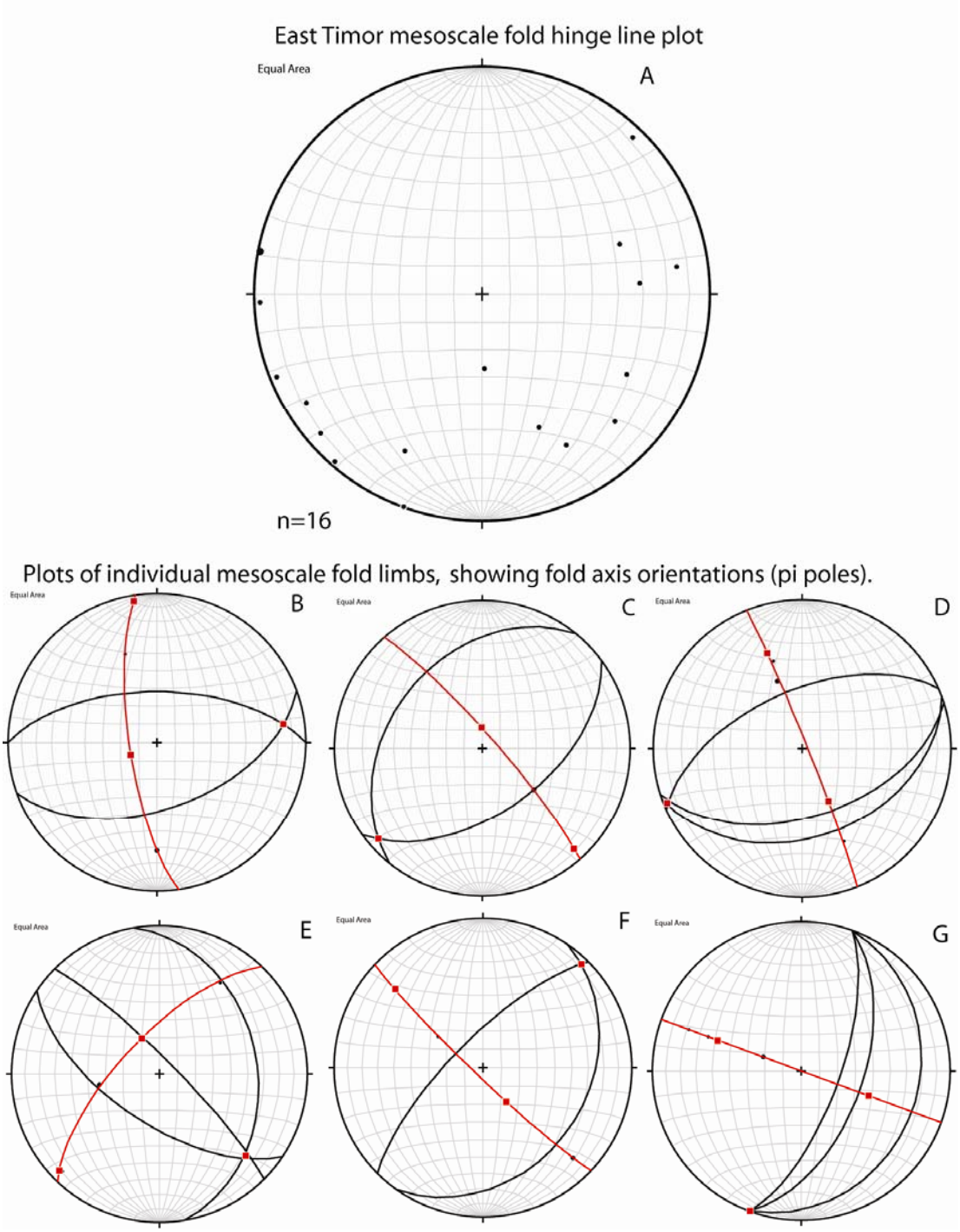

Figure 31. A. Equal area stereographic projection of East Timor mesoscale fold hinge lines. Two sets of hinge lines are evident, one oriented SW-NE and plunging shallowly in either direction. The second is oriented NW-SE plunging variably to the southeast. These fold orientations are consistent with either, two different directions of stress, or rotation within a constant stress field. B through G show plots of individual mesoscale fold limbs where pi girdles and pi poles are plotted as cylindrical best fits to represent individual fold axis orientations.

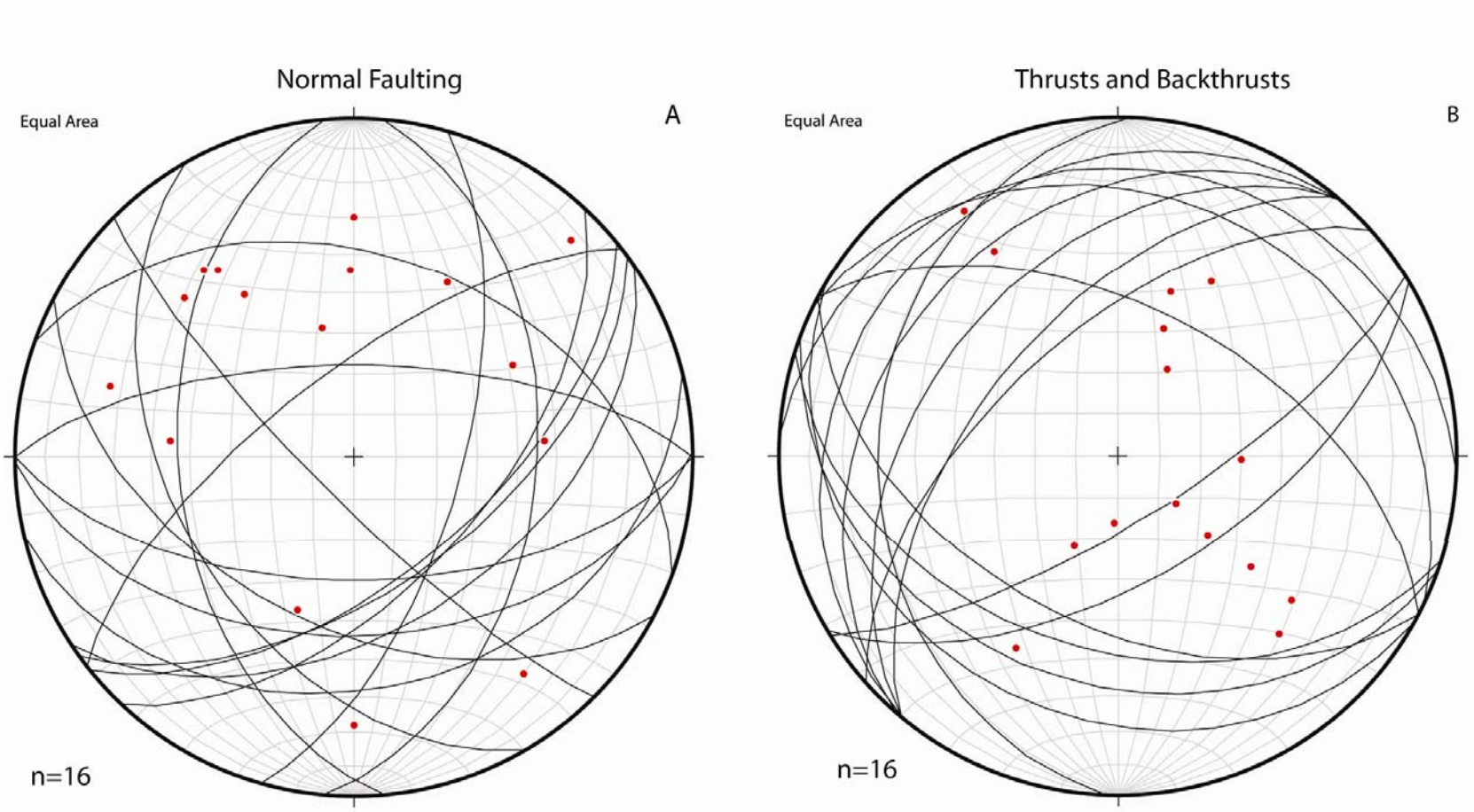

Figure 32. A) Normal fault planes and poles to planes found in the Bebe Susu and Lolotoi nappes. Eastward and Westward dipping normal faults are likely related to local relaxation along the boundaries of the nappes. Dominant southward and southeast oriented faults are likely related to regional extensional stresses. B) Poles to two main orientations of thrusting; one with SW-NE striking thrust and backstrust, the second with NW-SE striking thrust and backthrusts. Multiple thrust orientations may be related to rotation of rocks through a constant stress field, or to changes in the stress field during the brittle deformational history. Additional faults with unknown sense of shear have not been included in these plots.

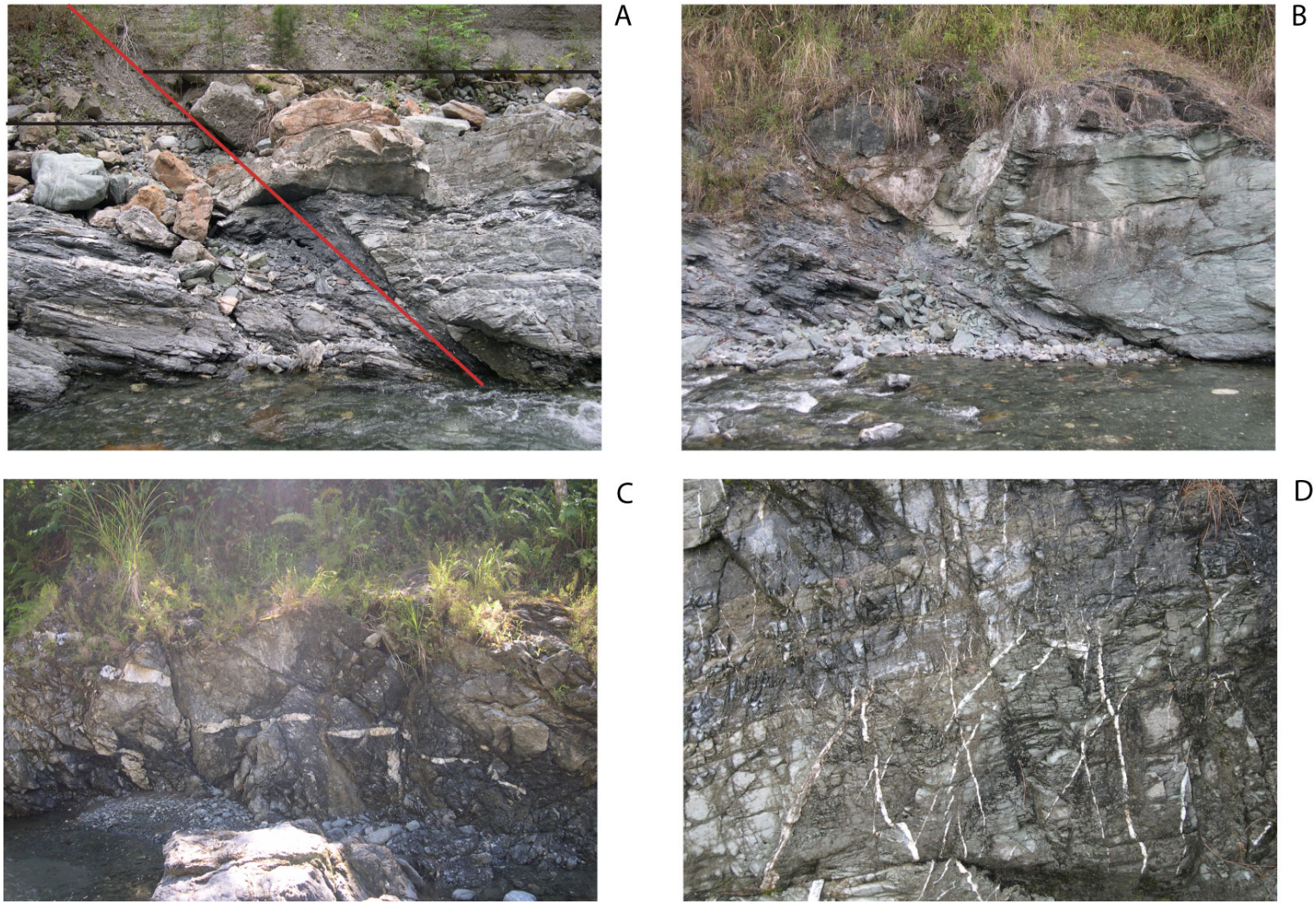

Figure 33. A) Thrust fault with recent movement. B) A well defined thrust fault with obvious truncation of greenschist against graphitic phyllite in the footwall. C) Extensional offset of a vein into a stair step pattern. D) Filled extensional and conjugate shear fractures from a near vertical sigma 1 (scale approx. 6 ft).

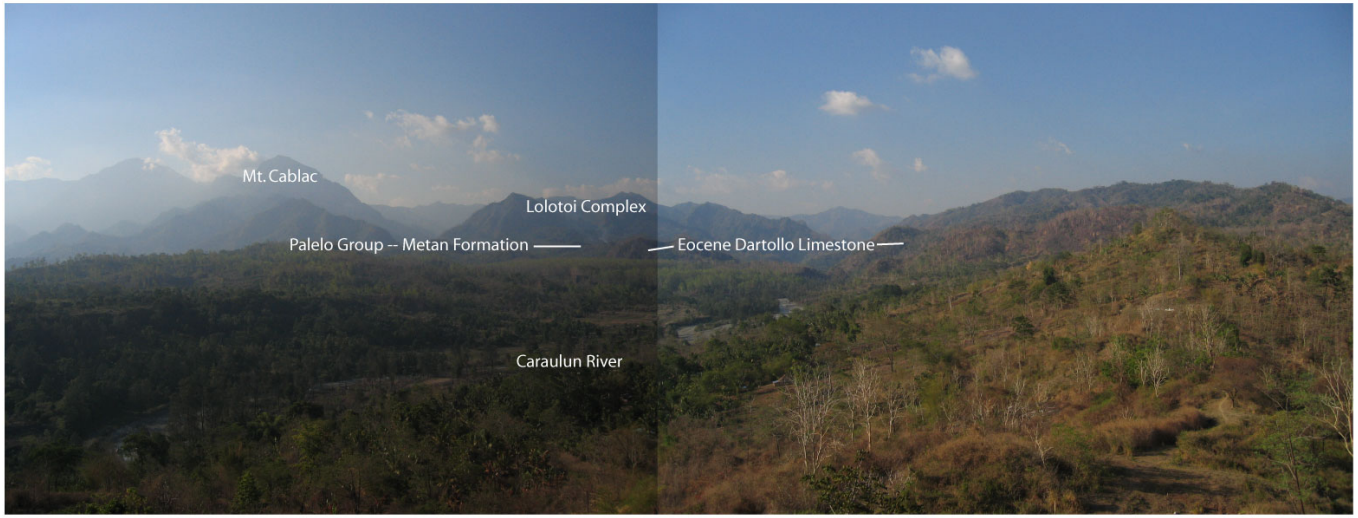


A


B

Figure 34. Above, Panorama of the southwestern edge of the Bebe Susu nappe. A) Basal Conglomerate of the Palelo Group immediately overlying monometamorphic units of the Lolotoi Complex. Igneous boulders from this unit yield Jurassic and Cretaceous U/Pb zircon ages (Harris, 2006). B) Clay rich Bobonaro mélange containing fragments of both Lolotoi metamorphics and Gondwana Sequence rocks is found commonly at the base of Lolotoi Complex massifs.

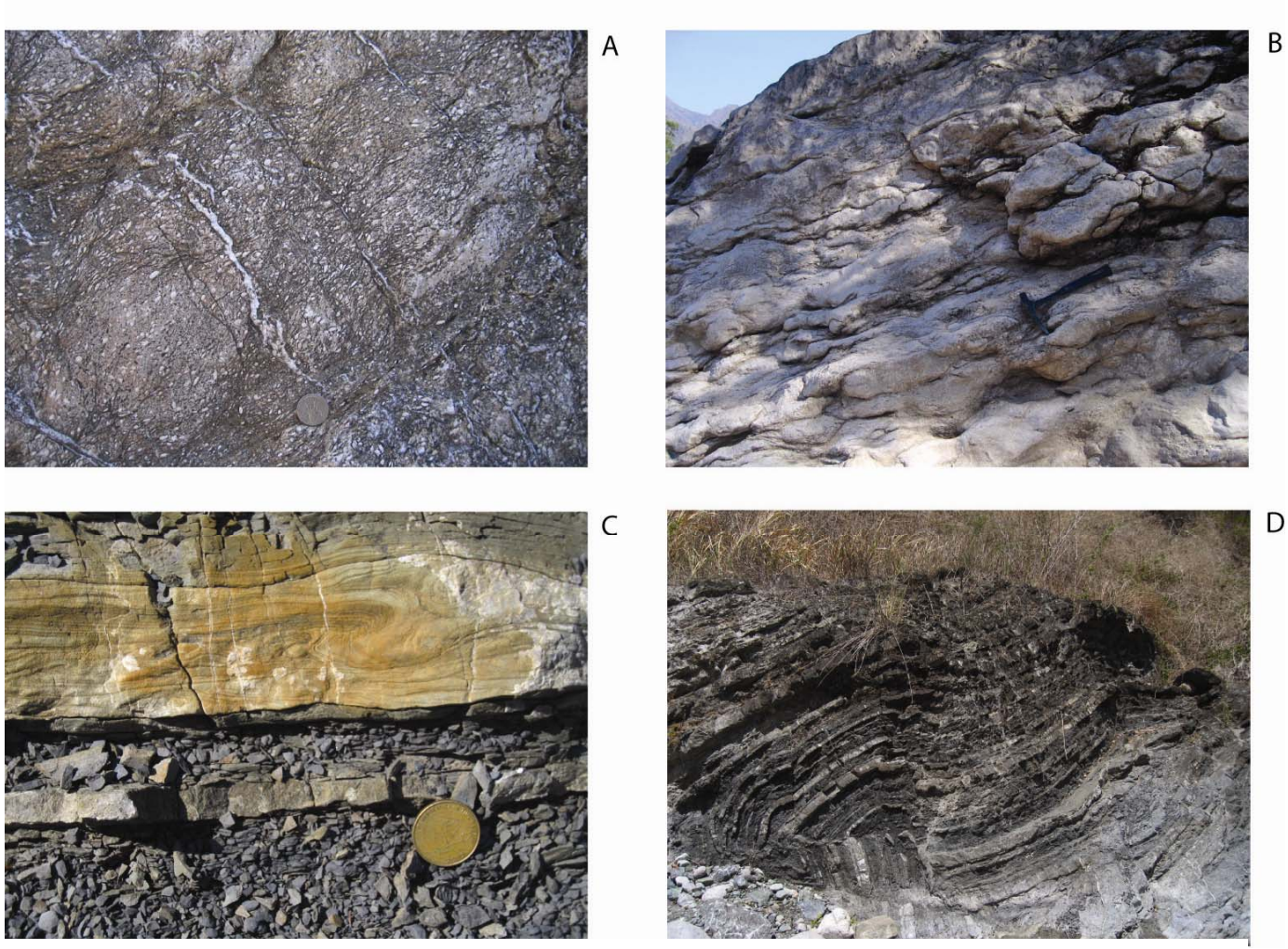

Figure 35. Palelo Group Formations found south of the Bebe Susu massif. A and B) Eocene Nummulitic Dartollu Limestone found in the Caraulun and Sui rivers, veins are perpendicular to layer parallel stylolites indicating a vertical sigma 1. C) Turbidites of the Haulasi Formation. D) Folded and thrusted sandstones and shales of the Haulasi Formation, showing Palelo Group sediments were also affected by late compressional stresses. The main thrust verges south with north verging backthrusts.

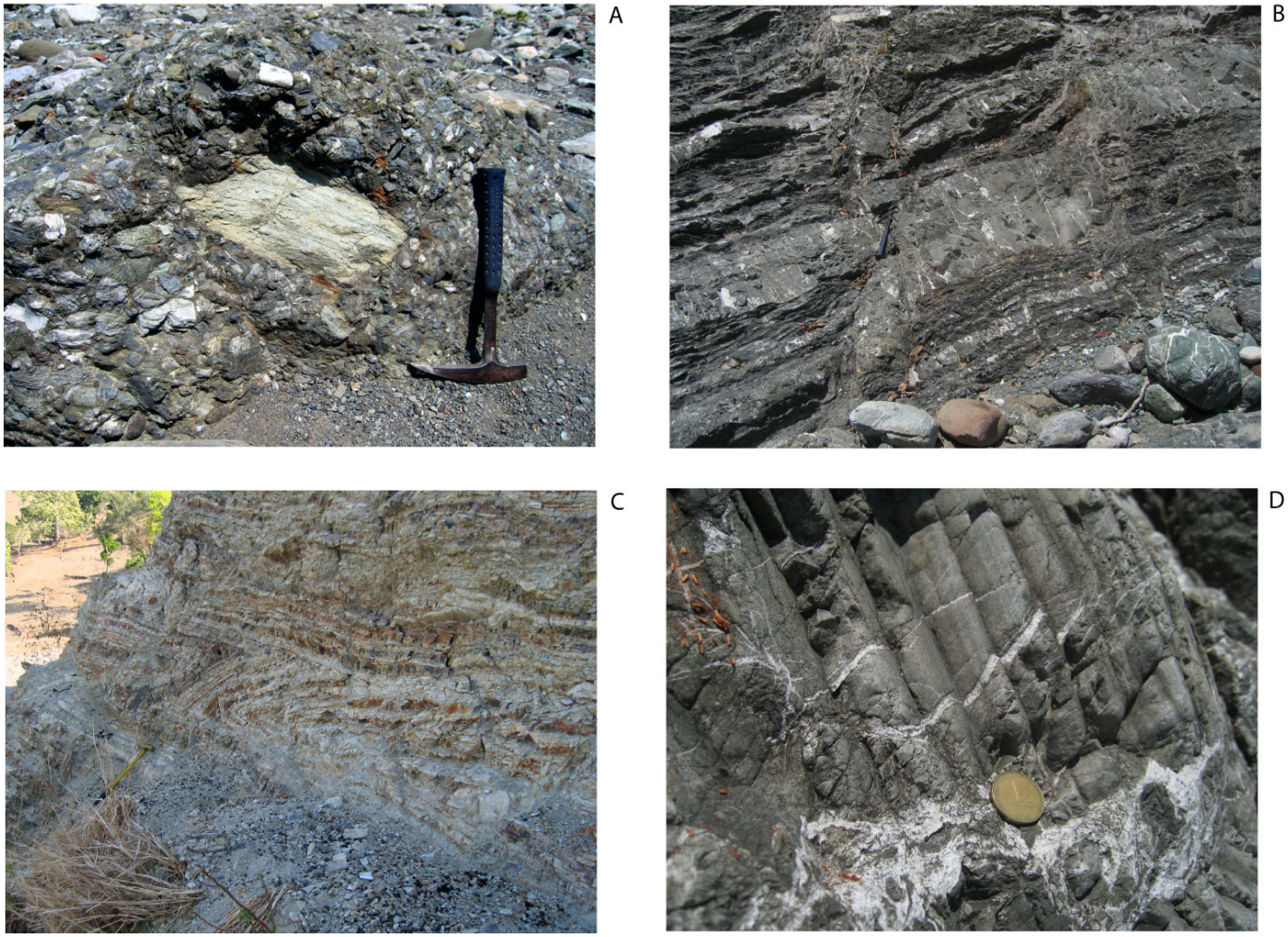

Figure36 A) Conglomerates of the Haulasi formations containing clasts of metamorphic, igneous, and carbonate rocks. B) South directed normal fault in Haulasi Formation sandstone. C) Outcrop of folded Palelo Group Noni Formation cherts and carbonates near at the base of the Mata Bia massif. D) Noni formation graded sandstones with near layer perpendicular pressure solution or movement along bedding planes.

CONCLUSION

Before this investigation there was considerable uncertainty about the age and origin of the Lolotoi Complex and its relation to other metamorphic units in Timor, such as the Mutis and Aileu Complexes and crystalline basement of Australia. Conclusions regarding the origin, structure and tectonic history of the metamorphic rocks in East Timor previously were made solely by either association with the Mutis Complex in West Timor or speculation. This study provides the first constraints needed to address these questions.

Petrologic analysis of Lolotoi metamorphic rocks suggests a sedimentary origin with original deposition of interlayered volcanogenic pelitic sediments (shales-graywackes) and volcanic deposits (basaltic to basaltic andesite compositions). Sedimentation of at least some of the protolith material must have taken place after the 80 Ma U/Pb age from zircons present in an amphibolite found at deep structural levels.

Provenance data obtained from discriminant diagrams, based on major and trace element whole rock geochemistry, indicates mixed MORB and volcanic arc affinities. These tectonomagmatic signatures are indicative of magma mixing associated with development of marginal and back arc basins. Evidence of arc splitting caused by slab rollback and later development of marginal and backarc basins such as the Banda Sea explain the MORB affinity provenance data. The volcanic and sedimentary protoliths are interpreted to have been deposited in a proximal forearc position on the southern edge of the eastern Great Indonesian arc before it collapsed to form the Banda arc.

Metamorphism is attributed to tectonic and sedimentary burial of sedimentary and volcanic rocks to pressures of up to 6-8 kbar with peak temperatures of 530 °C to 650 °C,

as shown by garnet-biotite geothermometry, GASP geobarometry and amphibole geothermobarometry. Metamorphic assemblages are consistent with medium pressure-temperature amphibolite and upper greenschist facies metamorphism.

The age of peak metamorphism is 45-46 Ma as indicated by Lu-Hf age analyses of monometamorphic garnets. Rocks were exhumed relatively quickly to above the partial annealing zone of apatite (150 °C to 100 °C) at a maximum of 41 Ma, then to the surface where they were overlain by shallow water Eocene to Oligocene carbonate. Extensional exhumation most likely contributed to the rapid ascent of the metamorphic rocks to the surface as demonstrated by large-displacement normal faults that juxtapose cover units with the Lolotoi Complex. This extensional event is likely related to slab rollback of the Australian/Indian plate. Continued slab rollback through this period resulted in the onset of suprasubduction zone seafloor spreading and marginal basin formation, which attenuated and dispersed the Great Indonesian arc-forearc and created new accommodation space for sediment deposition.

Eocene carbonates and volcanic units, and the Cablac Limestone were deposited over the Lolotoi Complex, which experienced burial temperatures of 120 to 140 °C as predicted by apatite fission-track modeling. Continued growth of the Banda Sea transported the Lolotoi and its cover units (Banda Terrane) southward and eastward until it was captured in the forearc of the Banda Arc. At around 3 Ma the NW continental margin of Australia clogged the subduction channel beneath the Banda Terrane, resulting in the present arc-continent collision. Collision initiated a period of rapid uplift of the Lolotoi Complex as indicated by the lack of any new 18 micron fission tracks.

Structural analyses and observations of contact relationships show that during tectonic emplacement, the Lolotoi Complex was thrust over Gondwana Sequence units of the Australian continental margin as evidenced by extensive outcrops of mélange and broken formation at the structural base of the Banda Terrane. This phase of deformation is recorded in the Banda Terrane by parallelism between the orientations and vergence directions of the structurally underlying Gondwana Sequence and overlying Banda Terrane thrust sheets. Thrust faulting, fold vergence, foliation orientations, and fracture orientations all show a dominant sigma 1 orientation that is perpendicular to the present orogenic front. Continued underthrusting of Gondwana Sequence units uplifted the Banda Terrane from a forearc basement position to higher than 2000 meters elevation in places. Erosion has removed much of the once continuous metamorphic terrane leaving only isolated klippen. Overlying Asian affinity Palelo Group, Metan Formation and Cablac Limestone units are extremely attenuated by extension and some post Eocene units lie unconformably on portions of the Lolotoi Complex.

The depositional, compositional, metamorphic, and structural characteristics between the Mutis and Lolotoi Complexes are very similar and thus, they should be regarded as having a closely related origin and tectonic evolution.

REFERENCES

Audley-Charles, M.G., 1968, The Geology of Portuguese Timor: Geological Society of London Memoirs, 4, 76.

Audley-Charles, M.G. and Carter, D.J., 1972, Palaeogeographical significance of some aspects of Paleogene and Early Neogene stratigraphy and tectonics of the Timor Sea region: Palaeogeography, Palaeoclimatology and Palaeoecology, v. 11, p. 247-264.

Audley-Charles, M.G. and Harris, R. A., 1990, Allochthonous terranes of the Southwest Pacific and Indonesia: Philosophical Transactions of the Royal Society of London, v. 331, p. 571-587.

Banno, S., Sakai, C., Higashino, T., 1986, Pressure-temperature trajectory of the Sanbagawa metamorphism deduced from garnet zoning: Lithos, v. 19, p. 51-63.

Barber, A.J. and Audley-Charles, M.G., 1976, The significance of the metamorphic rocks of Timor in the development of the Banda Arc, eastern Indonesia: Tectonophysics, v. 30, p. 119-128.

Barber, A. J., 1981, Structural interpretations of the island of Timor, eastern Indonesia: Geological research and development centre special publication, v. 2, p. 183-197.

Berry, R.F., and Grady, A.E., 1981, Deformation and metamorphism of the Aileu Formation, north coast, East Timor, and its tectonic significance: Journal of Structural Geology, v. 3, p. 143-167.

Berry, R.F., and McDougall, I., 1986, Interpretation of (super 40) Ar/ (super 39) Ar and K/Ar dating evidence from the Aileu Formation, East Timor, Indonesia: Chemical Geology; Isotope Geoscience Section, v. 59, no. 1, p. 43-58.

Bhatia, M.R., 1983, Plate tectonics and geochemical composition of sandstones: Journal of Geology, v. 91, p. 611-627.

Bhatia, M.R., and Crook, K.A.W., 1986, Trace element characteristics of graywackes and tectonic setting discrimination of sedimentary basins: Contributions to Mineralogy and Petrology, v. 92, no. 2, p. 181-193.

Blichert-Toft, J., 2001, On the Lu-Hf isotope geochemistry of silicate rocks: Geostandards Newsletter, vol. 25, no. 1, p. 41-56.

Brown, M., and Earle, M.M., 1983, Cordierite-bearing schists and gneisses from Timor, eastern Indonesia: P-T implications of metamorphism and tectonic implications: Journal of Metamorphic Geology, v. 1, p. 183-203.

Cabanis, B., and Lecolle, M., 1989, Le diagramme La/10-Y/15-Nb/8; un outil pour la discrimination des series volcaniques et la mise en evidence des processus de melange et/ou de contamination crustale. The La/10-Y/15-Nb/8 diagram; a tool for distinguishing volcanic series and discovering crustal mixing and/or contamination: Comptes Rendus de l'Academie des Sciences, Serie 2, Mecanique, Physique, Chimie, Sciences de l'Univers, Sciences de la Terre, v. 309, no. 20, p. 2023-2029.

Carter, D.J., Audley-Charles, M.G., and Barber, A.J., 1976, Stratigraphical analysis of island arc-continental margin collision in eastern Indonesia: Geological Society of London, v. 132, p. 179-198.

Chamalaun, F.H. and Grady, A.E., 1978, The tectonic evolution of Timor: A new model and its implications for petroleum exploration: Journal of the Australian Petroleum Exploration Association, v. 18, p. 102-108.

Chang, Z., Vervoort, J.D., McClelland, W.C., and Knaack, C., 2006, U-Pb dating of zircon by LA-ICP-MS: Geochemistry, Geophysics, Geosystems, v. 7, no. 5, p. 1-14.

Charlton, T. R., 2002, The structural setting and tectonic significance of the Lolotoi, Laclubar and Aileu metamorphic massifs, East Timor: Journal of Asian Earth Sciences, v. 20, p. 851-865.

de Roever, W.P., 1940, Geological Investigation in the Southwestern Moetis Region (Netherlands Timor) [Ph.D Thesis]: University of Amsterdam, 244 p.

de Waard, D., 1954a, Contributions to the geology of Timor 2; The orogenic main phase in Timor: Indonesian Journal of Natural Science, v. 110, p. 9-20.

de Waard, D., 1954b, Contributions to the Geology of Timor 5. Structural developments of the crystalline schists in Timor, tectonics of the Lalan Asu massif: Indonesian Journal for Natural Science, v. 110, p. 143-153.

de Waard, D., 1957, Zones of regional metamorphism in the Lalan Asu massif, Timor: K. Nederl. Akad. Wetens. v. 60, no. 5, p. 383-392.

de Waard, D., 1959, Anorthite content of plagioclase in basic and pelitic crystalline schists as related to metamorphic zoning in the Usu massif, Timor: American Journal of Science, v. 257, p. 553-562.

Donnelick, R.A., O'Sullivan, P.B., and Ketcham, R.A., 2005, Apatite Fission-Track Analysis, *in* Reiners, P.W., and Ehlers T.A., eds., Low-Temperature Thermochronology: Techniques, Interpretations, and Applications: Virginia, The Mineralogical Society of America, v. 58 p. 48-94.

Earle, M.M., 1980, A Study of Boi and Mollo, Two Metamorphic Massifs on Timor, Eastern Indonesia. [Ph.D Thesis]: University of London, 240 p.

Earle, M.M., 1981, The metamorphic rocks of Boi, Timor, eastern Indonesia, *in* Barber A.J., and Wiryosujono S., eds., The Geology and Tectonics of Eastern Indonesia, GRDC Special Publicatin 2, p. 239-251.

Fleischer, R.L., Price, P.B., and Walker, R.M., 1964, Fission Track Ages of Zircons: Journal of Geophysical Research, v. 69, p. 4885-4888.

Floyd, P.A., and Winchester, J.A., 1975, Magma type and tectonic setting discrimination using immobile elements: Earth and Planetary Science Letters, v. 27, no. 2, p. 211-218.

Genrich, J.F., Bock, Y., McCaffrey, R., Calais, E., Stevens, C.W., and Subarya, C., 1996, Accretion of the southern Banda Arc to the Australian Plate margin determined by Global Positioning System measurements: Tectonics, v. 15, no. 2, p. 288-295.

Gerya, T.V., Perchuk, L.L., Audren, C., and Sez'ko, A.I., 1997, Petrology of the Tumanshet zonal metamorphic complex, eastern Sayan: Petrology, v. 5, no. 6, p. 503-533.

Grady, A. E., 1975, A reinvestigation of thrusting in Portuguese Timor: Journal of the Geological society of Australia, v. 22, p. 223-227.

Grady, A. E., and Berry, R. F., 1977, Some Paleozoic-Mesozoic stratigraphic-structural relationships in East Timor and their significance to the tectonics of Timor: Journal of the Geological Society of Australia. v. 24, p. 203-214.

Haile, H.S., Barber, A.J., Carter, D.J., 1979, Mesozoic cherts on crystalline schists in Sulawesi and Timor: Geological Society of London. v. 136, p. 65-70.

Harris, R.A., 1991, Temporal distribution of strain in the active Banda orogen: a reconciliation of rival hypotheses: Journal of Southeast Asian Earth Sciences, v. 6, p. 373-386.

Harris, R.A., 1992, Peri-collisional extension and the formation of Oman-type ophiolites in the Banda Arc and Brooks Range, *in* Parson, L.M. Murton, B.J. and Browning, eds., Ophiolites and their Modern Oceanic Analogues: Geological Society of London Special, Publication, v. 60, p. 301-325.

Harris, R.A., Sawyer, R.K., and Audley-Charles, M.G., 1998, Collisional mélange development: Geologic associations of active mélange-forming processes with exhumed mélange facies in the western Banda orogen, Indonesia, v. 17, p. 458-479.

Harris, R.A., and Long, T., 2000, The Timor ophiolite, Indonesia: Model or myth?, *in* Dilek, Y., Moores, E.M., Elthon, D., and Nicolas, A., eds., Ophiolites and Oceanic Crust: New Insights from Field Studies and the Ocean Drilling Program: Geologic Society of America Special Paper, v. 349, p. 321-330.

Harris, R.A., Kaiser, J., Hurford, A., and Carter, A., 2000, Thermal history of Australian passive margin cover sequences accreted to Timor during Late Neogene arc-continent collision, Indonesia: Journal of Asian Earth Science, v. 18, p. 47-69.

Harris, R.A., 2004, Geodynamic patterns of ophiolites and marginal basins of the Indonesian and New Guinea regions, *in* Dilek, Y., and Robinson, P.T., eds., "Ophiolite in Earth History", Geological Society of London Special Publication, v. 218, p. 481-505.

Harris, R., 2006, Rise and fall of the Eastern Great Indonesian arc recorded by the assembly, dispersion and accretion of the Banda Terrane, Timor: Gondwana Research, v. 10, p. 207-231.

Hawkins, J.W., and Allan, J.F., 1994, Petologic evolution of Lau Basin Sites 834 through 839, *in* Hawkins, J., Parson, L., Allan, J., eds., Proceedings of the Ocean Drilling Program, Scientific Results, v. 135, p. 427-470.

Hawkins, J.W., 1995, The geology of the Lau Basin, *in* Taylor, B., ed., Backarc Basins: Tectonics and Magmatism, New York, Plenum Press, 523 p.

Johnston, C.R., and Bowin, C.O., 1981, Crustal reactions resulting from the mid-Pliocene to recent continent-island arc collision in the Timor region: Journal of Australian geology and geophysics. v. 6, p. 223-243.

Jenner, G.A., Cawood, P.A., Rautenschlein, M., and White, W.M., 1987, The geochemistry of the Lower Proterozoic Willyama Complex volanics, Broken Hill Block, New South Wales: Geological Society of London Special Publications, v. 33, p. 395-408.

Jovilet, L., Faccenna, C., D'Agostino, N., Fournier, M., and Worrall, D., 1999, The Kinematics of back-arc basins, examples from the Tyrrhenian, Aegean and Japan Seas, *in* Mac Niocaill, C., and Ryan, P.D., eds., Continental Tectonics, London, Geological Society, Special Publication, 341 p.

Kleemann, U., and Reinhardt, J., 1994, Garnet-biotite thermometry revisited; the effect of Al (super VI) and Ti in biotite: European Journal of Mineralogy, v. 6, no. 6, p. 925-941.

Kohn M.J., and Spear, F., 2000, Retrograde net transfer reaction insurance for pressure-temperature estimates: Geology, v. 28, no. 12, p. 1127-1130.

Leake, B.E., 1997, Nomenclature of Amphiboles: Report of the Subcommittee on Amphiboles of the International Mineralogical Association, Comminssion on new Minerals and Mineral Names: American Mineralogist, v. 82, no. 9-10, p. 1019-1037.

LeBas, M.J., LeMaitre, R.W., Streckeisen, A.L., and Zanettin, B., 1986, A chemical classification of volcanic rocks based on the total alkali-silica diagram: Journal of Petrology, v. 27, p. 745-750.

Macdonald, G.A., 1968, Composition and origin of Hawaiian lavas, *in* Coats, R.R., Hay, R.L., and Anderson, C.A., eds., Studies in volcanology: a memoir in honor of Howel Williams: Geological Society of America Memoir, v. 116, p. 477-522.

McDonough, W.F., Sun, S.-s., 1995, The composition of the Earth: Chemical Geology, v. 120 p. 223-253.

Maillet, P., Ruellan, E., Gerard, M., Person, A., Bellon, H., Cotton, J., Joron, J.-E., Nakada, S., and Price, R., 1995, Tectonics, Magmatism and Evolution of the New Hebrides Backarc Troughs (Southwest Pacific), *in* Taylor, B., ed., Backarc Basins: Tectonics and Magmatism, New York, Plenum Press, 523 p.

Meschede, M., 1986, A method of discriminating between different types of mid-ocean ridge basalts and continental tholeiites with the Nb-Zr-Y diagram: Chemical Geology, v. 56, no. 3-4, p. 207-218.

Mezger, K., 1990, Geochronology in granulites, *in* Vielzeuf, D., and Vidal, P., eds., Granulites and crustal evolution: NATO ASI Series C: Mathematical and Physical Sciences, v. 311, p. 451-470.

Mullen, E.D., 1983, MnO/TiO (sub 2) /P (sub 2) O (sub 5); a minor element discriminant for basaltic rocks of oceanic environments and its implications for petrogenesis: Earth and Planetary Science Letters, v. 62, no. 1, p. 53-62.

Naeser, C.W., 1976, Fission-track dating: U.S. Geological Survey Open-File Report 76-190, 65 p.

Naeser, C.W., 1979 Fission-track dating and geologic annealing of fission tracks. *in* Jager, E., and Hunziker, J.C., eds., Lectures in Isotope Geology: New York, Springer Verlag, p. 154-169.

Naeser, C.W., and Dodge, F.C.W., 1969, Fission-Track Ages of Accessory Minerals from Granitic Rocks of the Central Sierra Nevada Batholith, California: Bulletin of the Geological Society of America, v. 80. p. 2201-2212.

Naeser, N.D., Naeser, C.W., and McCulloh, T.H., 1989, The Application of Fission-Track Dating to the Depositional and Thermal History of Rocks in Sedimentary Basins, *in* Naeser, N.D., McCulloh, T.H., eds., Thermal History of Sedimentary Basins: New York, Springer-Verlag, p. 157-180.

Newton, R.C., and Haselton, H.T., 1981, Thermodynamics of the garnet-plagioclase-Al (sub 2) SiO (sub 5) – quartz geobarometer, *in* Saxena, S.K., ed., Thermodynamics of minerals and melts: New York, Springer-Verlag.

Nugroho, H., 2005, GPS Velocity Field in the transition from subduction to collision of the Eastern Sunda and Banda Arcs, Indonesia. Unpublished Masters Thesis, Brigham Young University.

Patchett, P.J., and Tatsumoto, M., 1980, A routine high precision method for Lu-Hf isotope geochemistry and chronology: Contributions to Mineral Petrology, v. 75, p. 263-267.

Patchett, P.J., and Ruiz, J., 1987, Nd isotopic ages of crust formation and metamorphism in the Precambrian of eastern and southern Mexico: Contributions to Mineral Petrology, v. 75, p. 523-528.

Pearce, J.A., 1982, Trace element characteristics of lavas from destructive plate boundaries. *in* Thorpe, R.S., ed., Andesites, Wiley, Chicchester, p. 525-548.

Pearce, J.A., 1983, Role of the sub-continental lithosphere in magma genesis at active volcanic rocks: Volcanology and Geothermal Research, v. 32, p. 51-65.

Pearce, J.A., and Cann, J.R., 1971, Ophiolite origin investigated by discriminant analysis using Ti, Zr, and Y: Earth and Planetary Science Letters, v. 12, 339-349.

Pearce, J.A., and Cann, J.R., 1973, Tectonic setting of basic volcanic rocks determined using trace element analyses: Earth and Planetary Science Letters, v. 19, no. 2, p. 290-300.

Pearce, J.A., and Gale, G.H., 1977, Identification of ore-deposition environment from trace-element geochemistry of associated igneous host rocks: Joint meeting of the Geological Society of London, Volcanic Studies Group, Institution of Mining and Metallurgy, London.

Pearce, J.A. and Norry, M.J., 1979, Petrogenetic implications of Ti, Zr, Y and Nb variations in volcanic rocks: Contributions to Mineralogy and Petrology, v. 69, no. 1, p. 33-47.

Pearce, J.A., Ernewein, M., Bloomer, S.H., Parson, L.M., Murton, B. J., and Johnson, L.E., 1994, Geochemistry of Lau Basin volcanic rocks: Geological Society of London Special Publications, v. 76 p. 373-403.

Pearce, J.A., 1996, A Users Guide to Basalt Discrimination Diagrams, *in* Wyman, D.A., ed., Trace Element Geochemistry of Volcanic Rocks: Applications for Massive Sulfide Exploration: Geological Association of Canada, Short Course Notes, v. 12, p. 79-113.

Pearce T.H., Gorman, B.E., and Birkett, T.C., 1975, The TiO2-K2O-P2O5 diagram: A method of discriminating between oceanic and non-oceanic basalts: Earth and Planetary Science Letters, v. 24, p. 419-426.

Pearce, T.H., Gorman B.E., and Birkett, T.C., 1977, The relationship between major element chemistry and tectonic environment of basic and intermediate volcanic rocks: Earth and Planetary Science Letters, v. 36, p. 121-132.

Prasetyadi, C., and Harris, R.A., 1996, Hinterland structure of the active Banda arc-continent collison, Indonesia: constraints from the Aileu Complex of East Timor. Proc. 25th Conv. Indonesian Association of Geology, p. 144-173.

Rollinson, H., 1993, Using geochemical data: evaluation, presentation, interpretation: Longman Sigamore Publishers, England, 352 p.

Roser, B.P., and Korsch, R.J., 1986, Determination of tectonic setting of sandstone-mudstone suites using SiO (sub 2) content and K (sub 2) O/Na (sub 2) O ratios: Journal of Geology, v. 94, no. 5, p. 635-650.

Roser, B.P., and Korsch, R.J., 1988, Provenance signatures of sandstone-mudstone suites determined using discriminant function analysis of major-element data: Chemical Geology, v. 67, no. 1-2, p. 119-139.

Saunders, A.D., and Tarney, J., 1979, The geochemistry of basalts from a back-arc spreading centre in the East Scotia Sea: Geochimica et Cosmochimica Acta, v. 43, p. 555-572.

Sguigna, A.P., Larabee, A.J. and Waddington, J.C., 1982, The half-life of 176Lu by a y-y coincidence measurement: Canadian Journal of Physics, v. 60, p. 361-364.

Shervais, J.W., 1982, Ti-V plots and the petrogenesis of modern and ophiolitic lavas: Earth and Planetary Science Letters, v. 59, no. 1, p. 101-118.

Sopaheluwakan, J., Helmers, H., Tjokrosapoetro, S., and Surya, N.E., 1989. Medium pressure metamorphism with inverted thermal gradient associated with ophiolite emplacement in Timor: Neatherlands Journal of Sea Research, v. 24, no. 2-3, p. 333-343.

Sopaheluwaken, J., 1990, Ophiolite obduction in Mutis Complex, Timor, Eastern Indonesia: An example of Inverted, Isobaric, Medium-High Pressure metamorphism. [PhD Thesis]: Amsterdam, Free University.

Sun, S., and McDonough, W.F., 1989, Chemical and isotopic systematics of oceanic basalts: Implications for mantle composition and processes, *in* Saunders, A.D., Norry, M.J., eds., Magmatism in the ocean basins, Boston, Blackwell Scientific, p. 313-345.

Sopaheluwakan, J., 1991, The Mutis metamorphic complex of Timor: A new view on the origin and its regional consequences: Proceedings of the Indonesian Association of Geologists, Twentieth annual convention.

Tappenbeck, D., 1939, Geologiedes Mollogebirges und Einiger Benachbanen Gebiete (Niederlandisch Timor). [Ph.D. Thesis]: Amsterdam.

Tatsumi, Y., and Kogisu, T., 2003, The subduction factory: its role in the evolution of the Earth's crust and mantle, *in* Larter, R.D., Leat, P.T., eds., Intra-Oceanic Subduction Systems: Tectonic and Magmatic Processes. Geological Society, London, special publication, v. 219, p. 55-80.

Taylor, S.R., and McClennen, S.M., 1985, The Continental Crust: its Composition and Evolution, Oxford, Blackwell Scientific, 312 p.

Winchester, J.A., and Floyd, P.A., 1976, Geochemical magma type discrimination; application to altered and metamorphosed basic igneous rocks: Earth and Planetary Science Letters, v. 28, no. 3, p. 459-469.

Wu, C.-M., and Cheng, B.-H., 2005, Valid garnet-biotite (GB) geothermometry and garnet-aluminum silicate-plagioclase-quartz (GASP) geobarometry in metapelitic rocks: Lithos, In press.

van Bemmelen, R.W., 1949, The Geology of Indonesia: General Geology of Indonesia and Adjacent Archipelgoes. Special Edition Indonesia Bur. Mines, Batavia.

van West, F.P., 1941, Geological investigations in the Miomaffo region [Ph.D. Thesis]: Amsterdam.

Vervoort, J.D., and Patchett, P.J., 1996, Behavior of halfnium and neodymium isotopes in the crust: Constraints from Precambrian crustally derived granites: Geochim. Cosmochim. Acta, v. 60, p. 3717-3733.

Vervoort, J.D. and Blichert-Toft, J., 1999, Evolution of the depleted mantle: Hf isotope evidence from juvenile rocks through time: Geochim. Cosmochim. Acta, v. 63, p. 533-556.

Vervoort, J.D., Patchett, J.P., and Soderlund, U., 2004, Isotopic composition of Yb and the determination of Lu concentrations and Lu/Hf rations by isotope dilution using MC-ICPMS: Geochemistry, Geophysics, Geosystems, v. 5, no. 11, p. 1-15.

Appendix I: List of Samples, Rock Types, Sample Locations, Analyses Performed, and Thin Section Descriptions

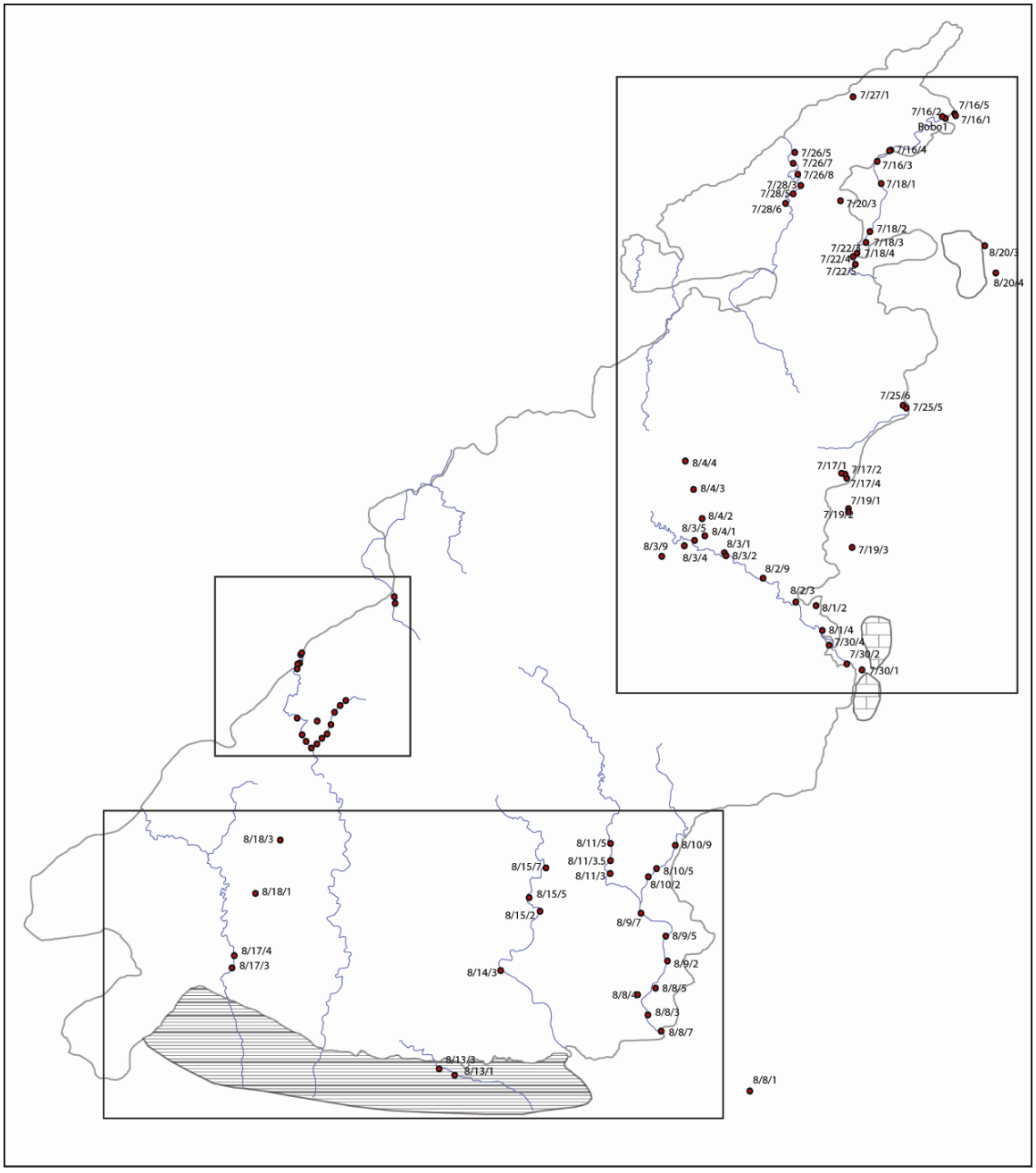

A) Sample Locations in the Bebe Susu massif

B) List of Samples, Rock Types, Locations and Analyses Performed

Sample #	Unit	Rock Type	Location	Lat (S)	Long (E)	Elev (m)	Analyses performed
7-16-1	Lolotoi Igneous	Altered Volcanic Breccia	Bobo River	S8.61608	E125.96693	237.1 m	TS,
7-16-2	Lolotoi Igneous	Igneous Dike, fine grained	Bobo River	S8.61726	E125.96311	182.5 m	ME, TE, TS
7-16-3	Palelo	Calcarenite	Bobo River	S8.63379	E125.93681	163.1 m	
7-16-4	Lolotoi Igneous	Altered Ultramafic	Bobo River	S8.62946	E125.94158	1064.8	ME, TE, TS
7-16-5	Lolotoi Igneous	Metatuff-Greenstone.	Bobo River	S8.61530	E125.96664	1094.6	ME, TE,
7-17-2	Lolotoi	Quartz-Graphite phyllite	Near Laclubar	S8.75526	E125.92406	1180.4	ME, TE, TBE
7-17-4	Lolotoi	Quartz-mica schist	Near Laclubar	S8.75698	E125.92473	1250.3	ME, TE, TS
7-18-1	Lolotoi Igneous	Ultramafic, altered to serpentine	Bobo River	----	----	----	----
7-18-2	Lolotoi	Amphibolite	Bobo River	----	----	----	----
7-18-3	Lolotoi	Graphite-quartz phyllite	Bobo River	----	----	----	----
7-18-4	Lolotoi	Epidote-Chlortie greenschist	Bobo River	----	----	----	----
7-19-1	Lolotoi	Altered Greenschist	Road to Soibada	S8.76869	E125.92536	1168.4	
7-19-2	Lolotoi Igneous	Igneous breccia	Road to Soibada	S8.76931	E125.92543	174.6 m	ME, TE, TS
7-19-3	Palelo	Carbonate cemented breccia	Road to Soibada	S8.78368	E125.92676	222.7 m	----
7-20-3	Palelo	Meta Calc Arenite	Ue Taur River	S8.64906	E125.92228	505.8 m	ME, TE, TS
7-22-4	Lolotoi	Greenschist	Bobo River	S8.67077	E125.92721	354.8 m	ME, TE,
7-22-3	Maubisse	Maubisse Limestone	Bobo River	S8.66933	E125.92882	366.4 m	----
7-22-5	BT Igneous	Lherzolite	Bobo River	S8.67073	E125.92731	290.0 m	ME, TE, TS
7-25-5	Lolotoi Igneous	Volcanic breccia	Sumasse River	S8.72946	E125.94799	205.8 m	TS,
7-25-6	Lolotoi Igneous	Graphitic Greenschist	Sumasse River	S8.72860	E125.94668	759.6 m	----
7-26-5	Lolotoi	Graphitic Greenschist	Ue Coi River	S8.63026	E125.90454	237.6 m	----
7-26-7	Lolotoi	Quartz-mica schist, garnet bearing	Ue Coi River	S8.63464	E125.90392	166.2 m	TS,
7-26-8	Palelo	Sed., with carbonate. and meta clasts	Ue Coi River	S8.63774	E125.90545	126.5 m	TS,
7-27-1	Lolotoi Igneous	Ultramafic altered to serpentine	Limestone Fensters	S8.60872	E125.92725	474.3 m	ME, TE, TS
7-28-3	Lolotoi	Green Amphibolite	Ue Coi River	S8.64076	E125.90570	279.6 m	TS,
7-28-5	Lolotoi	Greenschist	Ue Coi River	S8.64642	E125.90390	325.8 m	----
7-28-6	Lolotoi	Quartz and Calcite rich	Ue Coi River	S8.65007	E125.90282	274.1 m	ME, TE,
7-30-1	Palelo	Oolitic grainstone	Buarahum River	S8.83111	E125.93072	596.6 m	----
7-30-2	Lolotoi	Garnet-mica schist	Buarahum River	S8.82877	E125.92483	581.2 m	----
7-30-04	Lolotoi Igneous	Ultramafic, orthopyroxene rich	Buarahum River	S8.81599	E125.91529	616.6 m	ME, TE, TS,
8-01-2	Palelo	Foraminifera packstone	Buarahum River	S8.80626	E125.91277	605.3 m	TS,
8-01-4	Lolotoi Igneous	Gabbro	Buarahum River	S8.80486	E125.91372	637.0 m	TS,

B) List of Samples, Rock Types, Locations and Analyses Performed (continued)

Sample	Unit	Rock Type	Location	Lat (S)	Long (E)	Elev (m)	Analyses performed
8-02-9	Lolotoi	Fe rich conglomerate meta and volcanic	Buarahum River	S8.79193	E125.88520	679.1 m	----
8-02-3	Lolotoi	Quartz mica schist	Buarahum River	S8.80490	E125.90499	655.3 m	----
8-3-1	Lolotoi	Amphibolite schist	Buarahum River	S8.78577	E125.87725	844.4 m	ME, TE, TS, TBE, PT
8-3-2	Lolotoi	Garnet-mica schist	Buarahum River	S8.78473	E125.87228	748.7 m	ME, TE, TS, TBE, Hf/Lu, PT
8-3-4	Lolotoi	Quartz-Chlorite-muscovite schist	Buarahum River	S8.78433	E125.86699	887.4 m	ME, TE, TBE
8-3-5	Lolotoi	Garnet Amphibolite	Buarahum River	S8.78120	E125.86560	842.7 m	ME, TE, TS, TBE, Hf/Lu, PT
8-3-9	Lolotoi	Amphibolite	Buarahum River	S8.78718	E125.85282	1274.8	ME, TE, TS, TBE, U/Pb, PT
8-4-1	Lolotoi	Blue-Green Amphibolite	Mtns Above Buarahum	S8.77920	E125.86955	1402.9	TS, TBE, PT
8-4-2	Lolotoi	Green Amphibolite	Mtns Above Buarahum	S8.77258	E125.86874	1366.1	ME, TE, TS
8-4-3	Lolotoi	Altered sample	Mtns Above Buarahum	S8.76123	E125.86520	1395.5	----
8-4-4	Lolotoi	Green Amphibolite	Mtns Above Buarahum	S8.75013	E125.86196	1376.5	ME, TE, TS, TBE, PT
8-8-1		Batu Puti chalk	Clere (Cleric) River	S8.99474	E125.88718	171.0 m	----
8-8-4	Lolotoi	Graphitic phyllite	Clere (Cleric) River	S8.95728	E125.84353	201.5 m	----
8-8-5	Lolotoi	Greenschist	Clere (Cleric) River	S8.95482	E125.85049	243.3 m	ME, TE, TS
8-8-7	Lolotoi	Green amphibolite	Clere (Cleric) River	S8.96515	E125.84760	237.6 m	TS, TBE, PT
8-9-2	Palelo	Foraminifera packstone	Clere (Cleric) River	S8.94428	E125.85509	244.3 m	----
8-9-5	Palelo	Calc arenite	Clere (Cleric) River	S8.93453	E125.85438	277.0 m	ME, TE, TS
8-9-7	Maubisse	Maubisse breccia	Clere (Cleric) River	S8.92576	E125.84487	136.6 m	----
8-10-2	Lolotoi	Chlorite rich Greenschist	Quicleten River (Rt	S8.91151	E125.84782	273.1 m	ME, TE,
8-10-9	Maubisse	Maubisse Limestone	Quicleten River	S8.90836	E125.85078	360.4 m	----
8-10-5	Palelo	Very fine grained, layered	Quicleten River	S8.89700	E125.85872	265.7 m	ME, TE, TS, TBE
8-11-3	Lolotoi	Quartz-mica-garnet schist	Left Fork Clere River	S8.91029	E125.83280	360.4 m	----
8-11-3.5	Palelo	Fine grained palelo	Left Fork Clere River	S8.91029	E125.83280	360.4 m	ME, TE,
8-11-5	Lolotoi	Garnet-mica schist	Left Fork Clere River	S8.89858	E125.83291	253.4 m	ME, TE, TS, TBE, PT
8-13-1	Lolotoi Igneous	Volcanic conglomerate	Maran River	S8.98849	E125.77260	246.2 m	ME, TE, TS
8-13-3	Palelo	Foraminifera packstone	Maran River	S8.98608	E125.76650	327.0 m	TS,
8-14-3	Lolotoi Igneous	Serpentinite	Laclo de sur River	S8.94795	E125.79035	292.4 m	ME, TE,
8-15-2	Lolotoi	Serpentinized fault breccia	Laclo de sur River	S8.92491	E125.80565	393.8 m	ME, TE,
8-15-5	Lolotoi	Greenstone	Laclo de sur River	S8.90867	E125.80829	52.5 m	ME, TE, TS
8-15-7	Lolotoi	Greenstone	Laclo de sur River	S8.90823	E125.80795	348.8 m	----
8-17-3	Palelo	Lithic Arenite	Caraulun River	S8.95519	E125.68348	366.9 m	TS,
8-17-4	Lolotoi	Greenstone breccia	Caraulun River	S8.94689	E125.68599	320.2 m	ME, TE,

B) List of Samples, Rock Types, Locations and Analyses Performed (continued)

Sample #	Unit	Rock Type	Location	Lat (S)	Long (E)	Elev (m)	Analyses performed
8-18-1	Lolotoi	Greenstone	Caraulun Trail to Turiscai	S8.91794	E125.69504	1113.1	ME, TE,
8-18-3	Lolotoi	Quartz-mica-graphite schist	Caraulun Trail to Turiscai	S8.89729	E125.70466	1208.7	----
8-20-3	Lolotoi	Greenstone and breccia from float	Seperated Block of BT	----	----	----	----
8-20-4	Maubisse	Crinoidal limestone	Seperated Block of BT	----	----	----	----
8-21-4	Palelo	Massive limestone		S8.66653	E125.97824	971.3 m	
Clere River	Lolotoi	Quartz-mica-schist	Clere River	Float	Float	----	TS,
F1-1	Lolotoi	Mica rich-garnet schist	Soibada River	Float	Float	----	ME, TE, TS, PT
SF-2	Lolotoi	Garnet-mica schist	Soibada River	Float	Float	----	ME, TE, TS, Hf/Lu, TBE, PT
SF-3	Lolotoi	Garnet-mica schist	Soibada River	Float	Float	----	ME, TE, TS
SF-4	Lolotoi	Garnet-mica schist	Soibada River	Float	Float	----	
SF-5	Lolotoi	Garnet-mica schist	Soibada River	Float	Float	----	
Alt. Floats 1	Lolotoi	Igneous texture, amphibole rich	Sumasse?	Float	Float	----	
Alt. Floats 2	Lolotoi	Ultramafic, altered to serpentine	Sumasse?	Float	Float	----	----
Bobo River 1	Lolotoi	Quartz-mica-chlorite greenschist	Bobo River	Float	Float	----	----
Bobo River 2	Lolotoi	Very fine grained greenschist	Bobo River	Float	Float	----	TS,
04T-10	Palelo	Basaltic Trachyte	N. of Matebia	----	----	----	ME, TE,
04T-16	Barique Vol.	Basalt	SW of Bag	----	----	----	ME, TE,
04T-40	Lolotoi	Garnet-mica schist	Mara River	Float	Float	----	ME, TE, TBE
04T-9	Maubisse Vol.	Basalt	Quelicai	----	----	----	ME, TE,
04T-ML0	Lolotoi	Garnet-mica schist	Luca River	Float	Float	----	ME, TE, TS, TBE, Hf/Lu
04T-W51	Lolotoi	----	Same	----	----	----	ME, TE, TS, TBE
04TML2	Lolotoi	Amphibolite	Luca River	----	----	----	----
4T-14	Barique Vol.	Dacitic Tuff	Baguia	----	----	----	ME, TE,
4T-34	Viqueque	Dacitic Tuff	Viqueque	----	----	----	ME, TE,
CUA MC3	Lolotoi	----	Cua River	Float	Float	----	ME, TE,
MD-1	Lolotoi	Quartz-mica schist	Dilor River	Float	Float	----	ME, TE, TS, TBE
MD-2	Lototoi	----	Dilor River	Float	Float	----	ME, TE,
MM-3	Lolotoi	Amphibolite	Mara River	Float	Float	----	PT
MM-2	Lolotoi	Garnet-mica staurolite schist	Mara River	Float	Float	----	ME, TE, TS, TBE
MM-1	Lolotoi	Amphibolite	Mara River	----	----	----	PT
MT-1	Lolotoi	----	Tuca River	Float	Float	----	ME, TE, TS, TBE
MT-3	Lolotoi	Amphibole	Tuca River	S8.964582	E125.652786	----	TS, PT

B) List of Samples, Rock Types, Locations and Analyses Performed (continued)

Sample #	Unit	Rock Type	Location	Lat (S)	Long (E)	Elev (m)	Analyses performed
T3B	----	----	----	----	----	----	ME, TE,
T5	----	----	----	----	----	----	ME, TE, TBE
T5B	----	----	----	----	----	----	ME, TE,
MT-105F-91	Mutis	Metabasalt	Usu	----	----	----	ME, TE, AFT
MT-45-91	----	Coral	----	----	----	----	ME, TE,
MT-48-91	Aileu	Garnet schist	Kisar	----	----	----	ME, TE,
MT-55-91	----	Graphitic phyllite		----	----	----	ME, TE,
MT-99-C	Mutis	----	NW Timor	----	----	----	ME, TE,
04T-70	Palelo	Garnet schist	Same	----	----	----	ME, TE,
MT-112-91	----	Garnet gneiss	Nenas	----	----	----	AFT
MT-44	Aileu	Fine grained igneous	Kisar	----	----	----	AFT
MT-45-1	Aileu	Fine grained igneous	Kisar	----	----	----	AFT
MT-43-5	Aileu	----	Kisar	S8.01.0976	E27	----	AFT
MT-53A	Aileu	Graphytic phyllite	Kisar	S8.06.1520	127.09.3015	----	AFT
MT-64-91	----	Biotite hornblende gneiss	Kisar	----	----	----	AFT
04T-2g	Aileu	Graphitic Schist	Maubara	----	----	----	AFT
04T-67	Lolotoi	Garnet Schist	Caraulun River	----	----	----	AFT
MT-111-91	Mutis	Amphibolite	NW Mutis	----	----	----	AFT
MT106-91	Mutis	Metagabbro	W. Mutis	----	----	----	AFT
Kisar 43	----	----	Kisar	----	----	----	AFT

ME= major element
TE= Trace element
TS= Thin Section
TBE= Tetrabromoethane heavy liquid seperation
AFT= Apatite fission track analysis
Hf/Lu= Halfnium-Luticium age analysis
U/Pb= Uranium-Lead dating
PT= Pressure-Temperature analysis

C) Petrographic Observations

Sample 7-16-1
Igneous Breccia composed primarily of unmetamorphosed altered felsic igneous clasts containing phenocrysts of polysynthetically twinned plagioclase lathes, undulose quartz, chlorite, opaques and altered pyroxene. Some relatively unaltered pyroxene does persist at grain centers. A few grains are altered foliated metamorphic clasts. Extensive alteration to fine grained chlorite in both grain types is common. Matrix material between clasts is composed of finer grained material of similar composition. Secondary calcite veins are present.

Sample 7-16-2
Unmetamorphosed volcanic sample containing quartz, plagioclase, chlorite, and opaques. Very fined grained aphanitic texture. Alteration to chlorite is prolific.

Sample 7-16-4
Altered low-grade metaigneous rock containing large altered clinopyroxene grains up to 0.5 cm in size. Plagioclase, chlorite and quartz are other main phases, though plagioclase is mostly totally altered. A weak foliation does exist as evidenced by partial alignment of finer grained matrix particles between larger igneous grains.

Sample 7-17-4
Quartz-mica schist. Oriented sample, shows microfold vergence to the south. Main mineral constituents include quartz, muscovite, chlorite and plagioclase. Quartz rich and mica rich domains define a S1 foliation parallel to depositional layering. Quartz layers exhibit extensive folding.

Sample 7-19-2
Altered Basalt. Large twinned plagioclase phenocrysts account for 30% of the sample volume. Smaller plagioclase crystals form the majority of the matrix as well. Opaques and chlorite are also present. Blocky calcite is found in sparse large calcite veins

Sample 7-20-3
Meta Calcarenite. Composed of quartz and calcite with abundant calcite veins. Smaller amounts of mica and volcaniclastic grains are also present. Well aligned mica indicates low grade metamorphism, or possibly depositional alignment. Weak banding of quartz rich and calcite rich layers may be depositional as well.

Sample 7-22-5
Ultramafic Lherzolite. Composed of orthopyroxene, clinopyroxene, serpentine, muscovite, chlorite, and opaques. Pyroxene grains are very large, though extensive alteration has occurred. No metamorphic textures are observable. Calcite veins are present.

Sample 7-25-5
Volcanic Breccia. Altered volcanic clasts rich in plagioclase psuedomorphs. No unaltered plagioclase is present. Abundant vesicles are filled with both fibrous and blocky calcite. Alteration to serpentinite is extensive. No metamorphic textures are present.

Sample 7-26-7
Garnet-Quartz-Mica Schist. Main mineral assemblage is quartz, muscovite, biotite, garnet and opaques. Garnets are very sparse, very small in size 2-3 mm and have been significantly resorbed during retrograde reactions. Quartz grains are large compared to other quartz-mica schists. Fine grained micas are well aligned; late growing coarser grained micas are poorly aligned. Microfolds show vergence to the west.

Sample7-26-8
Fossiliferous Limestone dominated by blocky calcite (60%), but also contains whole fossils (20%) including brachiopods, crinoids, foraminifera, and brachiopod spines. Other grains (40%) include foliated quartz-mica schists, quartzite, greenschist. Very few igneous grains also present.

Sample 7-27-1
Altered ultramafic sample with psuedomorphs of pyroxene, olivine and minor Fe-Ti oxides. Highly altered to very fine grained serpentine. No metamorphic textures are observed. Quartz veins are present.

Sample 7-28-3
Amphibolite containing quartz, green amphibole, chlorite, and opaques, and minor sphene and apatite. Interlayers of quartz and green amphibole with chlorite. Gently folded Bands are approximately 5 mm thick. Size of amphiboles is bimodal, with larger porphyroblasts in a matrix of finer grains.

Sample 7-30-1
Oolitic grainstone from the base of Cablac Limstone. Ooids are .5 to 1.5 mm in size. Intergrain areas are filled with sparry calcite and carbonaceous mud. Some pore space is present at grain centers. Calcite veins also are present.

Sample 7-30-4
Altered Harzburgite. Large orthopyroxene grains altered at edges to serpentine. Serpentine alteration is extensive with only large (up to 1cm) pyroxene grains remaining. Unaltered calcite filled fractures are prolific. Modal abundances are pyroxene (30%), serpentine (40%) calcite veins (30%).

Sample 8-1-2
Foraminifera Packstone containing 40% large (up to 1.5 cm) nummulites forams. gastropods and bryzoans are also present (10%) Blocky calcite and mud fill intergrain areas (50%). Calcite veins are also present. Most likely part of the Eocene Dartollu Formation.

Sample 8-1-4
Gabbro. Coarse grained gabbro containing pyroxene, plagioclase, amphibole, opaques and minor chlorite, no quartz is present. Large unaltered interlocked polysynthetically twinned plagioclase grains dominate the sample. No evidence of metamorphism is present

Sample 8-3-1
Amphibolite. Green, fine-grained amphibole (45%), quartz (40%), calcite (10%), opaques, minor muscovite, chlorite, sphene and apatite. Very homogenous, no separate quartz and amphibolite domains have formed. Calcite veins and brittle fractures have formed perpendicular to foliations.

Sample 8-3-2
Garnet-quartz-mica schist. Quartz, biotite, muscovite, garnet, plagioclase (An_{44-52}), opaques, chlorite. Garnets are large, up to 1 cm, some are partly resorbed due to retrograde net transfer reactions, but most are well preserved with strait grain boundaries. Garnets contain very few inclusion and show little evidence of rotation.

Sample 8-3-5
Garnet amphibolite. Quartz (40%), amphibole (20%), chlorite (20%), chalcopyrite (10%) opaques (5%), garnet (5%). Amphibole is coarse grained and blue-green to blue in color. Amphiboles are well aligned and foliations are slightly folded. Garnets are sparse, but up to .5 cm in size. Garnets are relatively inclusion free, with no indications of grain rotation.

Sample 8-3-9
Amphibolite. Amphibole (80%), quartz (15%), opaques (4%), minor sphene and apatite. Amphibole is fine grained and is well foliated in quartz poor domains and poorly foliated in quartz rich domains. Quartz rich domains are highly folded.

Sample 8-4-1
Amphibolite. Amphibole, quartz, opaques, epidote, sphene, apatite. Coarse grained blue-green amphibole is very well foliated and exhibits no folding. Some portions are quartz rich or quartz poor, but no definite gneissic fabric exists.

Sample 8-4-2
Amphibolite. Green amphibole (75%), quartz (20%) opaques (2%) minor sphene and apatite. Sample is very homogenous and well-foliated; amphiboles are very small in size. No biotite or muscovite is present. Quartz veins with sutured grain contacts are present.

Sample 8-4-4
Amphibolite. Green amphibole (50%), quartz (40%), plagioclase (5%), opaques (5%), sphene and apatite. Amphibole is coarse grained and gneissic with domains of amphibole-rich and quartz-rich areas are very well-defined. Plagioclase grains are small and well twinned. Foliations have not been folded.

Sample 8-8-3
Altered Lherzolite. Large orthopyroxene and clinopyroxene grains have been largely altered to serpentine. Relict olivine grains do persist. Serpentine dominates the sample. Sample is very fractured.

Sample 8-8-7
Amphibolite. Amphibole, quartz, opaques, minor apatite and titanite. Sample is not foliated, texture is comprised of blebs of quartz containing abundant minor phases and very small amphibole grains. Amphibole fills in and meanders around the quartz blebs indicating a preserved igneous texture.

Sample 8-9-5
Calcarenite. Quartz and calcite dominate the sample, with minor chlorite and abundant calcite and quartz veins. Often, both quartz and calcite fill the same vein. Sample does not have a metamorphic texture, but shows evidence of abundant brittle deformations.

Sample 8-10-5
Chlorite mylonite. Chlorite has experienced significant localized grain size reduction. Sample is extremely fine grained. An abundant fine grained high relief mineral is also found. Quartz rich layers have been extremely folded.

Sample 8-11-5
Garnet-mica schist. Quartz, biotite, chlorite, muscovite, garnet, opaques, plagioclase, epidote, minor apatite, and amphibole. Garnets have abundant inclusions of epidote, and ilmenite. Garnets are altered and have some inclusion trails; inclusion halos indicate possibility of multiple generations of garnet growth. Garnets show little evidence of rotation. Quartz grains have abundant inclusions.

Sample 8-13-1
Volcanic conglomerate. Unmetamorphosed felsic volcanic clasts containing abundant altered plagioclase grains. Clasts are up to 1 cm in size. Matrix is composed of crushed volcanic material of identical composition. Matrix is optically identical to clasts.

Sample 8-13-3
Foraminifera packstone. Abundant large Nummulites forams up to 1 cm in size, with small amounts of brachiopods and bryzoans.

Sample 8-17-3
Lithic arenite. Quartz, volcanic clasts, metamorphic clasts (quartz-mica schist), calcite, and quartzite. Well sorted medium size rounded grains.

Sample Clere
Quartz-mica schist. Quartz, chlorite, biotite, muscovite, pyrite, opaques, apatite, titanite. Micas are locally aligned, but do not define a penetrative foliation. Pyrite grains are relatively large, up to 4 mm.

Sample F1-1
Garnet-mica schist. Quartz (50%), biotite (20%), muscovite (10%), garnet (15%), plagioclase (5%), kyanite (5%), minor staurolite and opaques. Sample is coarse grained, garnets contain abundant inclusions, mainly quartz. Little alteration to chlorite has taken place. Micas are poorly foliated in some areas apparently as a result of abundant stress shadows.

Sample SF-2
Garnet-mica schist. Quartz, chlorite, muscovite, biotite, garnet, plag, opaques, minor high relief grains. Well foliated with garnets containing abundant inclusions of ilmenite and epidote. Many garnets are very resorbed due to retrograde net transfer reactions, some are subhedral and up to 7 mm in size.

Sample SF-3
Garnet-mica schist. Quartz, biotite, muscovite, garnet, opaques, kyanite, feldspar. Garnets have abundant large inclusions. Feldspar exhibits some cross-hatch twinning.

Sample Bobo-2
Greenschist. Quartz, chlorite, opaques, epidote, calcite veins. Well foliated with thick quartz-rich and quartz-poor domains.

Sample 04T-MM-40
Garnet-mica schist. Quartz, biotite, muscovite, garnet, plagioclase. Garnets are anhedral up to 1.5 mm is size with numerous plagioclase inclusions. Garnet edges which are bounded by biotite are well preserved, while garnets bordering quartz rich domains are significantly resorbed due to retrograde reactions. Biotite is well foliated.

Sample MM-4
Quartz-mica schist. Quartz, biotite, muscovite, garnet, opaques, plagioclase. Garnet are sparse and anhedral, fairly resorbed. Thick bands of quartz and thin bands of quartz are intermixed with bands of well aligned muscovite and more poorly aligned biotite.

Sample MT-3
Amphibolite. Blue-green amphibole dominates the sample. Amphiboles are globbed together exhibiting no definite foliation, fabric likely represent a relict igneous texture. Individual amphibole grains are not aligned. Quartz is the other major phase, filling in between globs of amphibole.

Sample MM-3
Garnet Amphibolite. Quartz, green amphibole, garnet, opaques. Discontinuous bands of quartz and poorly oriented amphibole are the dominant fabric components. Garnets are very sparse and mostly resorbed.

Sample 04T-MLO
Garnet-mica schist. Quartz rich domains contain relatively large quartz grains with mica rich domains containing smaller quartz grains, biotites are up to 3 mm in size. Many biotites are altered to chlorite and not well aligned, while others are very well aligned, suggesting two generations of biotite growth. Garnets are large, euhedral, and nearly inclusion free. Some garnet edges adjacent to quartz domains have been slightly resorbed.

Appendix II: Whole Rock Geochemical Data

Major Element Measurements (weight %)

Sample	SiO2	TiO2	Al2O3	Fe2O3	MnO	MgO	CaO	Na2O	K2O	P2O5	Total	LOI	Total
Metabasites													
7.16.5	52.53	1.35	11.90	9.94	0.17	3.98	13.60	2.80	0.15	0.17	96.58	4.35	100.93
7.22.4	48.70	2.37	11.20	13.95	0.21	6.19	8.11	2.34	0.04	0.27	93.37	9.38	102.75
8.3.1	47.72	1.66	14.35	11.86	0.20	6.78	10.99	2.92	0.73	0.17	97.37	3.32	100.69
8.3.5	44.48	2.19	19.39	15.42	0.32	5.77	5.85	3.21	1.49	0.23	98.34	1.96	100.30
8.3.9	49.94	1.71	15.21	11.48	0.22	6.17	9.40	3.14	0.80	0.16	98.23	1.37	99.60
8.4.2	51.04	1.20	14.30	10.61	0.17	7.35	9.16	2.53	0.38	0.14	96.88	2.23	99.11
8.4.4	46.64	2.65	15.49	12.85	0.22	7.54	9.50	2.96	0.30	0.24	98.38	1.48	99.86
8.8.5	43.74	2.37	13.29	14.70	0.21	9.23	6.99	1.40	0.08	0.20	92.22	10.10	102.32
8.8.9	47.16	1.54	15.97	11.86	0.19	7.04	11.24	2.81	0.44	0.20	98.43	1.46	99.88
8.10.2	50.11	0.17	17.79	3.28	0.10	4.66	15.72	1.95	0.02	0.03	93.84	7.49	101.33
8.15.5	44.14	0.11	21.71	4.92	0.08	10.17	12.32	1.55	0.61	0.05	95.66	3.91	99.58
8.17.4	55.21	1.08	16.16	9.31	0.11	2.40	4.06	4.67	1.01	0.24	94.26	5.83	100.08
8.18.1	44.30	0.85	18.81	7.68	0.16	4.07	16.04	2.09	0.10	0.09	94.20	6.86	101.06
Metapelites													
7.17.2	43.00	2.30	15.27	11.07	0.20	4.90	8.77	4.31	0.51	0.44	90.78	11.08	101.86
7.17.4	69.66	0.56	13.09	4.54	0.07	2.10	1.74	4.00	0.99	0.15	96.90	3.42	100.33
8.3.2	60.04	0.81	17.52	7.96	0.16	3.03	4.31	2.14	2.57	0.19	98.73	1.37	100.10
8.3.4	48.96	1.22	23.07	10.19	0.23	3.69	3.89	3.65	2.37	0.12	97.39	2.86	100.26
8.11.5	54.27	1.63	14.58	10.14	0.16	4.10	5.91	3.64	1.88	0.26	96.56	1.79	98.35
SF-1	57.80	0.95	21.69	8.99	0.17	2.73	2.31	0.68	3.26	0.14	98.70	1.36	100.06
SF-2	58.35	0.86	18.64	8.62	0.19	3.23	2.13	1.83	3.51	0.11	97.46	2.47	99.92
SF-3	59.49	0.81	18.99	8.68	0.20	2.98	4.09	1.18	2.75	0.11	99.29	1.22	100.51
04T-40	62.46	0.82	16.78	7.37	0.19	2.85	3.08	2.24	2.33	0.11	98.22	1.62	99.84
04T-ML0	58.92	0.69	14.70	6.42	0.13	2.22	4.09	2.48	2.15	0.17	91.95	1.63	93.57
MD-1	68.70	0.49	10.94	4.10	0.07	1.93	3.71	3.09	1.51	0.13	94.67	6.08	100.75
MD-2	42.83	0.00	0.68	6.07	0.12	34.50	1.12	0.00	0.00	0.03	85.35		85.35
MM-2	59.40	0.87	18.28	7.49	0.10	3.22	3.15	2.13	2.67	0.15	97.47	1.73	99.19
MT-48-91	84.12	0.47	12.44	2.86	0.03	0.53	1.27	1.93	2.43	0.04	106.12	1.03	107.15
MT-55-91	64.54	0.90	18.73	7.07	0.07	1.82	1.03	1.08	3.93	0.13	99.30	3.85	103.15
04T-70	70.32	0.06	15.60	1.28	1.85	5.50	2.19	0.47	3.69	0.13	101.09	2.61	103.70

Major Element Measurements (weight %) continued

Sample	SiO2	TiO2	Al2O3	Fe2O3	MnO	MgO	CaO	Na2O	K2O	P2O5	Total	LOI	Total
Altered Igneous, ultramafic and misc. rock types													
8.21.3	47.12	1.67	13.63	11.39	0.19	6.70	11.54	3.15	0.10	0.20	95.68	4.21	99.89
04T-10	53.29	2.71	14.46	12.92	0.17	3.47	3.79	5.56	0.94	0.34	97.65	2.23	99.88
04T-16	49.50	1.77	14.75	12.44	0.19	5.73	8.01	4.10	0.80	0.19	97.48	3.37	100.85
04T-9	49.26	1.78	14.77	12.34	0.18	5.65	7.94	4.16	0.84	0.18	97.10	3.56	100.66
04T-W51	59.86	0.73	14.19	6.74	0.12	2.94	3.10	2.25	2.20	0.18	92.30		92.30
4T-14	61.51	0.23	10.51	2.30	0.18	0.67	10.64	2.33	1.00	0.04	89.39	13.75	103.14
4T-34	66.14	0.38	13.25	3.25	0.12	1.02	4.95	3.52	1.68	0.10	94.39	7.54	101.93
CUA MC3	50.27	0.97	17.12	8.85	0.15	4.94	11.20	3.44	0.18	0.11	97.22		97.22
MT-1	71.61	0.57	11.35	4.73	0.17	2.29	4.73	1.90	1.29	0.12	98.75	0.82	99.56
T3B	79.99	0.27	10.33	1.67	0.03	0.83	0.37	5.05	1.72	0.05	100.29	0.76	101.06
T5	41.82	3.81	13.21	18.05	0.24	7.60	12.09	1.68	0.89	0.41	99.80	2.37	102.17
T5B	44.00	0.03	1.63	5.74	0.14	38.85	2.40	0.10	0.00	0.03	92.91	3.45	96.36
MT-105F-91	59.76	0.83	17.95	8.17	0.10	3.81	2.91	2.39	1.96	0.14	98.02	2.89	100.91
MT-45-91	70.45	0.70	15.36	6.07	0.08	1.94	1.32	1.66	3.52	0.13	101.23	1.36	102.59
MT-99-C	59.53	0.89	18.21	8.05	0.06	3.70	2.66	2.23	2.66	0.14	98.13	3.02	101.15
N5-04T-12	49.64	0.70	15.79	9.62	0.12	3.72	0.00	2.74	0.48	0.09	82.90	5.14	88.04
CC-11306B	51.59	0.94	7.01	10.52	0.19	20.42	11.08	0.66	0.39	0.22	103.02		103.02
CD-30B	49.57	0.83	15.30	3.12	0.13	6.11	10.57	2.09	0.34	0.09	88.15	6.64	94.79
HS-05T-12	49.64	0.70	15.79	9.62	0.12	3.72	9.93	2.74	0.48	0.09	92.83	6.00	98.83
7.16.2	57.93	1.85	14.44	9.82	0.19	2.40	5.35	4.13	0.78	0.37	97.26	3.05	100.31
7.16.3	57.85	1.63	15.06	9.46	0.17	2.79	3.71	5.67	0.05	0.29	96.68	3.12	99.80
7.16.4	47.16	0.23	19.27	4.34	0.13	8.55	15.79	1.60	0.10	0.05	97.23	2.31	99.54
7.19.2	54.63	0.54	16.49	6.01	0.15	4.87	2.33	5.44	0.25	0.11	90.82	4.42	95.24
7.20.3	39.09	0.96	14.16	8.60	0.18	4.04	19.47	2.77	0.79	0.09	90.15	12.45	102.59
7.22.5	41.56	0.07	1.73	5.85	0.09	31.05	0.42	0.00	0.00	0.01	80.80	18.32	99.11
7.27.1	46.08	0.18	25.19	3.82	0.05	5.28	7.04	4.51	1.73	0.06	93.94	5.85	99.80
7.28.6	79.62	0.08	3.29	2.45	0.16	1.03	7.52	0.15	0.74	0.11	95.14	6.84	101.98
7.30.4	26.79	0.02	0.65	6.42	1.11	17.12	23.72	0.29	0.00	0.00	76.12	25.76	101.88
8.8.3	41.23	0.08	2.89	8.53	0.13	35.67	1.89	0.00	0.00	0.05	90.46	10.60	101.06
8.9.5	64.46	0.56	12.79	4.36	0.09	2.30	5.51	3.76	1.21	0.12	95.15	5.31	100.46

Major Element Measurements (weight %) continued

Sample	SiO2	TiO2	Al2O3	Fe2O3	MnO	MgO	CaO	Na2O	K2O	P2O5	Total	LOI	Total
8.10.5	30.31	1.65	20.83	10.27	0.30	23.00	2.18	0.01	0.00	0.18	88.72	10.71	99.44
8-11.3.5	45.40	2.08	22.10	13.08	1.84	3.86	5.56	3.79	0.40	0.06	98.17	3.84	102.00
8.13.1	60.17	1.25	14.65	7.95	0.18	2.15	5.43	4.04	0.81	0.40	97.02	3.84	100.85
8.14.3	39.04	3.66	14.67	17.56	0.17	8.86	9.11	1.37	0.00	0.30	94.74	6.69	101.42
8.15.2	40.62	0.08	3.45	6.22	0.15	33.37	1.14	0.00	0.03	0.03	85.08	13.07	98.15
Average Std.	50.00	2.72	13.61	12.21	0.17	7.24	11.32	2.28	0.54	0.27	100.37		100.37
Std. Values	49.94	2.71	13.80	11.40	0.17	7.23	11.40	2.26	0.52	0.27	99.70		99.70

Trace Element Measurements (In parts per million, PPM)

Sample	S	Cl	Sc	V	Cr	Ni	Cu	Zn	Ga	Rb	Sr	Y	Zr	Nb	Ba	La	Ce	Nd	Sm	Pb	Th	U	As	Co
Metabasites																								
7.16.5	0	56	35	215	152	44	28	88	18	2	215	28	94	5	20	9	22	0	9	0	0	0	3	24
7.22.4	599	54	46	372	40	39	45	142	22	0	85	52	158	4	0	10	26	0	15	0	4	0	4	1
8.3.1	61	56	45	312	235	79	29	130	18	22	131	42	102	1	20	7	19	0	7	10	3	0	1	25
8.3.5	419	39	48	202	356	119	340	208	25	87	161	52	128	8	107	12	26	0	11	19	3	3	1	17
8.3.9	0	43	43	276	207	64	76	111	19	23	148	38	112	3	38	0	9	0	5	0	0	3	2	35
8.4.2	0	40	42	253	341	93	33	97	17	7	124	31	84	2	0	0	0	0	5	0	2	0	2	32
8.4.4	0	44	52	331	248	79	20	122	21	4	124	57	178	4	0	14	31	0	6	4	3	0	1	30
8.8.5	0	45	63	505	230	131	55	139	26	3	201	49	134	0	0	0	0	0	9	0	5	0	19	21
8.8.9	145	48	42	302	284	85	44	127	20	7	157	36	101	3	12	0	11	0	4	4	3	0	1	37
8.10.2	52	41	24	69	392	74	54	21	16	0	160	7	21	0	4	0	11	0	1	0	1	0	4	22
8.15.5	0	184	17	53	3000	2005	4	43	7	0	12	2	14	1	0	0	0	0	0	0	3	0	7	77
8.17.4	24407	47	21	120	106	64	36	69	21	26	205	36	161	6	274	24	59	26	9	13	4	3	18	0
8.18.1	57	48	29	173	426	119	44	69	18	3	226	18	65	5	13	0	11	0	4	0	2	0	2	18
Metapelites																								
7.17.2	11	71	32	175	285	150	62	128	24	21	614	35	254	28	48	30	61	25	16	9	7	3	81	0
7.17.4	77	44	14	92	107	71	28	63	14	42	206	20	145	8	141	33	69	28	7	9	7	0	14	8
8.3.2	539	42	21	143	84	77	61	114	22	124	233	27	150	10	255	36	73	29	8	18	13	4	2	13
8.3.4	0	38	25	228	116	122	45	137	28	113	374	40	222	13	269	45	94	36	10	42	18	4	3	5
8.11.5	0	47	52	125	205	115	12	146	19	16	214	102	329	18	21	78	157	51	23	27	29	4	2	5
SF-1	237	38	16	127	80	78	242	134	20	121	88	32	178	13	322	38	76	28	1	14	16	4	2	18
SF-2	3	37	19	155	82	93	171	127	24	148	209	29	166	12	376	35	68	26	5	24	13	4	1	8
SF-3	49	38	17	126	77	62	51	99	21	120	128	27	146	19	231	33	67	25	5	23	13	3	2	22
04T-40	107	31	21	138	111	74	40	124	22	112	265	28	170	10	281	29	52	22	8	19	11	4	1	0
04T-ML0	3077	26	21	113	86	54	45	88	18	101	289	25	146	10	223	18	40	0	6	21	10	2	2	0
MD-1	609	38	14	80	166	57	9	69	13	65	231	22	152	9	231	13	32	0	9	14	8	0	3	27
MD-2	0	266	0	33	1308	2491	7	54	4	0	18	0	0	1	7	0	0	0	1	0	4	0	2	26
MM-2	673	28	20	148	131	89	35	140	24	120	251	30	181	12	287	32	57	26	4	21	13	4	25	2
MT-48-91	0	49	0	44	38	10	1	28	9	95	104	18	262	24	360	42	100	33	4	16	10	0	1	77
MT-55-91	0	49	10	157	67	24	52	64	24	186	124	35	302	41	486	54	113	40	7	24	23	4	2	31
04T-70			14	92	107	71	28	63	14	42	206	20	145	8	141	33	69	28	7	9	7	0		8

Trace Element Measurements (PPM) continued

Sample	S	Cl	Sc	V	Cr	Ni	Cu	Zn	Ga	Rb	Sr	Y	Zr	Nb	Ba	La	Ce	Nd	Sm	Pb	Th	U	As	Co
Altered Igneous, ultramafic and misc. rock types																								
8.21.3	21	46	42	306	271	105	46	96	19	1	171	43	118	2	8	0	11	0	6	0	0	0	2	39
04T-10	14	218	21	158	5	25	24	118	24	20	281	25	146	33	200	24	59	22	13	0	4	0	2	0
04T-16	1315	71	31	300	41	33	47	62	21	8	619	29	94	3	72	0	14	0	9	0	2	3	0	0
04T-9	1230	76	32	313	42	35	51	63	22	8	681	29	96	2	74	0	20	0	8	0	2	0	0	0
04T-W51	1103	34	17	125	117	62	64	103	19	98	272	21	151	10	249	20	44	0	9	15	11	2	19	0
4T-14	105	44	18	27	15	2	19	56	11	22	615	46	146	4	313	9	25	0	13	7	2	0	3	2
4T-34	2220	1219	14	41	14	8	14	67	16	43	261	29	134	4	305	12	30	0	9	10	6	0	11	0
CUA MC3	24	60	34	246	131	72	32	77	19	4	230	23	67	0	50	0	14	0	4	0	1	0	3	9
MT-1	454	33	15	104	251	68	11	53	12	47	237	20	169	8	235	18	38	0	5	11	7	0	3	83
T3B	122	191	0	32	13	8	0	25	12	59	59	19	171	10	455	34	75	29	5	9	12	0	1	5
T5	6	83	43	333	120	79	13	175	25	6	142	51	252	42	34	38	66	30	9	4	9	0	1	25
T5B	0	86	13	62	1958	1663	6	46	4	0	5	0	0	1	0	0		0	0	0	1	0	1	10
MT-105F-91	12	41	16	151	105	86	44	105	22	67	253	22	187	13	359	35	81	27	8	20	14	4	1	31
MT-45-91	1451	63	9	97	57	32	20	83	19	174	143	36	222	20	531	50	105	38	6	29	21	4	12	40
MT-99-C	0	46	12	155	106	72	69	109	21	129	230	30	197	13	361	35	94	31	9	20	12	3	1	37
N5-04T-12	14489	3837	41	235	0	23	35	81	18	6	375	21	71	3	41	0	15	0	12	5	2	3	1	80
CC-11306B	0	50	33	191	1732	513	2	92	13	15	101	20	94	7	9	12	33	0	0	5	3	0	2	71
CD-30B			24	31	3808	89	5	15	3	0	105	4	19	0	0	0	0	0	0	0	0	0		101
HS-05T-12			45	312	235	79	29	130	18	22	131	42	102	1	20	7	19	0	7	10	3	0		25
7.16.2	329	89	32	195	6	7	50	118	21	15	159	46	206	7	125	23	51	22	13	7	5	0	3	18
7.16.3	870	79	34	221	4	8	31	150	23	0	161	44	182	5	0	10	31	0	16	7	5	0	2	0
7.16.4	0	58	40	137	1147	102	40	41	12	1	99	9	22	0	0	0	0	0	0	0	0	0	2	36
7.19.2	3	68	15	100	26	24	21	78	22	4	317	15	103	3	54	0	14	0	10	0	3	0	3	109
7.20.3	19	76	35	216	308	62	38	72	16	19	202	31	63	1	0	0	11	0	10	0	1	0	4	11
7.22.5	0	41	0	45	3209	2511	0	41	5	0	7	1	15	1	0	0	0	0	0	0	5	0	8	96
7.27.1	22	52	6	31	432	192	32	28	14	53	689	0	35	1	885	0	0	0	0	0	1	3	3	9
7.28.6	39	51	12	51	18	19	82	41	6	36	70	20	37	2	125	31	54	25	10	0	2	0	5	7
7.30.4	0	152	24	31	3808	89	5	15	3	0	105	4	19	0	0	0	0	0	0	0	0	0	6	101
8.8.3	39	353	15	58	2607	2017	15	54	6	0	17	2	12	0	0	0	10	0	0	0	3	0	6	93
8.9.5	117	40	14	98	185	58	19	58	14	48	400	20	154	8	281	19	46	0	9	13	8	0	11	15

Trace Element Measurements (PPM) continued

Sample	S	Cl	Sc	V	Cr	Ni	Cu	Zn	Ga	Rb	Sr	Y	Zr	Nb	Ba	La	Ce	Nd	Sm	Pb	Th	U	As	Co
8.10.5	0	49	31	240	141	82	177	166	24	0	84	66	327	22	44	74	156	99	0	0	31	4	3	0
8-11.3.5	261	72	37	307	26	26	56	108	22	37	201	38	165	4	140	0	14	0	12	6	3	0	1	13
8.13.1	106	564	23	73	7	2	16	102	19	9	234	41	138	4	149	13	33	19	12	6	4	0	2	30
8.14.3	0	59	70	540	150	106	36	154	31	0	147	72	204	1	0	8	0	0	8	0	5	0	4	25
8.15.2	27	103	21	60	314	221	59	28	12	15	215	3	21	0	33	0	9	0	0	0	0	0	4	43
Average Std.	0	43	21	119	414	147	30	63	18	72	249	19	115	9	297	13	32	0	4	20	5	3		
Std. Values			19	130	465	142	29	63	16	68	252	18	119	10	317	16	33		3	19	5	2		

Appendix III: Mineral Chemistry

Amphibole Mineral Chemistry Results from Electron Microprobe Analysis (Based on 23 oxygens)

Sample	Na2O	MgO	Al2O3	SiO2	FeO	TiO2	MnO	CaO	K2O	Cl	Total	F	Cl	TOTAL
8-4-4core1.1	1.59	12.20	13.42	44.62	13.08	0.56	0.23	11.58	0.20	0.00	97.48	0.00	0.00	97.48
8-4-4rim1.1	1.49	12.59	13.15	45.03	12.47	0.49	0.21	11.47	0.23	0.01	97.14	0.00	-0.01	97.13
8-4-1grain2	1.94	10.67	13.69	42.71	15.83	0.66	0.26	11.07	0.31	0.03	97.17	0.00	-0.03	97.14
8-4-1grain2	1.89	10.52	13.81	43.05	15.62	0.66	0.28	11.06	0.31	0.00	97.19	0.00	0.00	97.19
8-4-1grain2	1.84	10.69	13.35	43.73	15.41	0.65	0.27	10.94	0.31	0.00	97.20	0.00	0.00	97.20
8-4-1grain2	1.89	10.89	13.48	43.07	15.46	0.67	0.30	11.05	0.30	0.02	97.13	0.00	-0.02	97.11
8-4-1grain2	1.77	10.80	13.18	44.11	15.25	0.55	0.26	10.73	0.28	0.01	96.95	0.00	-0.01	96.94
8-4-1grain2	1.85	10.41	13.82	43.56	15.81	0.66	0.32	10.60	0.31	0.03	97.37	0.00	-0.03	97.35
8-4-1grain2	1.92	10.80	13.60	42.93	15.83	0.60	0.25	11.29	0.28	0.00	97.50	0.00	0.00	97.50
8-4-1grain2	1.66	11.84	11.82	44.49	14.83	0.45	0.28	11.15	0.24	0.00	96.75	0.00	0.00	96.75
8-4-1grain2	1.79	11.16	13.00	43.48	15.71	0.60	0.26	10.90	0.26	0.00	97.15	0.00	0.00	97.15
8-4-1grain2	1.59	11.26	12.25	44.34	15.62	0.46	0.25	10.89	0.28	0.04	96.97	0.00	-0.04	96.94
8-3-5rim3.1	1.93	6.32	18.62	40.18	19.52	0.31	0.35	10.28	0.36	0.00	97.88	0.00	0.00	97.88
8-3-5rim3.2	1.87	6.15	17.98	40.52	19.44	0.36	0.46	9.97	0.27	0.00	97.03	0.00	0.00	97.02
8-3-5cor3.1	1.60	5.56	18.63	40.33	19.48	0.28	0.84	10.28	0.32	0.00	97.32	0.00	0.00	97.32
8-3-5cor3.2	1.83	5.76	18.70	40.10	19.98	0.29	0.57	9.73	0.29	0.02	97.28	0.00	-0.02	97.25
8-3-5rim4.1	1.72	6.94	17.03	41.19	19.37	0.35	0.20	10.53	0.47	0.00	97.80	0.00	0.00	97.80
8-3-5rim4.2	1.76	6.37	18.33	40.50	18.85	0.26	0.29	10.18	0.33	0.04	96.90	0.00	-0.04	96.86
8-3-5rim4.3	1.92	6.40	18.42	40.60	18.78	0.29	0.23	10.18	0.33	0.00	97.14	0.00	0.00	97.14
8-3-5core4.1	1.76	6.00	18.24	40.66	19.30	0.26	0.35	10.12	0.31	0.01	97.01	0.00	-0.01	97.00
8-3-5core4.2	1.85	5.74	18.64	40.61	19.52	0.28	0.57	10.01	0.30	0.00	97.51	0.00	0.00	97.51
8-3-5rim5.1	1.90	6.14	18.54	40.29	19.27	0.36	0.38	10.23	0.35	0.01	97.47	0.00	-0.01	97.46
8-3-5rim5.2	1.92	6.26	18.42	40.09	19.13	0.32	0.32	10.30	0.38	0.04	97.17	0.00	-0.04	97.14
8-3-5cor5.1	1.93	6.32	18.43	40.89	18.80	0.28	0.29	10.33	0.33	0.01	97.60	0.00	-0.01	97.59
8-3-5cor5.2	1.85	5.78	18.73	40.30	19.28	0.23	0.60	9.98	0.36	0.00	97.12	0.00	0.00	97.12
8-3-5cor2.1	1.87	5.91	18.86	40.31	19.74	0.22	0.59	10.06	0.34	0.01	97.90	0.00	-0.01	97.89
8-3-5cor2.2	1.88	6.41	18.15	40.54	19.10	0.30	0.38	10.30	0.30	0.00	97.34	0.00	0.00	97.34
8-3-5rim2.1	1.78	5.89	18.43	40.17	19.89	0.30	0.62	9.91	0.37	0.00	97.37	0.00	0.00	97.37
8-3-5rim2.2	1.92	6.08	18.52	40.58	19.59	0.33	0.39	10.09	0.34	0.02	97.85	0.00	-0.02	97.84
8-3-5int6.1	2.01	6.47	17.97	40.98	19.09	0.28	0.36	9.95	0.33	0.06	97.49	0.00	-0.06	97.43
8-4-1cor1.1	1.54	12.20	13.67	44.64	12.84	0.47	0.18	11.20	0.21	0.01	96.96	0.00	-0.01	96.95
8-4-1cor1.2	1.60	11.83	13.87	44.50	13.16	0.58	0.25	11.08	0.24	0.01	97.13	0.00	-0.01	97.12

Amphibole Mineral Chemistry Results from Electron Microprobe Analysis (Based on 23 oxygens)

Sample	Na2O	MgO	Al2O3	SiO2	FeO	TiO2	MnO	CaO	K2O	Cl	Total	F	Cl	TOTAL
8-4-1rim1.1	1.62	12.29	13.51	44.41	13.05	0.62	0.17	11.51	0.22	0.00	97.38	0.00	0.00	97.38
8-4-1rim1.2	1.56	12.24	13.48	44.52	13.12	0.55	0.20	11.26	0.23	0.00	97.16	0.00	0.00	97.16
8-4-1rim2.2	1.64	12.08	13.83	44.71	12.78	0.57	0.22	11.31	0.19	0.00	97.31	0.00	0.00	97.31
8-4-1rim2.3	1.39	13.65	11.35	46.83	11.87	0.42	0.19	11.44	0.14	0.02	97.29	0.00	-0.02	97.27
8-4-1cor2.1	0.96	15.16	8.25	49.81	10.78	0.27	0.22	11.24	0.08	0.01	96.76	0.00	-0.01	96.76
8-4-1cor3.1	1.29	12.21	13.02	45.40	13.21	0.45	0.19	11.45	0.19	0.00	97.40	0.00	0.00	97.40
8-4-1cor3.2	1.60	11.68	14.31	44.19	13.30	0.55	0.22	11.30	0.23	0.03	97.40	0.00	-0.03	97.37
8-4-1rim3.1	1.51	12.27	13.04	44.92	13.40	0.56	0.19	11.56	0.17	0.01	97.65	0.00	-0.01	97.64
8-4-1rim3.2	1.60	11.82	13.46	44.65	13.10	0.54	0.18	11.50	0.22	0.05	97.12	0.00	-0.05	97.07
8-4-1int4.1	1.59	12.42	13.23	44.87	12.81	0.46	0.26	11.16	0.20	0.00	97.00	0.00	0.00	97.00
8-4-4cor1.1	1.82	10.94	13.08	43.62	15.57	0.64	0.24	11.25	0.30	0.01	97.46	0.00	-0.01	97.45
8-4-4cor1.3	1.87	10.73	13.60	43.30	15.40	0.58	0.29	11.02	0.30	0.02	97.11	0.00	-0.02	97.08
8-4-4rim1.1	1.97	10.28	13.94	42.54	16.08	0.64	0.27	10.78	0.32	0.00	96.81	0.00	0.00	96.81
8-4-4rim1.2	1.74	11.19	12.32	44.55	15.39	0.53	0.29	11.11	0.28	0.00	97.39	0.00	0.00	97.39
8-4-4cor3.2	1.87	11.05	13.02	43.74	15.33	0.64	0.30	11.30	0.29	0.02	97.55	0.00	-0.02	97.53
8-4-4rim3.1	1.77	11.02	12.92	44.02	15.40	0.68	0.26	10.94	0.29	0.00	97.30	0.00	0.00	97.30
8-4-4rim3.2	1.77	11.89	12.03	45.70	14.80	0.51	0.26	11.19	0.24	0.01	98.38	0.00	-0.01	98.37
8-4-4int4.1	1.87	11.17	12.94	43.85	15.41	0.60	0.27	10.94	0.28	0.00	97.33	0.00	0.00	97.33
8-4-1line1	1.91	10.88	13.11	43.73	15.75	0.67	0.26	11.02	0.31	0.02	97.65	0.00	-0.02	97.64
8-4-1line1	1.73	11.11	13.17	43.70	15.21	0.62	0.25	11.00	0.28	0.00	97.06	0.00	0.00	97.06
8-4-1line1	1.92	10.82	13.13	43.73	15.54	0.59	0.29	11.14	0.31	0.00	97.47	0.00	0.00	97.46
8-4-1line1	1.96	10.87	13.16	43.42	15.52	0.63	0.33	10.91	0.28	0.01	97.09	0.00	-0.01	97.09
8-4-1line1	1.89	10.83	13.57	43.36	15.57	0.53	0.27	10.84	0.30	0.02	97.16	0.00	-0.02	97.14
8-4-1line1	1.85	10.78	13.15	43.59	15.59	0.55	0.30	11.02	0.27	0.01	97.11	0.00	-0.01	97.10
8-4-1line1	1.80	11.02	13.03	43.83	15.59	0.62	0.29	10.85	0.28	0.00	97.31	0.00	0.00	97.31
8-4-1line1	1.90	10.76	14.08	43.10	15.30	0.67	0.28	10.85	0.31	0.00	97.24	0.00	0.00	97.24
8-4-1line1	1.60	11.95	11.76	45.14	14.74	0.46	0.31	10.81	0.28	0.00	97.05	0.00	0.00	97.05
8-4-1line1	1.84	10.95	13.25	43.91	15.85	0.66	0.29	10.81	0.32	0.02	97.89	0.00	-0.02	97.88
8-3-5line1	0.00	0.00	25.87	38.06	10.33	0.08	0.32	22.21	0.00	0.01	96.87	0.00	-0.01	96.86
8-3-5line1	0.00	0.00	25.40	38.07	10.35	0.07	0.42	22.51	0.00	0.00	96.83	0.00	0.00	96.83
8-3-5line1	1.70	5.81	18.47	40.56	19.36	0.24	0.74	10.08	0.33	0.02	97.30	0.00	-0.02	97.28
8-3-5line1	1.72	5.68	18.57	40.57	19.51	0.29	0.70	10.02	0.34	0.01	97.40	0.00	-0.01	97.40

Amphibole Mineral Chemistry Results from Electron Microprobe Analysis (Based on 23 oxygens)

Sample	Na2O	MgO	Al2O3	SiO2	FeO	TiO2	MnO	CaO	K2O	Cl	Total	F	Cl	TOTAL
8-3-5line1	1.74	5.58	18.69	40.42	19.27	0.22	0.80	10.02	0.29	0.02	97.05	0.00	-0.02	97.03
8-3-5line1	1.80	5.61	18.94	40.23	19.45	0.25	0.76	9.75	0.27	0.01	97.07	0.00	-0.01	97.06
8-3-5line1	1.76	5.83	18.70	40.33	19.63	0.26	0.80	9.85	0.29	0.02	97.48	0.00	-0.02	97.46
8-3-5line1	1.74	5.79	18.70	40.08	19.78	0.24	0.78	10.05	0.34	0.00	97.49	0.00	0.00	97.49
8-3-5line1	1.80	5.75	18.68	40.22	19.66	0.30	0.77	9.75	0.30	0.02	97.25	0.00	-0.02	97.22
8-3-5line2	1.93	6.18	18.37	40.39	19.44	0.27	0.35	10.18	0.32	0.02	97.43	0.00	-0.02	97.42
8-3-5line2	1.88	6.39	17.96	40.68	19.79	0.30	0.44	10.06	0.32	0.00	97.83	0.00	0.00	97.83
8-3-5line2	1.81	5.85	18.58	40.04	19.79	0.25	0.74	9.80	0.32	0.01	97.18	0.00	-0.01	97.17
8-3-5line2	1.80	5.87	18.70	40.02	19.96	0.28	0.63	9.68	0.29	0.02	97.25	0.00	-0.02	97.22
8-3-5line2	1.91	5.70	18.61	40.05	20.03	0.30	0.70	9.89	0.34	0.00	97.53	0.00	0.00	97.53
8-3-5line2	1.88	5.81	19.38	39.78	19.71	0.23	0.53	9.90	0.30	0.01	97.52	0.00	-0.01	97.51
8-3-5line2	1.84	5.87	18.76	39.86	19.59	0.26	0.63	10.03	0.28	0.00	97.13	0.00	0.00	97.13
8-3-5line2	1.81	5.88	18.84	40.48	19.39	0.23	0.39	10.15	0.38	0.00	97.54	0.00	0.00	97.54
8-3-5line2	1.74	5.77	18.70	40.65	19.46	0.23	0.71	10.07	0.37	0.02	97.73	0.00	-0.02	97.71
8-4-1line1	0.00	0.00	27.74	37.68	8.19	0.13	0.14	22.22	0.00	0.00	96.10	0.00	0.00	96.10
8-4-1line1	1.59	12.41	13.52	44.67	12.44	0.51	0.21	11.04	0.22	0.01	96.62	0.00	-0.01	96.61
8-4-1line1	1.52	11.99	14.12	44.23	12.84	0.52	0.25	10.96	0.20	0.00	96.63	0.00	0.00	96.63
8-8-7int1.4	1.71	10.93	13.71	43.21	14.87	0.58	0.26	11.57	0.57	0.00	97.39	0.00	0.00	97.39
8-8-7int1.5	0.01	0.00	27.18	38.22	8.82	0.08	0.21	23.57	0.02	0.00	98.12	0.00	0.00	98.12
8-8-7int2.2	0.03	0.00	27.25	38.27	8.43	0.12	0.19	23.78	0.00	0.00	98.07	0.00	0.00	98.07
8-8-7int2.3	1.71	10.94	13.51	43.44	14.95	0.58	0.24	11.81	0.58	0.01	97.77	0.00	-0.01	97.76
8-8-7int3.1	1.68	10.84	13.63	43.74	15.18	0.67	0.24	11.75	0.56	0.01	98.28	0.00	-0.01	98.27
8-8-7rim3.1	1.58	11.07	12.57	44.28	14.77	0.52	0.24	11.77	0.55	0.00	97.34	0.00	0.00	97.34
8-8-7rim3.2	1.69	11.03	13.59	43.48	14.67	0.56	0.26	11.48	0.54	0.03	97.32	0.00	-0.03	97.30
8-8-7cor3.1	1.81	11.01	13.73	43.81	15.06	0.64	0.27	11.99	0.60	0.00	98.90	0.00	0.00	98.90
8-8-7cor3.2	1.76	11.14	13.58	43.68	15.26	0.67	0.27	11.91	0.59	0.00	98.84	0.00	0.00	98.83
8-3-9int1.1	1.64	11.09	12.47	44.21	15.30	0.44	0.33	11.64	0.33	0.04	97.48	0.00	-0.04	97.44
8-3-9int1.2	1.60	11.04	11.69	43.11	16.69	0.33	0.33	11.67	0.49	0.02	96.97	0.00	-0.02	96.96
8-3-9int1.4	1.49	12.50	10.25	45.72	14.66	0.33	0.34	11.53	0.27	0.01	97.10	0.00	-0.01	97.08
8-3-9int1.5	1.68	11.11	12.51	43.51	15.79	0.46	0.38	11.34	0.42	0.00	97.20	0.00	0.00	97.20
8-3-9rim2.1	1.81	10.84	12.73	43.96	15.82	0.48	0.38	11.20	0.45	0.00	97.66	0.00	0.00	97.66
8-3-9cor2.1	0.02	0.00	24.51	37.68	11.92	0.03	0.30	23.32	0.00	0.00	97.78	0.00	0.00	97.78

Amphibole Mineral Chemistry Results from Electron Microprobe Analysis (Based on 23 oxygens)

Sample	Na2O	MgO	Al2O3	SiO2	FeO	TiO2	MnO	CaO	K2O	Cl	Total	F	Cl	TOTAL
8-3-9cor2.2	1.81	11.03	12.31	43.91	15.79	0.43	0.35	11.72	0.36	0.02	97.73	0.00	-0.02	97.71
8-3-9cor2.3	1.82	10.99	12.41	43.56	15.51	0.48	0.34	11.29	0.41	0.00	96.79	0.00	0.00	96.79
8-3-9cor2.4	1.81	11.29	12.54	43.90	15.53	0.44	0.31	11.38	0.42	0.01	97.64	0.00	-0.01	97.63
8-3-1int1.1	1.29	11.54	11.46	45.75	14.50	0.43	0.32	11.62	0.37	0.00	97.28	0.00	0.00	97.28
8-3-1int1.2	1.71	10.28	13.91	42.99	15.68	0.57	0.28	11.69	0.42	0.01	97.53	0.00	-0.01	97.52
8-3-1int1.3	1.79	10.44	13.61	43.55	15.62	0.45	0.29	11.70	0.33	0.01	97.78	0.00	-0.01	97.77
8-3-1int2.2	1.56	10.38	13.29	43.38	14.98	0.58	0.29	11.78	0.59	0.00	96.81	0.00	0.00	96.81
8-3-1int2.3	1.74	9.50	14.83	42.72	15.90	0.47	0.32	11.62	0.60	0.01	97.70	0.00	-0.01	97.70
8-3-1int2.4	1.64	10.13	13.66	43.13	15.78	0.53	0.29	11.42	0.49	0.00	97.06	0.00	0.00	97.06
8-3-1line1	1.71	9.55	14.60	42.35	15.88	0.42	0.30	11.71	0.59	0.01	97.11	0.00	-0.01	97.10
8-3-1line1	1.70	10.35	13.96	43.18	15.42	0.61	0.21	11.64	0.49	0.03	97.58	0.00	-0.03	97.55
8-3-1line1	2.09	9.55	14.36	44.01	14.95	0.56	0.29	11.06	0.56	0.03	97.46	0.00	-0.03	97.43
8-3-1line1	1.59	10.40	13.83	44.46	15.59	0.57	0.29	11.66	0.50	0.02	98.90	0.00	-0.02	98.89
8-3-1line1	8.10	0.00	25.02	55.94	0.23	0.00	0.00	6.96	0.06	0.03	96.32	0.00	-0.03	96.30
8-3-1line1	1.48	11.07	13.32	44.93	15.38	0.58	0.22	11.72	0.57	0.00	99.26	0.00	0.00	99.26
8-3-1line2	1.48	10.68	12.60	44.71	15.85	0.47	0.29	11.67	0.50	0.00	98.25	0.00	0.00	98.25
8-3-1line2	1.26	11.17	10.99	44.80	15.18	0.45	0.27	11.51	0.41	0.01	96.04	0.00	-0.01	96.03
8-3-1line2	1.36	9.93	14.35	42.61	16.09	0.60	0.29	11.22	0.61	0.00	97.06	0.00	0.00	97.06
8-3-1line2	1.33	11.66	10.70	45.58	14.82	0.40	0.28	11.34	0.39	0.04	96.54	0.00	-0.04	96.49
8-3-1line2	1.26	11.75	10.90	45.75	14.72	0.50	0.26	11.71	0.33	0.05	97.22	0.00	-0.05	97.17
8-3-1line3	1.62	9.70	14.00	42.69	16.06	0.63	0.28	11.58	0.63	0.01	97.19	0.00	-0.01	97.19
8-3-1line3	1.05	12.90	8.84	48.36	14.08	0.28	0.23	11.85	0.28	0.01	97.86	0.00	-0.01	97.85
8-3-1line3	0.90	13.70	7.44	49.11	13.76	0.13	0.32	11.54	0.20	0.00	97.11	0.00	0.00	97.11
8-3-9line1	1.74	11.18	12.53	43.48	15.83	0.46	0.32	11.41	0.39	0.01	97.33	0.00	-0.01	97.33
8-3-9line1	1.62	11.35	12.46	43.82	15.45	0.41	0.35	11.47	0.30	0.00	97.21	0.00	0.00	97.21
8-3-9line1	1.47	11.01	11.93	44.18	16.17	0.45	0.27	11.85	0.45	0.00	97.79	0.00	0.00	97.78
8-3-9line1	0.00	0.00	24.07	36.95	12.59	0.04	0.24	23.20	0.00	0.02	97.09	0.00	-0.02	97.07
8-3-9line1	1.54	11.28	11.78	44.44	15.80	0.37	0.33	11.30	0.34	0.00	97.18	0.00	0.00	97.18
8-3-9line1	1.69	11.23	12.42	43.87	15.77	0.46	0.36	11.65	0.42	0.01	97.87	0.00	-0.01	97.86
8-3-9line1	0.79	12.78	12.19	43.56	15.41	0.76	0.29	8.19	3.30	0.00	97.25	0.00	0.00	97.25
8-3-9line1	1.70	11.16	11.82	43.64	16.29	0.36	0.32	11.53	0.40	0.00	97.21	0.00	0.00	97.21
8-3-9line1	1.08	10.97	11.18	44.82	15.33	0.31	0.27	12.59	0.46	0.01	97.01	0.00	-0.01	97.01

Amphibole Mineral Chemistry Results from Electron Microprobe Analysis (Based on 23 oxygens)

Sample	Na2O	MgO	Al2O3	SiO2	FeO	TiO2	MnO	CaO	K2O	Cl	Total	F	Cl	TOTAL
8-3-9line2	1.67	10.64	12.92	42.41	17.26	0.39	0.25	11.99	0.53	0.00	98.05	0.00	0.00	98.05
8-3-9line2	1.51	11.02	12.40	42.41	17.08	0.44	0.35	11.33	0.68	0.00	97.21	0.00	0.00	97.21
8-3-9line2	0.01	0.11	22.98	37.33	13.39	0.05	0.24	23.02	0.04	0.00	97.18	0.00	0.00	97.18
8-3-9line2	1.33	8.81	15.12	42.00	15.28	0.44	0.33	13.51	0.36	0.00	97.17	0.00	0.00	97.17
8-3-9line2	1.59	11.02	12.54	44.09	15.60	0.41	0.33	11.46	0.30	0.00	97.32	0.00	0.00	97.32
8-3-9line2	0.64	15.67	5.15	52.63	11.54	0.14	0.36	11.55	0.16	0.00	97.84	0.00	0.00	97.84
8-3-9line2	1.38	11.76	12.39	44.98	14.48	0.35	0.29	10.84	0.67	0.00	97.14	0.00	0.00	97.14
8-3-9line2	1.62	11.40	12.12	44.44	15.47	0.43	0.31	11.46	0.36	0.00	97.60	0.00	0.00	97.60
8-3-9line2	1.74	11.00	12.96	43.15	15.69	0.49	0.31	11.36	0.40	0.03	97.13	0.00	-0.03	97.11
8-3-9line2	0.90	7.55	15.86	42.45	13.69	0.25	0.35	15.94	0.18	0.01	97.18	0.00	-0.01	97.17
8-3-9line2	0.37	3.07	21.30	39.51	12.64	0.15	0.24	20.29	0.10	0.01	97.66	0.00	-0.01	97.65
8-3-9line2	0.72	4.28	20.41	39.99	14.00	0.19	0.28	18.85	0.17	0.00	98.87	0.00	0.00	98.87
8-3-9line2	1.62	11.32	11.83	44.18	15.77	0.38	0.35	11.46	0.37	0.01	97.28	0.00	-0.01	97.27
8-3-9line2	1.66	11.22	12.51	43.91	15.76	0.44	0.31	11.62	0.41	0.00	97.84	0.00	0.00	97.84
8-3-9line2	1.63	10.96	13.02	43.07	16.08	0.48	0.29	11.55	0.49	0.00	97.56	0.00	0.00	97.56
8-3-9line2	1.57	11.09	12.17	43.30	16.21	0.44	0.29	11.56	0.42	0.00	97.05	0.00	0.00	97.05
8-3-9line2	1.03	14.22	8.53	47.46	13.67	0.29	0.34	11.03	0.53	0.03	97.12	0.00	-0.03	97.09
8-3-9line2	1.68	11.67	11.87	44.58	15.59	0.38	0.37	11.23	0.35	0.00	97.72	0.00	0.00	97.72
8-3-9line2	1.58	11.61	11.89	44.18	15.19	0.44	0.31	11.25	0.54	0.03	97.03	0.00	-0.03	97.00
8-8-7line1	1.65	10.51	13.79	42.89	15.21	0.58	0.26	11.70	0.55	0.04	97.17	0.00	-0.04	97.13
8-8-7line1	1.67	10.82	13.88	42.94	15.04	0.49	0.22	11.53	0.54	0.01	97.15	0.00	-0.01	97.13
8-8-7line1	1.68	11.03	13.06	43.39	15.28	0.55	0.24	11.67	0.50	0.00	97.39	0.00	0.00	97.39
8-8-7line1	1.79	10.66	13.91	42.80	15.19	0.60	0.21	11.58	0.49	0.00	97.23	0.00	0.00	97.23
8-8-7line1	1.65	10.81	13.55	43.19	15.29	0.58	0.23	11.59	0.52	0.01	97.41	0.00	-0.01	97.41
8-8-7line1	1.70	11.05	13.21	43.19	14.99	0.54	0.21	11.59	0.53	0.00	97.02	0.00	0.00	97.02
8-8-7line1	1.73	11.01	13.46	42.97	14.96	0.60	0.27	11.78	0.56	0.00	97.35	0.00	0.00	97.35
8-8-7line1	1.68	10.93	13.37	43.31	14.87	0.58	0.21	11.56	0.57	0.00	97.08	0.00	0.00	97.08
8-8-7line1	1.66	10.95	13.38	43.45	15.06	0.61	0.27	11.72	0.63	0.04	97.76	0.00	-0.04	97.72
8-8-7line1	1.17	9.37	12.94	41.23	14.19	0.48	0.26	11.24	0.49	0.03	91.39	0.00	-0.03	91.36
8-8-7line1	1.56	10.79	14.22	42.72	15.36	0.61	0.27	11.69	0.55	0.01	97.78	0.00	-0.01	97.77
8-8-7line1	1.66	11.18	13.12	43.74	15.23	0.52	0.25	11.64	0.55	0.01	97.89	0.00	-0.01	97.88
8-8-7line1	1.75	11.15	13.30	42.93	15.25	0.68	0.23	11.87	0.59	0.00	97.76	0.00	0.00	97.76

Amphibole Mineral Chemistry Results from Electron Microprobe Analysis (Based on 23 oxygens)

Sample	Na2O	MgO	Al2O3	SiO2	FeO	TiO2	MnO	CaO	K2O	Cl	Total	F	Cl	TOTAL
8-8-7line1	1.63	11.16	13.23	43.28	15.27	0.57	0.23	11.77	0.53	0.03	97.70	0.00	-0.03	97.67
8-8-7line1	1.55	11.10	13.15	43.37	15.07	0.59	0.25	11.74	0.53	0.00	97.36	0.00	0.00	97.36
8-8-7line1	0.00	0.00	27.31	37.69	8.99	0.14	0.15	22.93	0.00	0.01	97.21	0.00	-0.01	97.21
8-8-7line1	1.40	9.90	13.20	42.67	17.81	0.42	0.23	12.05	0.45	0.01	98.14	0.00	-0.01	98.14
8-8-7line1	1.58	11.30	12.82	44.66	14.53	0.50	0.21	11.32	0.47	0.00	97.40	0.00	0.00	97.40
8-8-7line1	1.66	11.34	13.23	43.99	15.05	0.47	0.23	11.53	0.47	0.00	97.96	0.00	0.00	97.96
8-8-7line2	1.46	12.33	11.50	45.69	13.65	0.42	0.27	11.68	0.32	0.03	97.35	0.00	-0.03	97.32
8-8-7line2	1.79	11.19	13.83	43.41	14.84	0.52	0.24	11.26	0.51	0.00	97.58	0.00	0.00	97.58
8-8-7line2	1.51	11.01	13.62	43.32	14.77	0.54	0.27	11.56	0.47	0.00	97.06	0.00	0.00	97.06
8-8-7line2	1.74	10.74	13.74	43.09	15.14	0.63	0.24	11.35	0.55	0.00	97.23	0.00	0.00	97.23
8-8-7line2	1.78	10.84	13.86	42.94	14.99	0.53	0.27	11.24	0.50	0.01	96.97	0.00	-0.01	96.96
8-8-7line2	1.74	11.43	13.17	43.47	15.14	0.47	0.26	11.09	0.54	0.08	97.39	0.00	-0.08	97.31
8-8-7line2	1.71	10.84	14.00	42.73	14.82	0.69	0.21	11.48	0.55	0.01	97.05	0.00	-0.01	97.04
8-8-7line2	1.28	13.35	7.95	49.74	12.70	0.22	0.17	11.62	0.20	0.00	97.23	0.00	0.00	97.22
8-8-7line2	1.63	10.94	14.05	43.50	15.23	0.60	0.27	11.55	0.61	0.01	98.37	0.00	-0.01	98.37
mt-3icore1.1	0.69	15.35	6.62	50.64	10.62	0.20	0.25	13.70	0.08	0.00	98.14	-0.05	0.00	98.09
mt-3int1.2	0.52	16.83	3.82	52.65	9.49	0.13	0.18	13.63	0.05	0.01	97.30	-0.04	0.00	97.26
mt-3rim1.2	1.43	11.29	14.25	44.16	14.09	0.39	0.25	13.12	0.25	0.00	99.23	-0.07	0.00	99.16
mt-3rim2.1	1.37	11.55	13.54	45.04	12.66	0.43	0.20	13.35	0.20	0.01	98.35	-0.03	0.00	98.32
mt-3core2.2	0.63	16.30	4.86	52.08	9.98	0.15	0.23	13.78	0.12	0.00	98.12	-0.03	0.00	98.10
mt-3rim2.3	1.02	12.85	9.67	47.64	12.36	0.30	0.18	13.50	0.35	0.01	97.88	-0.05	0.00	97.82
mm3-1rim1.3	1.23	8.48	17.34	42.30	14.93	0.43	0.33	13.53	0.43	0.02	99.01	-0.06	0.00	98.96
mm3-1int2.1	1.12	9.11	16.29	42.66	15.14	0.43	0.17	13.61	0.28	0.00	98.80	-0.07	0.00	98.73
mt-3.grain4	0.35	16.88	3.93	52.53	10.13	0.06	0.23	14.30	0.10	0.00	98.51	-0.02	0.00	98.49
mt-3.grain4	0.49	16.57	4.63	51.84	9.94	0.08	0.21	14.06	0.11	0.00	97.94	-0.05	0.00	97.89
mt-3.grain4	0.62	16.28	5.03	52.03	9.87	0.15	0.29	13.82	0.08	0.00	98.16	-0.06	0.00	98.10
mt-3.grain4	1.10	13.26	10.31	47.24	11.97	0.33	0.16	13.82	0.16	0.01	98.35	-0.03	0.00	98.31
mm-3.grain4	1.06	9.70	15.49	43.38	14.87	0.39	0.22	12.89	0.25	0.00	98.24	-0.07	0.00	98.17
mm-3.grain4	1.16	8.44	17.41	41.77	15.14	0.42	0.29	12.88	0.32	0.00	97.84	-0.05	0.00	97.79
mm-3.grain3	1.13	9.82	15.13	43.72	14.85	0.47	0.25	12.73	0.30	0.01	98.39	-0.08	0.00	98.31
mm-3.grain3	1.18	9.95	14.65	43.44	14.54	0.49	0.30	12.61	0.26	0.02	97.43	-0.07	0.00	97.36
04t-ml-2.grain1	1.32	13.04	12.23	45.71	12.68	0.46	0.18	11.98	0.27	0.01	97.88	-0.02	0.00	97.86

Amphibole Mineral Chemistry Results from Electron Microprobe Analysis (Based on 23 oxygens)

Sample	Na2O	MgO	Al2O3	SiO2	FeO	TiO2	MnO	CaO	K2O	Cl	Total	F	Cl	TOTAL
04t-ml-2.grain1	1.28	12.49	12.53	45.24	12.87	0.51	0.20	11.82	0.28	0.01	97.21	-0.05	0.00	97.16
04t-ml-2.grain1	1.32	12.86	11.75	45.66	12.77	0.43	0.26	12.05	0.24	0.01	97.35	-0.04	0.00	97.31
04t-ml-2.grain2	1.41	12.74	12.71	45.35	12.80	0.47	0.22	11.78	0.27	0.01	97.74	-0.05	0.00	97.68
04t-ml-2.grain2	1.36	13.10	11.97	46.01	12.44	0.34	0.16	11.66	0.23	0.02	97.29	-0.04	0.00	97.25
04t-ml-2.grain3	1.38	12.77	12.68	45.37	12.56	0.41	0.21	11.69	0.28	0.00	97.34	-0.03	0.00	97.31
04t-ml-2.grain3	0.01	0.03	26.25	40.00	8.30	0.11	0.02	22.79	0.02	0.01	97.53	-0.07	0.00	97.47
mm-3grain3	1.06	8.88	17.10	43.05	14.98	0.43	0.31	11.49	0.33	0.00	97.62	-0.06	0.00	97.56
mm-3grain3	1.06	8.43	17.91	42.59	15.22	0.40	0.16	11.54	0.39	0.00	97.70	-0.08	0.00	97.62
mt-3grain5	1.49	11.40	14.36	44.73	13.20	0.43	0.22	11.53	0.27	0.00	97.63	-0.06	0.00	97.57
mt-3grain5	0.88	14.74	8.14	49.69	11.53	0.27	0.28	11.93	0.14	0.01	97.60	-0.05	0.00	97.55
04t-mm1.rim3.1	1.77	8.58	11.51	42.32	20.76	0.63	0.34	11.09	0.49	0.00	97.50	0.00	0.00	97.50
04t-mm1.cor3.1	1.86	8.42	11.65	41.83	20.82	0.64	0.36	11.13	0.56	0.00	97.27	0.00	0.00	97.27
TSA-2.rim1.1	2.46	10.62	12.30	40.74	16.84	1.17	0.26	11.83	0.62	0.01	96.86	0.00	-0.01	96.84
TSA-2.rim2.1	2.54	10.60	12.39	40.22	16.99	1.13	0.29	11.76	0.63	0.03	96.58	0.00	-0.03	96.55
tsa2.grain3.1	2.51	10.56	13.31	40.23	16.68	1.11	0.25	11.93	0.63	0.02	97.22	0.00	-0.02	97.20
tsa2.grain3.2	2.41	10.95	12.75	40.59	16.89	0.99	0.25	11.90	0.55	0.01	97.27	0.00	-0.01	97.27
tsa2.grain1.1	2.53	11.80	11.90	42.53	15.50	0.88	0.22	11.95	0.48	0.00	97.80	0.00	0.00	97.80
tsa2.grain1.1	2.54	11.01	12.59	40.95	16.40	1.08	0.27	11.72	0.65	0.00	97.19	0.00	0.00	97.19
tsa2.grain1.1	2.53	11.80	11.90	42.53	15.50	0.88	0.22	11.95	0.48	0.00	97.80	0.00	0.00	97.80
o4t-mm-1.grain1.1	6.64	2.65	14.79	52.63	6.69	5.68	0.08	8.69	0.23	0.02	98.10	0.00	-0.02	98.09
o4t-mm-1.grain1.2	1.87	7.82	12.39	41.60	20.63	0.68	0.33	11.13	0.67	0.01	97.12	0.00	-0.01	97.11
o4t-mm-1.grain1.3	1.82	8.20	11.85	41.89	20.71	0.59	0.36	11.09	0.64	0.00	97.14	0.00	0.00	97.14
o4t-mm-1.grain2.2	1.77	8.74	10.86	43.07	20.10	0.52	0.30	11.31	0.38	0.02	97.07	0.00	-0.02	97.04

B) Feldspar Mineral Chemistry (Based on 8 oxygens)

Feldspars	Na	Al	Si	K	Ca	Fe	Total	Albite	Orthoclase	Anorthite
Albite	11.232	20.185	68.437	0.289	0.37	0	100.513	96.603	1.636	1.761
sf-2grain1.1	7.565	26.103	59.671	0.047	7.266	0.055	100.707	65.152	0.268	34.58
sf-2grain1.2	7.828	25.584	60.816	0.051	6.478	0.023	100.78	68.417	0.294	31.288
sf-2grain2.1	7.044	26.904	58.378	0.062	8.066	0.027	100.481	61.031	0.351	38.619
sf-2grain2.2	7.765	26.129	60.022	0.087	6.892	0.021	100.916	66.764	0.491	32.746
sf-2grain3.1	7.682	25.975	59.552	0.052	6.889	0.011	100.161	66.665	0.297	33.038
sf-2grain3.2	7.623	25.855	59.641	0.056	7.138	0	100.313	65.691	0.317	33.992
sf-2grain4.1	7.223	26.594	59	0.075	7.437	0.063	100.392	63.459	0.434	36.107
sf-2grain4.2	7.845	25.852	60.101	0.12	6.756	0.139	100.813	67.3	0.675	32.025
albite	11.29	20.051	67.937	0.273	0.352	0.023	99.926	96.794	1.541	1.666
8-11-5grain1.1	8.568	24.679	61.686	0.028	5.488	0.065	100.514	73.742	0.158	26.1
8-11-5rim1.1	8.307	24.931	61.325	0.069	5.694	0.205	100.531	72.241	0.396	27.363
8-11-5int1.2	8.876	23.969	62.19	0.074	4.725	0.089	99.923	76.944	0.423	22.633
8-11-5cor1.2	8.616	24.718	61.791	0.088	5.272	0.05	100.535	74.358	0.502	25.14
8-11-5grain2.1	8.696	24.168	61.984	0.178	4.982	0.019	100.027	75.186	1.011	23.802
8-11-5grain2.2	8.799	24.182	61.868	0.087	4.985	0	99.921	75.78	0.496	23.724
8-11-5grain2.3	8.785	24.04	62.452	0.042	4.7	0.022	100.041	76.993	0.244	22.763
8-11-5grain2.4	8.129	24.816	61.041	0.019	5.821	0.021	99.847	71.569	0.111	28.319
8-11-5grain3.1	9.177	23.462	63.03	0.186	4.027	0.038	99.92	79.629	1.061	19.31
8-11-5grain3.2	8.376	24.743	61.85	0.068	5.529	0.051	100.617	72.985	0.391	26.623
8-11-5grain3.3	8.525	24.386	61.22	0.036	5.517	0.065	99.749	73.507	0.207	26.286
f1-1cor1.2	4.405	30.688	52.192	0.054	12.347	0.049	99.735	39.109	0.315	60.576
f1-1cor1.3	4.141	31.084	51.874	0.041	12.83	0.05	100.02	36.785	0.237	62.978
f1-1cor1.4	5.951	28.582	56.044	0.062	9.766	0.06	100.465	52.255	0.357	47.388
f1-1cor1.5	5.429	29.139	55.03	0.04	10.532	0.012	100.182	48.15	0.233	51.617
f1-1int1.6	5.912	28.804	55.828	0.06	9.831	0	100.435	51.933	0.348	47.719
f1-1rim1.7	5.073	29.5	54.203	0.077	11.252	0.05	100.155	44.73	0.445	54.824
f1-1rim1.8	6.118	28.274	56.273	0.046	9.903	0.013	100.627	52.647	0.261	47.093
f1-1rim2.1	4.079	30.938	51.697	0.026	13.039	0.083	99.862	36.09	0.154	63.756
f1-1rim2.2	4.288	30.927	52.324	0.03	12.637	0.02	100.226	37.979	0.176	61.845
f1-1int2.1	5.064	29.061	54.248	0.344	11.011	0	99.728	44.518	1.99	53.492
f1-1int2.2	4.089	31.284	52.01	0.041	13.067	0.006	100.497	36.068	0.236	63.696

B) Feldspar Mineral Chemistry (continued)

Feldspars	Na	Al	Si	K	Ca	Fe	Total	Albite	Orthoclase	Anorthite
f1-1icor2.1	5.613	28.885	55.236	0.058	10.145	0.032	99.969	49.86	0.339	49.802
sf-3cor1.1	5.1	29.594	53.912	0.087	11.42	0.007	100.12	44.471	0.5	55.029
sf-3cor1.2	5.118	29.616	54.093	0.071	11.327	0.035	100.26	44.798	0.409	54.793
sf-3int1.1	4.186	30.785	52.197	0.072	13.234	0.002	100.476	36.254	0.408	63.338
sf-3int1.2	4.208	31.101	52.017	0.05	12.909	0.005	100.29	36.992	0.289	62.718
sf-3rim1.2	4.496	30.846	53.03	0.033	12.525	0.047	100.977	39.305	0.19	60.505
sf-3rim1.1	3.838	31.514	51.099	0.02	13.482	0.098	100.051	33.964	0.115	65.92
sf-3cor.1.1	5.3	29.498	54.229	0.117	11.067	0.017	100.228	46.117	0.667	53.216
sf-3cor.1.3	3.895	31.621	51.415	0.031	13.646	0.015	100.623	33.997	0.179	65.825
sf-3cor.2.1	5.639	28.76	54.959	0.048	10.56	0.03	99.996	49.008	0.277	50.716
sf-3cor.2.2	5.749	28.818	55.251	0.066	10.274	0	100.158	50.125	0.376	49.499
sf-3rim.2.1	5.573	28.679	55.029	0.025	10.367	0	99.673	49.242	0.143	50.615
sf-3rim.2.2	5.371	29.389	54.591	0.042	10.871	0.027	100.291	47.092	0.241	52.667
8-3-5grain.1.1	8.765	24.251	61.534	0.142	5.086	0.049	99.827	75.113	0.802	24.085
8-3-5grain.1.3	8.008	24.397	61.546	1.053	4.862	0.084	99.95	70.32	6.086	23.594
8-3-5grain.1.4	7.935	25.464	60.614	0.248	6.485	0.08	100.826	67.925	1.397	30.677
8-3-2grain.1.1	6.343	27.693	57.205	0.075	9.207	0.02	100.543	55.251	0.431	44.318
8-3-2grain.1.2	6.358	27.857	57.36	0.141	8.929	0.005	100.65	55.846	0.815	43.339
8-3-2grain.1.3	6.497	28.059	57.255	0.1	8.952	0.02	100.883	56.448	0.572	42.98
8-3-2grain.1.4	6.265	28.093	56.957	0.365	8.948	0.036	100.664	54.717	2.096	43.187
8-3-2grain.2.1	5.683	28.958	55.582	0.044	10.279	0.047	100.593	49.888	0.252	49.86
8-3-2grain.2.2	5.427	29.338	55.116	0.061	10.744	0.043	100.729	47.586	0.35	52.063
8-3-2grain.2.3	5.957	28.617	56.25	0.086	9.892	0.042	100.844	51.894	0.49	47.615
8-3-2grain.2.4	5.328	29.44	54.803	0.041	10.801	0.048	100.461	47.054	0.237	52.709

C) Biotite Mineral Chemistry (Based on 22 oxygens)

Sample	F	Na2O	MgO	Al2O3	TiO2	K2O	Cl	SiO2	CaO	MnO	FeO	Total	F	Cl	Total
sf-2bio1.2	0.311	0.291	9.952	18.023	1.319	8.871	0.003	35.187	0.041	0.037	20.509	94.544	-0.311	-0.003	94.23
sf-2bio1.3	0.402	0.133	9.745	17.722	1.444	8.651	0.006	34.855	0.05	0.065	21.335	94.408	-0.402	-0.006	94
sf-2bio1.4	0.351	0.233	9.613	18.953	1.568	9.16	0.003	35.419	0	0.018	19.414	94.732	-0.351	-0.003	94.378
sf-2bio1.5	0.321	0.238	9.679	18.629	1.435	8.904	0.007	35.295	0	0.026	19.9	94.434	-0.321	-0.007	94.106
sf-2bio3.1	0.284	0.205	9.994	18.552	1.419	8.693	0.009	35.144	0.018	0.047	19.987	94.352	-0.284	-0.009	94.059
sf-2bio3.2	0.301	0.159	10.032	17.349	1.391	8.857	0.003	35.741	0.028	0.045	20.588	94.494	-0.301	-0.003	94.19
sf-2mus1.1	0.025	1.389	0.601	35.668	0.261	9.567	0.025	46.092	0	0.006	1.956	95.59	-0.025	-0.025	95.54
sf-2mus1.2	0.078	1.338	0.576	35.593	0.282	9.659	0.031	45.876	0.005	0	1.777	95.215	-0.078	-0.031	95.106
sf-2mus2.1	0.044	1.286	0.685	34.821	0.269	9.339	0	46.076	0.015	0	2.094	94.629	-0.044	0	94.585
lemhi	0.27	0.092	2.759	17.552	1.277	9.022	1.169	33.051	0	0.044	31.015	96.251	-0.27	-1.169	94.812
8-3-2grain1.1	0.234	0.107	9.722	18.722	1.891	9.327	0.004	36.014	0.049	0.053	20.244	96.367	-0.234	-0.004	96.129
8-3-2grain1.2	0.262	0.235	10.339	19.103	1.746	9.084	0.009	36.167	0.002	0.08	18.961	95.988	-0.262	-0.009	95.717
8-3-2bio1.3	0.199	0.091	9.648	19.395	1.518	9.102	0	35.653	0.018	0.109	19.79	95.523	-0.199	0	95.324
8-3-2bio2.1	0.254	0.157	11.225	19.252	1.547	9.167	0.004	36.227	0.018	0.046	16.941	94.838	-0.254	-0.004	94.58
8-3-2bio2.2	0.272	0.223	10.935	19.712	1.644	9.355	0.007	35.924	0.014	0.06	16.531	94.677	-0.272	-0.007	94.398
8-3-2bio3.1	0.193	0.27	10.98	19.59	1.694	8.968	0.018	36.175	0.023	0.024	17.808	95.743	-0.193	-0.018	95.532
8-3-2bio3.2	0.217	0.205	10.802	19.554	1.982	9.127	0	35.965	0.014	0.041	17.623	95.53	-0.217	0	95.313
8-3-2mus1.1	0.021	1.059	0.823	35.665	0.308	9.513	0.007	46.526	0	0	1.164	95.086	-0.021	-0.007	95.058
8-3-2mus1.2	0.089	1.105	0.778	35.75	0.477	9.715	0	46.39	0.02	0.013	1.183	95.52	-0.089	0	95.431
8-3-2mus1.3	0.081	1.083	0.716	35.784	0.496	9.726	0	46.194	0.01	0.043	1.015	95.148	-0.081	0	95.067
8-3-2mus2.1	0.001	1.151	0.794	36.209	0.233	9.652	0.015	46.075	0.008	0	1.169	95.307	-0.001	-0.015	95.291
sf-3bio1.2	0.359	0.125	11.75	18.526	1.597	9.325	0	36.407	0.002	0.035	16.744	94.87	-0.359	0	94.511
sf-3bio1.3	0.255	0.267	12.251	19.031	1.789	9.133	0.028	36.471	0.005	0.029	15.603	94.862	-0.255	-0.028	94.579
sf-3biocore2.2	0.278	0.192	12.203	19.188	1.928	9.599	0.006	37.04	0.011	0	15.851	96.296	-0.278	-0.006	96.012
sf-3biorim2.1	0.323	0.158	12.208	19.027	1.813	9.389	0	36.531	0.045	0.014	15.757	95.265	-0.323	0	94.942
sf-3mus1.1	0.078	0.951	1.011	35.84	0.867	10.241	0.001	47.21	0.016	0.011	1.44	97.666	-0.078	-0.001	97.587
sf-3mus1.2	0.114	0.899	0.916	34.747	0.921	9.724	0.004	46.697	0	0	1.356	95.378	-0.114	-0.004	95.26
sf-3mus2.1	0.049	0.937	0.917	34.892	0.686	9.941	0	46.444	0.026	0	1.382	95.274	-0.049	0	95.225
sf-3mus2.2	0.095	0.948	0.915	34.89	0.803	9.951	0.01	46.203	0	0.008	1.366	95.189	-0.095	-0.01	95.084
lemhi	0.293	0.167	2.764	17.684	1.264	8.947	1.228	33.055	0.016	0.05	30.761	96.229	-0.293	-1.228	94.708
f1-1biocore1.1	0.312	0.298	11.965	19.092	1.853	9.218	0.038	36.566	0	0	16.04	95.382	-0.312	-0.038	95.032
f1-1bioint1.1	0.27	0.23	11.905	18.702	1.813	9.001	0.006	36.009	0.012	0	16.288	94.236	-0.27	-0.006	93.96

C) Biotite Mineral Chemistry

Sample	F	Na2O	MgO	Al2O3	TiO2	K2O	Cl	SiO2	CaO	MnO	FeO	Total	F	Cl	Total
f1-1bioint1.2	0.286	0.319	11.976	18.921	1.754	9.203	0.033	36.284	0.013	0.028	16.28	95.097	-0.286	-0.033	94.778
f1-1biorim1.1	0.328	0.209	11.589	19.054	1.743	9.371	0	36.392	0	0.047	16.107	94.84	-0.328	0	94.512
f1-1biocor1.2	0.303	0.354	11.79	18.819	1.901	9.122	0	36.408	0	0	15.76	94.457	-0.303	0	94.154
f1-1bioint2.1	0.254	0.367	12.069	18.986	1.789	8.543	0.014	36.211	0.023	0.031	16.294	94.581	-0.254	-0.014	94.313
f1-1biorim3.1	0.324	0.242	11.485	18.536	1.926	9.176	0.006	36.391	0.01	0.031	16.807	94.934	-0.324	-0.006	94.604
f1-1bioint3.1	0.315	0.178	11.686	18.838	1.83	8.999	0	36.197	0.007	0.047	16.486	94.583	-0.315	0	94.268
f1-1bioint4.2	0.369	0.253	12.255	18.967	1.751	9.327	0.035	36.3	0	0	15.419	94.676	-0.369	-0.035	94.272
f1-1mus1.1	0.11	1.005	0.992	34.459	0.705	10.059	0	45.876	0.004	0	1.701	94.911	-0.11	0	94.801
f1-1mus1.2	0.087	0.952	1.01	34.077	0.817	9.987	0	46.318	0.014	0.003	1.63	94.895	-0.087	0	94.808
f1-1mus1.3	0.048	0.946	0.906	34.553	0.809	9.662	0	45.611	0.002	0	1.622	94.159	-0.048	0	94.111
f1-1mus2.1	0.05	0.97	0.943	34.786	0.718	10.002	0.007	45.785	0.004	0	1.576	94.841	-0.05	-0.007	94.784
f1-1mus2.2	0.189	0.967	1.062	33.698	1.864	9.215	0.012	46.223	1.572	0	1.854	96.656	-0.189	-0.012	96.455
8-11-5bio3.1	0.472	0.133	12.539	17.324	1.341	8.46	0	35.992	0.055	0.271	17.856	94.443	-0.472	0	93.971
8-11-5bio5.1	0.414	0.245	12.552	17.774	1.453	8.747	0.02	37.087	0.027	0.184	16.763	95.266	-0.414	-0.02	94.832
8-11-5bio5.2	0.378	0.186	12.945	17.784	1.396	8.383	0.017	36.539	0.008	0.286	16.539	94.461	-0.378	-0.017	94.066
8-11-5bio5.3	0.41	0.179	12.287	18.133	1.389	9.048	0	36.772	0.033	0.266	16.756	95.273	-0.41	0	94.863
8-11-5bio5.4	0.362	0.207	12.226	17.935	1.471	9.408	0.003	36.609	0	0.232	16.484	94.937	-0.362	-0.003	94.572
8-11-5mus1.1	0.066	2.384	0.639	34.305	0.262	7.779	0.007	46.873	0.349	0.019	2.355	95.038	-0.066	-0.007	94.965
8-11-5mus1.2	0.123	1.927	0.687	34.482	0.295	8.316	0.003	45.609	0.04	0.051	2.475	94.008	-0.123	-0.003	93.882
8-11-5mus1.3	0.066	1.89	0.592	34.958	0.297	8.626	0	45.58	0	0	2.484	94.493	-0.066	0	94.427

D) Garnet Mineral Chemistry Data from Microprobe Analysis (Based on 12 oxygens)

Sample	MgO	Al2O3	CaO	TiO	FeO	MnO	SiO2	Total
garrv	7.265	22.864	18.579	0.385	11.45	0.184	40.023	100.75
F1-1rim1.1	3.413	21.738	6.196	0.038	31.532	0.294	37.609	100.82
F1-1rim1.2	3.436	21.55	6.467	0.038	30.849	0.672	37.272	100.284
F1-1rim1.3	3.544	21.778	5.483	0.042	32.061	0.453	37.433	100.794
F1-1int1.1	2.297	21.59	8.145	0.061	31.039	0.215	37.374	100.721
F1-1int1.2	2.977	21.486	6.253	0.012	31.566	0.829	37.412	100.535
F1-1cor1.1	1.299	21.644	9.005	0.065	31.31	0.715	37.244	101.282
F1-1cor1.2	1.652	21.435	8.865	0.061	30.787	0.391	37.507	100.698
F1-1cor1.3	2.352	21.537	7.712	0.057	31.117	0.337	37.207	100.319
F1-1rim2.1	3.88	21.658	4.437	0.017	32.226	0.854	37.309	100.381
F1-1rim2.2	3.824	21.801	4.78	0.032	32.065	0.664	37.589	100.755
F1-1rim2.3	3.8	21.556	4.518	0	32.034	1.025	37.373	100.306
F1-1cor2.1	0.961	21.33	9.048	0.036	30.054	1.805	36.876	100.11
F1-1cor2.2	1.131	21.397	9.04	0.034	30.472	0.982	37.002	100.058
F1-1cor2.3	1.049	21.271	8.936	0.07	30.21	1.749	37.005	100.29
8-11-5rim1.1	2.653	21.334	3.71	0.024	28.996	6.436	36.925	100.078
8-11-5rim1.2	2.692	21.257	3.513	0.02	29.173	6.424	36.702	99.781
8-11-5rim1.3	2.65	21.332	3.441	0	29.314	6.412	36.994	100.143
8-11-5cor1.1	1.781	21.26	5.511	0.107	26.67	8.057	36.86	100.246
8-11-5cor1.2	1.522	21.17	5.768	0.114	25.953	8.683	36.653	99.863
8-11-5cor1.3	1.8	21.026	5.674	0.091	26.507	7.814	36.664	99.576
8-11-5rim2.1	2.739	21.419	3.675	0.048	28.984	6.525	36.858	100.248
8-11-5rim2.2	2.742	21.335	3.155	0.014	29.453	6.634	36.987	100.32
8-11-5cor2.1	2.62	21.301	3.444	0.062	28.791	6.88	36.783	99.881
8-11-5cor2.2	2.532	21.236	3.661	0.043	28.905	6.797	36.763	99.937
8-11-5rim3.1	2.535	21.379	5.574	0.105	23.459	9.952	37.048	100.052
8-11-5rim3.2	2.715	21.598	4.07	0.048	27.613	7.769	37.376	101.189
8-11-5rim3.3	2.594	21.325	4.239	0.014	26.91	7.964	36.778	99.824
8-11-5cor3.2	1.422	21.2	4.409	0.043	24.787	11.566	36.976	100.403
8-11-5cor3.3	1.236	21.104	5.628	0.072	24.116	11.146	36.682	99.984
SF-2rim1.1	2.16	21.357	4.931	0.071	31.973	3.023	36.887	100.402
SF-2rim1.2	2.083	21.302	5.492	0.039	31.927	2.568	36.351	99.762
SF-2int1.1	1.753	21.216	4.522	0.146	27.528	8.58	36.695	100.44
SF-2int1.2	1.636	21.264	3.689	0.057	26.395	10.638	36.598	100.277
SF-2cor1.1	1.481	20.971	4.048	0.237	25.561	10.989	36.149	99.436
SF-2cor1.2	1.449	20.936	3.941	0.271	25.575	11.087	36.41	99.669
SF-2rim2.1	2.085	21.374	5.353	0.071	32.046	2.623	36.785	100.337
SF-2rim2.2	2.263	21.439	4.58	0.029	32.759	2.776	36.857	100.703
SF-2int2.1	2.1	21.126	4.354	0.1	31.559	4.112	36.791	100.142
SF-2int2.2	2.166	21.365	4.095	0.035	32.114	3.673	36.771	100.219
SF-2cor2.1	2.225	21.252	4.363	0.055	32.129	3.313	36.581	99.918
SF-2cor2.2	2.228	21.451	4.484	0.058	32.432	3.123	36.743	100.519
f1-1line1	3.03	21.646	6.938	0.032	30.529	0.425	37.337	99.937
f1-1line1	3.528	21.715	5.121	0.022	32.113	1.092	37.447	101.038
f1-1line1	2.159	21.198	5.817	0	33.377	0.623	36.143	99.317
f1-1line1	1.57	21.431	8.066	0.034	31.264	0.997	36.71	100.072
f1-1line1	1.232	20.915	9.024	1.96	30.186	0.627	35.811	99.755
f1-1line1	1.294	21.339	9.19	0.039	30.717	0.526	36.649	99.754

D) Garnet Mineral Chemistry Data from Microprobe Analysis

Sample	MgO	Al2O3	CaO	TiO	FeO	MnO	SiO2	Total
f1-1line1	2.268	21.411	5.735	0.014	33.686	0.569	36.74	100.423
f1-1line1	1.688	21.639	8.501	0.016	31.475	0.372	37.238	100.929
f1-1line1	1.746	21.552	8.971	0.068	30.793	0.226	37.294	100.65
f1-1line1	2.687	21.596	7.177	0.032	31.547	0.579	37.335	100.953
f1-1line1	3.615	21.327	4.271	0	33.033	0.935	36.814	99.995
8-11-5line1	2.747	21.523	3.925	0.028	28.381	6.727	37.246	100.577
8-11-5line1	2.576	21.493	5.667	0.08	24.999	8.307	37.205	100.327
8-11-5line1	2.509	21.543	5.406	0.046	25.411	8.434	37.237	100.586
8-11-5line1	2.018	21.245	5.581	0.058	27.487	6.042	36.643	99.074
8-11-5line1	2.054	21.237	5.151	0.032	26.77	7.356	37.177	99.777
8-11-5line1	1.8	21.192	5.61	0.112	25.818	8.912	37.053	100.497
8-11-5line1	1.283	20.81	5.523	0.065	24.214	11.113	36.371	99.379
8-11-5line1	1.122	20.722	6.437	0.176	22.596	11.902	36.497	99.452
8-11-5line1	1.286	20.876	5.79	0.181	23.807	11.032	36.506	99.478
8-11-5line1	1.644	21.356	5.103	0.079	25.618	9.77	36.781	100.351
8-11-5line1	1.662	21.257	5.829	0.106	27.681	7.025	36.85	100.41
8-11-5line1	1.834	21.356	5.597	0.083	28.588	6.017	37.085	100.56
8-11-5line1	2.157	21.387	5.592	0.094	28.108	6.198	37.085	100.621
8-11-5line1	2.366	21.375	5.457	0.092	26.198	7.543	37.013	100.044
8-11-5line1	2.886	21.394	3.152	0	29.553	6.148	36.915	100.048
sf-2line1	2.179	21.388	4.329	0.085	31.293	4.719	36.92	100.913
sf-2line1	2.194	21.382	4.147	0.075	30.914	4.79	36.376	99.878
sf-2line1	1.944	21.3	3.744	0.093	29.412	6.957	37.041	100.491
sf-2line1	1.763	21.444	4.561	0.129	27.461	8.457	36.966	100.781
sf-2line1	1.655	21.396	4.334	0.149	26.647	9.743	36.977	100.901
sf-2line1	1.613	21.204	4.365	0.14	26.128	9.904	36.92	100.274
sf-2line1	1.634	21.19	4.257	0.145	26.088	10.189	36.82	100.323
sf-2line1	1.767	21.408	4.216	0.111	27.999	8.345	37.113	100.959
sf-2line1	1.85	21.347	3.901	0.118	28.481	7.955	36.913	100.565
sf-2line1	1.829	21.29	4.194	0.074	28.697	7.45	36.579	100.113
sf-2line1	1.918	21.325	3.86	0.072	29.296	7.133	36.941	100.545
sf-2line1	2.021	20.933	4.084	0.096	30.265	5.924	36.285	99.608
rvm752	7.191	22.927	18.58	0.371	11.434	0.192	39.948	100.643
SF-3rim1.1	3.923	21.891	3.856	0.013	32.335	1.514	37.199	100.731
SF-3rim1.2	3.893	21.696	4.139	0.02	32.26	1.243	37.16	100.411
SF-3rim1.3	3.974	21.81	4.056	0	32.303	1.36	37.065	100.568
SF-3int1.1	1.118	21.355	9.104	0.104	30.458	1.195	36.745	100.079
SF-3int1.2	1.217	21.492	9.113	0.082	30.58	0.912	36.998	100.394
SF-3cor1.1	3.782	21.41	4.202	0.006	32.001	1.666	37.205	100.272
SF-3cor1.2	3.934	21.905	3.815	0.026	32.059	1.601	37.215	100.555
SF-3cor1.3	3.906	21.633	4.075	0.005	32.151	1.591	37.156	100.517
SF-3rim2.1	3.761	21.892	4.922	0.045	31.991	0.953	37.357	100.921
SF-3rim2.2	3.751	21.852	4.995	0.024	32.127	0.871	37.372	100.992
SF-3rim2.3	3.897	21.742	4.342	0	32.236	1.05	37.193	100.46
SF-3int2.1	1.597	21.469	9.287	0.056	30.438	0.362	37.109	100.318
SF-3int2.2	1.417	21.492	9.471	0.075	30.43	0.601	37.052	100.538
SF-3cor2.1	1.977	21.445	8.599	0.047	30.249	1.019	37.024	100.36

D) Garnet Mineral Chemistry Data from Microprobe Analysis

Sample	MgO	Al2O3	CaO	TiO	FeO	MnO	SiO2	Total
SF-3cor2.3	1.651	21.587	9.406	0.071	30.234	0.72	37.087	100.756
8-3-5rim1.1	2.244	21.291	4.867	0.059	30.647	4.306	36.921	100.335
8-3-5rim1.2	2.256	21.663	5.042	0.034	30.615	4.058	36.863	100.531
8-3-5rim1.3	2.245	21.436	4.72	0.033	30.547	4.604	36.743	100.328
8-3-5int1.1	2.097	21.279	5.076	0.051	29.325	5.685	36.92	100.433
8-3-5int1.2	1.882	21.073	4.77	0.081	28.248	7.328	36.621	100.003
8-3-5int1.3	1.994	21.282	5.398	0.097	28.548	6.277	36.74	100.336
8-3-5cor1.1	2.107	21.392	4.492	0.073	29.283	6.574	36.982	100.903
8-3-5cor1.2	1.977	21.163	4.719	0.14	28.587	7.008	36.727	100.321
8-3-5cor1.3	1.796	21.252	4.761	0.098	27.652	7.996	36.705	100.26
8-3-5cor1.4	1.791	21.244	4.85	0.12	27.443	8.277	36.945	100.67
8-3-5rim2.1	2.147	21.417	5.328	0.052	30.668	4.225	37.067	100.904
8-3-5rim2.2	2.201	21.544	5.19	0.044	30.886	4.161	37.005	101.031
8-3-5int2.2	2.293	21.482	4.532	0.054	30.353	5.247	36.937	100.898
8-3-5int2.4	2.049	21.384	4.419	0.089	29.55	6.569	37.054	101.114
8-3-2rim1.1	3.495	21.762	3.58	0.002	33.37	1.571	37.19	100.97
8-3-2rim1.2	2.45	21.662	6.876	0.049	30.783	1.688	37.231	100.739
8-3-2rim1.3	2.55	21.787	6.253	0.058	31.376	1.993	37.172	101.189
8-3-2int1.2	1.251	21.372	7.151	0.109	30.185	3.771	36.801	100.64
8-3-2cor1.2	1.148	21.535	7.302	0.06	29.739	4.234	36.913	100.931
8-3-2cor1.3	1.143	21.41	7.535	0.052	29.567	4.148	37.026	100.881
8-3-2rim2.1	1.841	21.445	6.77	0.079	32.063	1.738	37.169	101.105
8-3-2rim2.2	1.222	21.593	7.447	0.104	30.053	3.771	36.909	101.099
8-3-2cor2.2	0.889	21.379	8.133	0.109	27.194	6.046	36.76	100.51
8-3-2cor2.3	0.862	21.502	8.148	0.126	26.964	6.18	37.057	100.839
8-3-2line1	2.062	21.507	7.057	0.076	31.569	1.388	37.127	100.786
8-3-2line1	1.874	21.652	7.184	0.065	31.834	1.359	37.321	101.289
8-3-2line1	1.42	21.489	7.033	0.105	31.061	2.919	37.155	101.182
8-3-2line1	1.235	21.429	7.513	0.103	29.863	3.728	37.237	101.108
8-3-2line1	1.104	20.771	7.415	0.049	28.965	4.032	37.163	99.499
8-3-2line1	1.005	21.373	8.099	0.086	28.439	4.614	36.937	100.553
8-3-2line1	1.128	21.334	7.676	0.084	29.417	4.129	36.978	100.746
8-3-2line1	1.274	21.472	7.309	0.072	30.02	3.608	36.705	100.46
8-3-2line1	1.331	21.421	6.931	0.115	30.92	3.235	37.103	101.056
8-3-5line1	2.271	21.406	4.829	0.063	30.591	4.29	37.102	100.552
8-3-5line1	2.257	21.438	5.004	0.035	29.702	5.07	37.24	100.746
8-3-5line1	2.07	21.353	4.744	0.089	29.087	6.226	37.047	100.616
8-3-5line1	1.992	21.232	4.653	0.112	28.856	6.872	36.95	100.667
8-3-5line1	1.967	21.394	4.984	0.084	28.494	6.698	36.977	100.598
8-3-5line1	1.957	21.524	4.732	0.033	28.955	6.865	36.969	101.035
8-3-5line1	1.993	21.38	4.758	0.092	28.567	6.945	37.025	100.76
8-3-5line1	1.856	21.453	5.148	0.096	28.091	7.138	37.275	101.057
8-3-5line1	1.925	21.469	4.345	0.08	29.112	6.99	37.012	100.933
8-3-5line1	1.987	21.389	4.855	0.043	28.658	6.992	37.143	101.067
8-3-5line1	1.999	21.203	4.832	0.086	28.638	6.755	37.044	100.557
8-3-5line1	2.198	21.307	4.334	0.073	29.922	5.803	37.233	100.87
8-3-5line1	2.284	21.503	4.965	0.106	30.677	4.365	37.359	101.259

D) Garnet Mineral Chemistry Data from Microprobe Analysis

Sample	MgO	Al2O3	CaO	TiO	FeO	MnO	SiO2	Total
SF-3line1	3.689	21.985	5.416	0	31.105	1.384	37.648	101.227
SF-3line1	2.929	21.278	7.223	0.029	30.222	1.086	36.626	99.393
SF-3line1	1.634	21.869	9.116	0.052	30.454	0.701	37.334	101.16
SF-3line1	1.963	21.616	7.776	0.055	29.437	2.627	37.324	100.798
SF-3line1	2.895	22.08	4.682	0.076	29.452	3.558	37.305	100.048
SF-3line1	3.193	21.527	4.867	0.045	29.939	3.522	36.87	99.963
SF-3line1	3.31	21.624	5.335	0.031	30.363	2.199	36.973	99.835
SF-3line1	0.017	0.291	0.075	0.29	0	0.036	98.91	99.619
SF-3line1	3.034	21.605	5.656	0.036	31.65	1.538	37.048	100.567
SF-3line1	3.084	21.71	6.731	0	30.928	0.813	37.193	100.459
04t-mlogarnet1	2.221	21.584	37.031	3.462	0.007	2.493	32.973	99.771
04t-mlogarnet1	2.496	21.404	36.943	2.898	0.004	2.478	33.464	99.687
04t-mlogarnet1	2.474	21.327	37.075	3.142	0.006	2.775	32.871	99.67
04t-mlogarnet1	2.39	21.276	37.117	3.082	0.019	3.201	32.614	99.699
04t-mlogarnet1	2.334	21.384	37.014	3.188	0.031	3.477	31.891	99.319
04t-mlogarnet1	2.205	21.356	37.139	3.636	0.051	3.81	31.735	99.932
04t-mlogarnet1	2.247	21.36	37.046	3.407	0.046	4.372	31.639	100.117
04t-mlogarnet1	2.039	21.471	37.323	4.075	0.041	4.614	30.329	99.892
04t-mlogarnet1	2.031	21.262	36.825	3.713	0.061	4.968	30.544	99.404
04t-mlogarnet1	1.961	21.29	37.023	4.451	0.077	5.061	29.715	99.578
04t-mlogarnet1	1.97	21.48	36.921	4.08	0.046	5.538	29.354	99.389
04t-mlogarnet1	1.864	21.276	37.071	4.776	0.071	5.608	28.324	98.99
04t-mlogarnet1	1.839	21.24	37.055	4.439	0.057	5.93	28.726	99.286
04t-mlogarnet1	1.901	21.295	37.011	4.358	0.055	5.744	28.968	99.332
04t-mlogarnet1	1.813	21.429	37.015	4.704	0.043	5.82	28.869	99.693
04t-mlogarnet1	1.779	21.358	36.686	4.109	0.021	6.061	28.425	98.439
04t-mlogarnet1	1.747	21.241	36.839	4.799	0.114	5.949	27.578	98.267
04t-mlogarnet1	1.784	21.323	36.939	4.515	0.079	6.293	28.057	98.99
04t-mlogarnet1	1.739	21.308	36.736	4.806	0.07	6.306	27.413	98.378
04t-mlogarnet1	1.675	21.231	36.664	4.616	0.065	6.664	27.702	98.617
04t-mlogarnet1	1.795	21.388	36.787	4.668	0.075	5.79	28.242	98.745
04t-mlogarnet1	1.689	21.269	37.176	4.823	0.077	6.769	27.454	99.257
04t-mlogarnet1	1.704	21.101	36.719	4.788	0.075	6.614	27.004	98.005
04t-mlogarnet1	1.694	21.293	36.862	4.579	0.084	6.965	27.485	98.962
04t-mlogarnet1	1.629	21.457	37.182	4.74	0.082	6.62	27.693	99.403
04t-mlogarnet1	1.617	21.383	37.002	4.803	0.071	6.696	27.017	98.589
04t-mlogarnet1	1.617	21.258	36.674	4.498	0.113	6.811	27.546	98.517
04t-mlogarnet1	1.696	21.272	37.041	4.561	0.061	6.753	27.809	99.193
04t-mlogarnet1	1.697	21.341	36.673	4.689	0.081	6.657	27.129	98.267
04t-mlogarnet1	1.709	21.291	36.614	4.546	0.053	6.581	27.856	98.65
04t-mlogarnet1	1.803	21.236	36.825	4.381	0.055	5.971	28.252	98.523
04t-mlogarnet1	1.738	21.333	36.617	4.384	0.077	6.521	27.992	98.662
04t-mlogarnet1	1.745	21.349	36.847	4.446	0.06	6.294	28.202	98.943
04t-mlogarnet1	1.768	21.26	36.663	4.353	0.076	6.453	28.339	98.912
04t-mlogarnet1	1.855	21.506	36.883	4.612	0.059	5.904	28.17	98.989
04t-mlogarnet1	1.833	21.375	36.917	4.277	0.053	6.131	28.901	99.487

D) Garnet Mineral Chemistry Data from Microprobe Analysis

Sample	MgO	Al2O3	CaO	TiO	FeO	MnO	SiO2	Total
04t-mlogarnet1	1.889	21.291	36.862	3.981	0.068	5.823	29.204	99.118
04t-mlogarnet1	2.084	21.372	36.651	3.791	0.054	4.777	29.959	98.688
04t-mlogarnet1	2.278	21.477	36.951	3.318	0.026	3.718	31.784	99.552
04t-mlogarnet1	2.384	21.563	36.975	3.299	0.023	3.399	32.207	99.85
04t-mlogarnet1	2.491	21.638	36.836	2.916	0.024	3.134	32.361	99.4
04t-mlogarnet1	2.515	21.414	36.428	2.8	0.011	2.471	32.934	98.573
04t-mlogarnet1	2.528	21.491	36.492	2.89	0.013	2.447	32.815	98.676
04t-mlogarnet2	2.443	21.501	37.228	3.186	0.002	2.362	33.43	100.152
04t-mlogarnet2	2.517	21.362	37.032	2.878	0	2.495	32.915	99.199
04t-mlogarnet2	2.514	21.425	37.194	2.849	0.012	3.033	32.65	99.677
04t-mlogarnet2	2.352	21.548	37	2.938	0.019	3.528	32.052	99.437
04t-mlogarnet2	2.208	21.362	36.932	3.065	0.018	4.342	30.983	98.91
04t-mlogarnet2	1.944	21.351	36.89	4.031	0.055	5.314	29.54	99.125
04t-mlogarnet2	1.818	21.201	36.915	4.432	0.142	6.022	28.27	98.8
04t-mlogarnet2	1.731	21.27	36.886	4.627	0.086	6.133	28.192	98.925
04t-mlogarnet2	1.733	21.355	36.741	4.769	0.059	6.377	27.664	98.698
04t-mlogarnet2	1.595	21.335	36.876	5.128	0.076	6.544	27.095	98.649
04t-mlogarnet2	1.594	21.347	37.005	5.495	0.112	6.384	26.868	98.805
04t-mlogarnet2	1.48	21.253	36.892	6.045	0.121	7.082	25.662	98.535
04t-mlogarnet2	1.406	21.481	36.964	6.072	0.127	7.34	25.304	98.694
04t-mlogarnet2	1.354	21.444	36.783	6.388	0.092	7.596	24.933	98.59
04t-mlogarnet2	1.447	21.259	37.021	6.406	0.14	7.312	25.051	98.636
04t-mlogarnet2	1.638	21.321	37.069	5.185	0.078	6.463	27.05	98.804
04t-mlogarnet2	1.649	21.271	36.93	4.963	0.087	6.45	27.187	98.537
04t-mlogarnet2	1.621	21.571	36.627	4.417	0.069	6.104	28.257	98.666
04t-mlogarnet2	1.824	21.502	36.512	4.207	0.067	6.081	28.613	98.806
04t-mlogarnet2	2.081	21.477	36.511	3.854	0.048	4.764	30.133	98.868
04t-mlogarnet2	2.306	21.483	36.759	3.152	0.031	3.864	31.344	98.939
04t-mlogarnet2	2.546	21.697	36.716	2.804	0.015	2.796	32.605	99.179
04t-mlogarnet2	2.498	21.652	36.766	2.841	0.016	2.559	32.915	99.247
04t-mlogarnet2	2.046	21.615	36.95	4.25	0.018	2.261	32.032	99.172
04t-mlogarnet3	2.287	21.268	37.038	3.296	0.007	2.319	33.069	99.284
04t-mlogarnet3	2.55	21.381	37.332	2.826	0.001	2.408	33.289	99.787
04t-mlogarnet3	2.564	21.459	37.336	2.91	0.017	2.743	33.089	100.118
04t-mlogarnet3	2.416	21.312	37.167	3.255	0.013	3.054	32.091	99.308
04t-mlogarnet3	2.282	21.338	37.187	3.488	0.025	3.429	31.056	98.805
04t-mlogarnet3	2.286	21.209	37.206	3.632	0.025	3.655	31.163	99.176
04t-mlogarnet3	2.21	21.206	37.176	3.667	0.029	3.846	30.858	98.992
04t-mlogarnet3	2.062	21.226	37.17	3.487	0.036	4.254	30.699	98.934
04t-mlogarnet3	2.041	21.276	37.122	3.775	0.044	4.419	29.963	98.64
04t-mlogarnet3	2.006	21.21	37.135	3.788	0.051	4.877	29.734	98.801
04t-mlogarnet3	1.814	21.477	36.643	4.251	0.059	5.739	28.7	98.683
04t-mlogarnet3	1.632	20.756	35.373	4.492	0.12	6.031	28.422	96.826
04t-mlogarnet3	1.679	21.404	36.941	4.569	0.064	6.562	27.354	98.573
04t-mlogarnet3	2.049	21.33	36.93	3.695	0.044	4.862	30.032	98.942
04t-mlogarnet3	2.023	21.386	36.752	3.846	0.038	4.82	29.82	98.685
04t-mlogarnet3	2.283	21.633	36.701	3.292	0.03	3.729	30.922	98.59

Appendix IV: Analytical Procedures

U/Pb Dating Analytical Procedures.

A complete description of instrumentation, operational parameters, corrections and data reduction used at Washington State University is provided by Chang et al., (2006), the analytical details described below are summarized from this paper.
All U/Pb analyses were conducted using a New Wave UP-213 laser ablation system in conjunction with a ThermoFinnigan Element2 single collector double focusing magnetic sector ICP-MS at Washington State University. The Element2 is tuned before each analytical session using an NIST 612 glass standard to maximize signal intensity and stability. During a session, a zircon standard is analyzed two to three times every 5 to 10 analyses to assure that $^{206}Pb/^{238}U$ and $^{207}Pb/^{206}Pb$ ratios are within or near 1% of standard values. Fixed 30 to 40 diameter spots were used with a laser frequency of 10 Hz. The ablated material is delivered to the torch by He and Ar gas. Each analysis consists of a 6 second warm-up, and 8 second delay to enable the sample to reach the plasma and 35 seconds of rapid scanning across masses ^{202}Hg $^{204}(Hg + Pb)$, ^{206}Pb, ^{207}Pb, ^{208}Pb, ^{235}Th, ^{235}U, and ^{238}U. Each analysis consists of 300 sweeps which takes about 35 seconds. For individual analyses the accuracy and precision of determined ages is better than 4% at the 2 sigma level. For a detailed account of error calculations and data reduction, the reader is again referred to Chang et al., (2006).

Analytical Procedures for Hf/Lu Age Dating

The tabletop dissolution method employed at Washington State University is described below.

1. In Savilex Teflon beakers approximately .250 grams of sample is cleaned in 4 mL of 4 M HCL, then rinsed with 5 mL H_2O.

2. Sample is dissolved with 3 drops of 14 M HNO_3 and 30 drops 29 M HF, and then dried on a hotplate.

3. 1 mL 14 M HNO_3 and 9 mL 29 M HF are added to the sample, the sample is capped and placed on a hotplate at 100 °C for 24 hours. Whole rock samples are placed in steel jacketed PTFE dissolution vessels for 5 days.

4. Sample is then uncapped and allowed to dry.

5. 2.5 mL of Boric Acid and 5 mL of 6 M HCL are added to the sample, the sample is capped and placed on a hotplate for 24 hours.

6. Sample is uncapped and allowed to dry.

7. For whole rock samples, 6 M HCL is added, heated overnight and allowed to dry.

8. 10 mL of 6 M HCL is added to the sample and allowed to equilibrate. A 100 µL aliquot is then taken for preliminary trace element analysis to obtain spiking information.

9. Samples are spiked with mixed ^{176}Lu–^{180}Hf tracer solutions to determine Lu concentrations and $^{176}Lu/^{177}Hf$ ratios.

10. Samples are then centrifuged at 3500 rpm for 15 minutes in preparation for HF and Lu separation column chemistry.

Separation chemistry involves 3 different separation columns for hafnium and 2 for lutetium. Separation of elements is achieved by flushing the solution through a resin, which retains the desired element while releasing most others. The desired element is eventually eluted and released from the resin with an appropriate acid. For details of

separation chemistry the reader is referred to; Patchett and Tatsumoto, 1980; Vervoort and Blichert-Toft, 1999; Blitchert-Toft, 2001; and Vervoort et al., 2004.
After complete seperation of Hf and Lu the samples are dried down on a hotplate and then dissolved in 500 µL 2% HNO_3 in preparation for analysis.

Samples were analyzed using a ThermoFinnigan Neptune ICP-MS multi-collector. Standards and backgrounds were measured several times at the beginning of each session and after every 3 to 5 samples. During each lutetium analysis 30 individual measurements were taken, for each Hf analysis 75 individual measurements were recorded. After each sample analysis the system was cleaned by aspirating 2% HNO_3 and 0.1% HF for several minutes until background measurements dropped at least three orders of magnitude below the sample signals. Explanations for sample nebulization, background calculations, faraday cup configurations, mass bias corrections, and fractionation corrections are provided by Vervoort et al., (2004). Ages were determined from the slopes of multipoint isocrons with ^{176} Hf/^{177}Hf plotted on the ordinate axis and ^{176}Lu/^{177}Hf plotted on the abscissa.